Optical Vortices: Scattering through Random Media

A THESIS

submitted for the Award of Ph.D. degree of

MOHANLAL SUKHADIA UNIVERSITY

in the

Faculty of Science

by

Salla Gangi Reddy

Under the Supervision of

Prof. Ravindra P Singh

Professor

Atomic, Molecular, and Optical Physics Division

Physical Research Laboratory

Ahmedabad, India.

DEPARTMENT OF PHYSICS

MOHANLAL SUKHADIA UNIVERSITY

UDAIPUR

Year of submission: 2015

To

My Parents

Amma-Nanna

DECLARATION

I, **Mr. Salla Gangi Reddy***, S/o Mr. Venkata Subba Reddy, resident of Room No. C-103, PRL Students Hostel, Navrangpura, Ahmedabad, 380009, hereby declare that the research work incorporated in the present thesis entitled,* **"Optical Vortices: Scattering through Random Media"** *is my own work and is original. This work (in part or in full) has not been submitted to any University for the award of a Degree or a Diploma. I have properly acknowledged the material collected from secondary sources wherever required. I solely own the responsibility for the originality of the entire content.*

Date:

(Salla Gangi Reddy)

CERTIFICATE

I feel great pleasure in certifying that the thesis entitled, **"Optical Vortices: Scattering through Random Media"** embodies a record of the results of investigations carried out by Mr. Salla Gangi Reddy under my guidance. He has completed the following requirements as per Ph.D regulations of the University.

(a) Course work as per the university rules.

(b) Residential requirements of the university.

(c) Regularly submitted six monthly progress reports.

(d) Presented his work in the departmental committee.

(e) Published a minimum of one research paper in a referred research journal.

I am satisfied with the analysis, interpretation of results and conclusions drawn. I recommend the submission of the thesis.

Date:

Prof. Ravindra P Singh
(Thesis Supervisor)
Professor, AMOPH,
Physical Research Laboratory,
Ahmedabad - 380 009

Countersigned by

Head of the Department

Acknowledgements

This thesis is the end of my long journey in obtaining the doctoral degree. A journey is easier when you travel together. Interdependence is certainly more valuable than independence. This thesis is the result of five years of work whereby I have been accompanied and supported by many people. It is a pleasant aspect that I have now the opportunity to express my sincere gratitude for all of them.

I am deeply indebted to my supervisor R. P. Singh for his able guidance and continued encouragement for the fulfilment of the research work. I believe I don't have words which could fully encompass the amount of gratitude and respect I have for him. For his simple attitude yet thorough professionalism, I thank him, for his supervision and scientific expertise provided during this period. His company and assurance at the time of crisis (both scientific and personal) would be remembered lifelong. I appreciate his many useful comments on this work, but even more so, I appreciate his advices and willingness to discuss any questions or ideas that I have had.

I am very much thankful to Prof. Jagannath Banerji for his continued support and encouragement in my research work. With great pleasure I express my sincere gratitude to him for fruitful discussions, numerous suggestions and constructive criticism throughout the period. I take this opportunity to express my sincere thanks to Prof. Rajaiah Simon, IMSc Chennai for his collaboration and also for imparting knowledge as well as motivation towards research. I am thankful to Dr. Goutam K. Samanta for his help in my research work. I would like to say my sincere thanks to Prof. K. P. Subramanian for his kind support during my project as well as Ph.D.

I take this opportunity to express my profound respect to PRL for providing the basic infrastructural facilities for carrying out the research work. I thank Prof. Jitesh Bhatt, Prof. M. M. Sarin, Prof. S. Ramachandran, Prof. R. Ramesh, Dr. Bhuvan Joshi, Dr. Abhijit Chakravarty, Dr. Bijaya Sahoo, Prof. S. Goswami, Dr. Navinder Singh, Prof. R. Rangarajan, Prof. Varun Sheel, Dr. D. Chakravarty, and Dr. K. K. Marhas for taking various courses in physics. My special thanks goes to the academic committee and my thesis experts Prof. Pallam Raju and Prof. Dilip Angom for thoroughly reviewing my work. Their guidance has served me well and I owe them my heartfelt appreciation.

I am thankful to Dr. Ashok Kumar and Dr. Priya (bhabhi ji), for their encouragement and guidance in both the professional and personal life. I consider Dr. Ashok Kumar as my guide and philosopher. I always like to have scientific discussions with him and to learn how

to perform the experiments as well as how to write research papers. I would like to thank Dr. Pravin Vaity and Dr. Shashi Prabhakar for their help at the initial stage of my research career and also in computing programs. Special thanks to Shashi for helping me to complete the thesis as well as for his personal support. I greatly enjoyed working with all my lab mates Dr. Sunita Kedia, Dr. Jitendra Bhatt, Aadhi, Chithrabhanu, Apurv, Vinayak, Ali, Jabir, Nijil, Aavesh and all the project associates who have completed their project work in our lab. I specially thank Apurv for providing me the good drawings of the experimental set ups and Chithra, Ali, Nijil for the careful reading of my thesis. I thank them all for their full cooperation and ever needed help throughout to carry this work and also for being around all the time. Many thanks to Chithra and Apurv for scientific discussions and political debates which have made life enjoyable. I will be thankful to Dr. A. K. Jha (IITK), Dr. Goutam Paul (ISI) and Dr. R. K. Singh (IIST) for their kind help and discussions during my Ph.D.

I would like to say thanks to all my seniors and juniors for making my stay in PRL comfortable. I must acknowledge my batch mates Avdhesh, Girish, Arko, Yashpal, Gaurav[2]*, Priyanka, Bhavya, Lekshmy and Midhun, Anjali, Tanmoy, Gulab, Monojit, Debasis, Uma, Latha, Dinesh*[2]*, Ashok, Naveen, Dillip, Upendra, Wageesh for providing the enjoyable company. I must say thanks to my friends Eswar Reddy, Ramanaiah, Pawan, Govardhan, Umadhar, Ashok (Dg), Hari, Has, Pratap, Balu, Sowmya, Goutami, K (R) V Krishnaiah, Deva, Madhu, Sriram, Uday, Jalpa, Asha, Vijay, Zeen and Akhilesh, Prasad and Prasanna for their valuable company during my education and trips. I would like to say thanks to all my students at RGUKT (specially, Pujitha, Amala, Meenakshi, Giri, Vivek, Saieesh, Durga, Siva, Goutham) for teaching me Physics. I also thank my RGUKT colleagues Raghava Reddy, Ramakrishna, Anji, Tirupathi Reddy, Umakanth, Munichandu, Uma, Srinivas Siddhi, Venkata Rao, Haritha, Soujanya, Srinivas, Sreedhar, and Ashok for their nice company and parties while I was in RGUKT.*

I will be always thankful to Prof. V. Rajagopal Reddy, who motivated me to join PRL and supported through out my Ph.D career. My special thanks to Prof. K. T. Ramakrishna Reddy, Prof. P. Sreedhara Reddy, Prof. S. Buddhudu, Mr. Jagan Mohanacharyulu (My School Teacher), Dr. Ramesh, Dr. Chalapathi and Venkata Lakshmi for their encouragement, inspirations and guiding me at different levels of my education. I must acknowledge the company of my Andhra mates Dr. Suneel Krishna, Dr. B. Srinivas, Durga Prasad, Krishna Veni, Dr. Aditya, Aslam, Teja, Jyothi, Maniteja, Ejaj, Satti (Nellore), Rajesh (HCU), Damodar, Venkatesh, Samir, Satish, Kiran, Dr. Tirupataiah and family, Vamseedhar Reddy (IITGn) who have always relieved me from the work loads. Special thanks to Dr. Suneel

Krishna for his dinner parties and friendly company. I am always thankful to Sambhasiva Rao (CISF) and his family for giving me homely atmosphere and also for providing such a nice food. I would like to thank Krishna Reddy sir and Saraswathi madam for their precious help in my life.

I am grateful to all the staff members of PRL library, computer center, dispensary and administration staff for their sincere support. Its my duty to acknowledge Google scholar, Arxiv for keeping me updated.

I have no words to express appreciation to my family. Without their love, inspiration and support I would not have been able to complete this work. I am grateful for my Father Shri Venkata Subba Reddy, my Mother Smt. Rama Lakshumma, my mama Muniratnam Naidu and my atta Vasantamma, my brothers and vadina (bhabhi ji) Venkata Subba Reddy and Praveena; Eswar Reddy and Nageswari; Rajesh and Muni Kumari, Sv Subba Reddy (both), Siva, my Sisters and brother in laws Rama Tulasi and Linga Reddy; Narayanamma and Subba Reddy, Vasanta, Sameepa, Chinna, Vijay, Manohar, and their kids Veena, Baby, Bhavani, Charan, Vijay, Jyoshna, Teja^2*, Charith, Keerthana, Prarthana. I am always thankful to my friend and brother Dr. A. Venkateswarlu and his family who made my life easier and comfortable. I am also thankful to all my relatives for their love, support and encouragement. And last, but not the least, to my wife, Prasanna Kumari, who shares my dreams and passion. I feel blessed to have such a life partner who understands me always in a better way. She entered officially into my life when I was in crisis and I was able to solve all the problems with her support in both personal and professional life that I have faced. This Thesis would not have been possible without her. I dedicate this work to my parents.*

I gratefully acknowledge the financial support provided by PRL in the form of junior/senior research fellowships during the period of research.

Salla Gangi Reddy

ABSTRACT

Optical vortices, whirlpools of light, are phase singularities in the light field. These vortex beams have helical wave front and their Poynting vector rotates around the propagation axis. They carry an orbital angular momentum of $m\hbar$, m being the topological charge or order defined as the number of helices in one wave length. Such beams have an azimuthal phase dependence of $\exp(im\phi)$, where $\phi = tan^{-1}(y/x)$ is the azimuthal angle. Vortex beams can be generated by a number of methods. Few of them are an astigmatic mode converter, computer generated holography and spiral phase plates. However, vortices of first order naturally exist in the speckles that can be formed by the scattering of a coherent light beam through a rough surface. Speckles are due to the mutual interference of a number of scattered wave fronts from inhomogeneities of the random medium. It would be very interesting to study the speckles generated by the optical vortices as they themselves contain vortices. This thesis concerns with the study of optical vortices and their scattering through random media.

The spatial intensity profile of optical vortices has been studied using two novel and measurable parameters, inner and outer radii along with their propagation through free space. We show that the propagation characteristics depend only on width of the host Gaussian beam and its intensity profile at the source plane. We have also studied the divergence of vortex beams, considering it as the rate of change of inner and outer radii with the propagation distance (z), and found that it varies with the order in the same way as that of the inner and outer radii at $z = 0$. The corresponding experimental and theoretical results have been presented.

We have embedded a pair of vortices with different topological charges in a Gaussian beam and studied their evolution through an astigmatic optical system, a tilted lens. The propagation dynamics is explained by a closed-form analytical expression. Furthermore, we show that a careful examination of the intensity distribution at a predicted position, past the lens, can determine the charge present in the beam. To the best of our knowledge, our method is the first non-interferometric technique to measure the charge of an arbitrary vortex pair. Our theoretical results are well supported by experimental observations.

We have experimentally generated higher order optical vortices and scattered them through a ground glass plate resulting in speckle formation. Intensity autocorrelation measurements of speckles show that their size decreases with increase in the order of the vortex. It implies increase in angular diameter of the vortices with their order. The characterization of vortices in terms of the annular bright ring also helps us to understand these observations. We

have generated the ring shaped beams from the speckles generated by the scattering of LG and BG beams. We also show that these ring-shaped beams have the same vorticity as the incident beam falling on the rough scattering surface. The vorticity is measured through a novel method that uses a non separable state of polarization and orbital angular momentum of light. The observed vorticity is found to be independent of the amount of scattered light collected. Therefore, vortices can be used as information carriers even in the presence of scattering media. The experimental results are well supported by the theoretical results.

We have generated perfect optical vortices (POV), whose intensity distribution are independent of the order, using Fourier transform of Bessel–Gauss (BG) beams and scatter them through a rough surface. We show that the size of produced speckles is independent of the order and their Fourier transform gives the random non-diffracting fields. The invariant size of speckles over the free space propagation verifies their non-diffracting or non-diverging nature. The size of speckles can be easily controlled by changing the axicon parameter, used to generate the BG beams.

Keywords : Optical vortices, Scattering, Random media, Speckles, Astigmatic system, Perfect optical vortices.

List of Abbreviations

OAM	Orbital Angular Momentum
HG	Hermite Gaussian
LG	Laguerre Gaussian
CGH	Computer Generated Hologram or Holography
SPP	Spiral Phase Plate
VL	Vortex Lens
GGP	Ground Glass Plate
POV	Perfect Optical Vortex
BG	Bessel-Gauss
SLM	Spatial Light Modulator
PMT	Photomultiplier Tube
GSM	Gaussian Schell Model
LGSM	Laguerre Gaussian Schell Model
BGSM	Bessel Gaussian Schell Model
RGG	Rotating Ground Glass
CCD	Charge Couple Device
FWHM	Full Width Half Maxima

Contents

Acknowledgements **i**

Abstract **v**

List of Abbreviations **vii**

Contents **ix**

List of Tables **xiii**

List of Figures **xv**

1 Introduction **1**

1.1 Optical vortices 1

1.1.1 Astigmatic mode converter 3

1.1.2 Spiral phase plate or vortex lens 4

1.1.3 Computer generated holography 5

1.2 Speckle phenomena 8

1.3 Scattering of optical vortices 9

1.4 Perfect optical vortices 10

1.5 Objective of the thesis 11

1.6 Overview of the thesis 12

2 Propagation Dynamics of Optical Vortex Beams **15**

2.1 Inner and Outer radii of an optical vortex beam 16

2.2 Free space propagation of vortex beams 20

2.3 Divergence of the vortex beam 22

2.4 Conclusion 24

3 Pair of Vortices through an Astigmatic Optical System 25

3.1 Theory . . . 26

3.1.1 Determination of net topological charge . . . 28

3.1.1.1 Vortices with topological charges of the same sign . . . 29

3.1.1.2 Vortices with topological charges of opposite signs . . . 29

3.1.2 Propagation dynamics away from the critical plane ($z > z_c$) . . . 30

3.1.3 Propagation dynamics when the lens is not tilted . . . 30

3.2 Experimental set-up . . . 31

3.3 Experimental results . . . 33

3.3.1 Intensity distribution at the critical plane ($z = z_c$) . . . 33

3.3.2 Evolution of vortices beyond the critical plane . . . 40

3.4 Conclusion . . . 40

4 Scattering of Optical Vortices and Formation of Speckles 41

4.1 Experimental set up . . . 41

4.2 Speckle patterns of vortex beams . . . 42

4.2.1 Auto-correlation for finding the speckle size . . . 42

4.2.2 Speckle size vs order . . . 43

4.3 Theoretical modelling . . . 46

4.4 Intensity correlation vs order of the vortex . . . 47

4.5 Scattering and the focal plane . . . 49

4.6 Conclusion . . . 50

5 Speckles and Formation of Ring Shaped Beams 51

5.1 Experimental set up . . . 52

5.2 Results and discussion . . . 53

5.3 Theoretical analysis . . . 57

5.4 Conclusion . . . 60

6 Vorticity of the Scattered Optical Vortices 61

6.1 Interferometry of a scattered optical vortex . . . 62

6.2 Entanglement in classical optics . . . 64

6.3 Experimental set up . . . 65

6.4 Confirmation of vorticity . . . 66

6.5 Theory . . . 67

6.6 Conclusion . . . 69

7 Perfect Optical Vortices and the Non-Diffracting Speckles 71

7.1 Generation of perfect optical vortices 72

7.2 Scattering of POV beams: a comparison with ordinary vortices 75

7.3 Non-diffracting speckles 76

7.4 Conclusion 79

8 Summary and Scope for Future Work 81

8.1 Summary of the work-done 81

8.2 Scope for future work 83

Bibliography 85

List of Publications 101

Publications attached with the thesis 107

List of Tables

2.1 Numerical solutions for Eqs. 2.3a and 2.3b 17

List of Figures

1.1 The intensity distribution (a), wavefront (b) and the phase (c) of a Gaussian beam (top) and the optical vortices of orders +1 (middle) and -1 (bottom). . 2

1.2 The schematic of the input and output spatial modes of an astigmatic mode converter consisting of two cylindrical lenses with a given separation. 3

1.3 Changing the planar wavefronts to helical wavefronts using a spiral phase plate. 4

1.4 The computer generated holograms with sinusoidal (a), binary (b) and blazed (c) transmission functions for making an optical vortex of order +1. 6

1.5 The schematic for the generation of optical vortices by passing a Gaussian beam through a branch point of the hologram. 6

1.6 The interference patterns of a Gaussian beam (left) and the vortex beams of order +1 (middle) and −1 (right) with planar (top) and spherical (bottom) wavefront. 7

1.7 The speckle patterns generated by the scattering of a Gaussian (a), optical vortex (b) and perfect optical vortex of order +1 (c) through the ground glass plate (d). 8

1.8 The axicon holograms with a (a) sinusoidal, (b) binary and (c) blazed transmission functions. This hologram is used to generate the Bessel–Gauss beams. 11

1.9 Theoretically obtained intensity distributions of the POV beams of orders 0, 10, 20, 30 (from left to right) and at axicon parameters of 10, 13, 16 /mm (from top to bottom). 12

2.1 The transverse intensity profile of an optical vortex of order 1 and its line profile. 16

2.2 Numerically obtained values of $\chi_2 + \chi_1$ (filled squares) and the line $y = m + 1.3$ as functions of m. 18

2.3 Line profiles along the vortex centres of optical vortices for orders 0 to 5 that are produced in the laboratory. 19

2.4 Experimental and theoretical results showing the variation of (a) inner and outer radii and (b) area of bright annular region with the order of a vortex. . 19
2.5 The inner radius for vortices of orders $m = 1$ to 4 at different distances. . . . 21
2.6 The outer radius for vortices of orders $m = 1$ to 4 at different distances. . . . 21
2.7 The divergence i.e. the rate of change of inner (top) and outer (bottom) radii with the order of vortex beams obtained experimentally (blue diamonds) as well as theoretically (red dots). 23

3.1 Experimental set-up for the determination of the net charge of an arbitrary vortex pair embedded in a Gaussian beam. 32
3.2 The intensity distributions of a vortex pair embedded in a Gaussian beam and the corresponding interferograms at 96 cm (left) and 147 cm (right) from the SLM with the orders (top) m=n=1; (bottom) m=n=2. 32
3.3 The theoretical (first two rows) and experimental (last two rows) results for the intensity patterns of a vortex pair with topological charges of the same sign, at $z = z_c$ for $x_0 = 0.1w_0$. 34
3.4 The theoretical results for the intensity patterns of a vortex pair with topological charges of the same sign with varying separation at $z = z_c$, (top) m=4, n=1; (bottom) m=n=2. 35
3.5 The experimental images corresponding to Figure 3.4. 35
3.6 The line profiles of intensity distributions along the center of the lobes corresponding to Figure 3.5 at $x_0 = 0.4w_0$, (left) m=4, n=1; (right) m=n=2. . . . 35
3.7 The theoretical (first two rows) and experimental (last two rows) results for the intensity patterns of an off-axis vortex of charge 2, at $z = z_c$ for different values of x_0 as labelled in the insets. 36
3.8 The theoretical (first two rows) and experimental (last two rows) results for the intensity patterns of a vortex pair with topological charges of opposite signs, at $z = z_c$ for $x_0 = 0.1w_0$. 37
3.9 The theoretical (top row) and experimental (bottom row) results for the intensity patterns of a dipole vortex of charge (2,-2), at $z = z_c$ for different values of x_0 as labelled in the figures. 37
3.10 Theoretical results for the intensity patterns of a vortex pair with topological charges (top) m= n=2; (bottom) m=2, n=3, at $z = z_c$ corresponding to the tilt angle $\theta = 6°$. As the tilt angle moves away from 6°, the sharpness of the patterns decreases, as expected. 38

3.11 The experimental images corresponding to Figure 3.10 at $z = z_c$. 38
3.12 Theoretical intensity patterns of a vortex pair of different charges (as given on the top) at various values of the propagation distance z (as given on the left). 39
3.13 The experimental images corresponding to Figure 3.12. 39

4.1 The experimental set-up for generating the speckles by scattering the optical vortex beams. Here, A–Aperture, M–Mirror, BS–Beam splitter, SLM–Spatial light modulator, and GGP–Ground glass plate. 42
4.2 The speckle patterns formed by the scattering of optical vortices with orders $m = 0 - 5$ at a given plane. 43
4.3 (a) The obtained speckle pattern of first order optical vortex, (b) the distribution of auto correlation function, (c) and (d) are the variation of autocorrelation function in transverse directions X and Y respectively. 44
4.4 The plot of $\ln S_m$ versus $\ln A_m$ where S_m and A_m are the experimentally obtained speckle size and area of bright region of optical vortices respectively, (Inset, the same plot for a Gaussian beam with different sizes/areas). The solid line is the best fit to our experimental data. 45
4.5 The plot of speckle divergence vs order of the vortex. 45
4.6 The numerically obtained speckle patterns for optical vortices with orders m=0–5. 47
4.7 The experimentally obtained temporal intensity correlation curves for the optical vortices of orders m=0–7. 48
4.8 The experimentally obtained spatial intensity correlation curves for the optical vortices of orders m=1–6. 48
4.9 Plot showing the shift in focal plane with the position of lens from the GGP for different beam widths. 50

5.1 Experimental set up for the generation of ring shaped beams. 53
5.2 Images showing the intensity distributions of scattered second order LG (a-d) and BG (e-h) beams; (a, e) are recorded after the ground glass and (b, f) after the lens, while (c, g) and (d, h) are recorded at same places when the ground glass is rotating (linear speed 72.1 cm/sec). 53
5.3 Far field intensity distribution of the scattered LG beams of different azimuthal indices ($l = 2, 4, 6$) through a RGG plate for different widths of the incident beam, 0.496 mm (top), 0.412 mm (middle) and 0.321 mm (bottom). 54

5.4 Far field intensity distribution of the scattered BG beams for same conditions as in Figure 5.3 55

5.5 The line profiles along the core of ring shaped beams generated from scattered second order LG (left) and BG (right) beams at different speeds of the RGG plate (top) and for different incident beam widths. (bottom) 56

5.6 The line profiles (intensity distribution) along the centers of far field intensity distributions of scattered LG (a) and BG (b) beams for l = 1-6 56

5.7 Theoretical results for far field intensity distribution of the scattered LG beams of different azimuthal indices ($l = 2, 4, 6$) through a RGG plate for different w_0 values 0.496 mm (top), 0.412 mm (middle) and 0.321 mm (bottom). . . . 59

5.8 (a) The experimental (top) and theoretical (bottom) far field intensity distributions of the scattered LG beam of azimuthal index ($l = 1$) through a RGG plate for different w_0 values, 0.496 mm (left), 0.412 mm (middle) and 0.140 mm (right). (b) The line profiles of theoretical far field intensity distributions of scattered first order vortex for different incident beam widths. 59

6.1 The experimental set up for scattering the vortex beam and to observe the vortex-vortex interference fringes. M1, M2, M3, M4 - mirrors; VL - Vortex lens; BS - Beam Splitter; L1, L2 - Plano-convex lenses. 62

6.2 The intensity distributions of a scattered optical vortex of order 2 after the GGP (left), immediately after the lens (middle) and the Fourier plane (right) correspond to different speeds of the GGP (top) 0 cm/s and (bottom) 194.7 cm/s. 63

6.3 Experimentally obtained interference fringes for coherent (top) and scattered (bottom) optical vortex beams of order m = 0–3 (from left to right). 63

6.4 The theoretical intensity distributions of a non separable state of polarization and OAM for the different projections – horizontal, vertical, anti–diagonal and diagonal from left to right of m = 2 (top) and 3 (bottom). 65

6.5 The experimental set up for observing the vorticity in scattered optical vortex. M1, M2, M3, M4 - mirrors; HWP - half wave plate; PBS - polarizing beam splitter; VL - vortex lens; i/p state - non–separable state; GGP - ground glass plate; P - polarizer; L - plano convex lens. 66

6.6 Experimentally obtained far field intensity distributions for different projections in polarization after scattering through a ground glass plate. These results correspond to the non-separable states with $m = 2$ (top), 3 (bottom) for w_0=1.92 mm. 67

6.7 The theoretical far field intensity distributions that correspond to the images shown in Figure 6.6. 68

6.8 The experimental (top) and simulated (bottom) far field intensity distributions for the projection on diagonal polarization of a scattered non-separable light beam of $m = 2$ at different speeds of the GGP given at top of the figure. . . . 69

7.1 The experimental set up for the generation of POV beams using the Fourier transform of BG beam. Here, M-Mirror, SLM-Spatial light modulator, BS-Beam splitter, BD-Beam dumper used to block the unwanted beams, L1-plano convex lens of focal length $f_1 = 60$ cm. 73

7.2 Experimentally obtained intensity distributions for POV beams of orders m = 0, 2, 4, 6 (from left to right) at different axicon parameters of 7.29 /mm (top), 10.93 /mm (middle) and 14.58 /mm (bottom). 73

7.3 The experimentally observed lobes due to the superposition of two equal and oppositely charged POV beams of given orders. 74

7.4 The experimental set-up for the scattering of POV beams through the ground glass plate and to generate the non-diffracting speckles. Here, L1 and L2 are plano-convex lenses of focal lengths $f_1 = 60$ cm and $f_2 = 50$ cm respectively. . 75

7.5 The speckle patterns correspond to scattering of the ordinary optical vortices (top) and the POV beams (bottom) of orders $m = 0$–3 (from left to right). . 76

7.6 The intensity distributions of non-diffracting speckles obtained by taking the Fourier transform of speckles generated by the scattering of POV beams of orders m =2, 5, 8 (from top to bottom) at an axicon parameter of $a = 14.58$ /mm corresponding to different propagation distances of $z = 0.12$ m, 0.27 m, 0.42 m and 0.57 m (from left to right). 77

7.7 The intensity distribution of non-diffracting speckles obtained by taking the Fourier transform of speckles generated by the scattering of POV beams of orders m =0, 3, 6, 9 (from left to right) and at axicon parameters a =14.58, 17.01, 21.87 /mm (from top to bottom). 77

7.8 The variation of speckle size with the propagation distance (top) and the order (bottom) at different axicon parameters showing no difference with respect to either of them. 78

Chapter 1

Introduction

Vortices are fascinating topological features which are ubiquitous throughout the physical systems [1–13]. In optics, these vortices have quantized orbital angular momentum (OAM) that leads to the use of vortices in a number of scientific and technical applications such as particle manipulation, quantum information, free space optical communication, and wireless communications [14–27]. This thesis addresses the propagation of optical vortices through a linear optical system, and its effect on the variation of size and divergence of the beam along with the consequences of an astigmatic optical system and scattering through random media like a ground glass plate. In this chapter, I will be giving a brief introduction to optical vortices and vortices with constant intensity distribution, their scattering, formation of speckles and their characteristics.

1.1 Optical vortices

Vortices have been observed in a variety of natural phenomena such as hurricanes, tornadoes, and even while pouring the water from one container to another [1, 28]. However, vortices have gained an extra importance after their mathematical representation and theory by Berry and Nye. It has been shown that the mathematical equation representing these vortices is the solution for Maxwell's electromagnetic wave equation which implies the possibility of vortices in light beams [29]. Nowadays, optical vortices have become more than a mathematical curiosity and have proved their practical value in numerous fields [30–34].

An optical vortex beam is characterized by a doughnut–shaped intensity distribution with a phase singularity and hence zero field amplitude at the center [35–37]. Optical vortices have a screw–shaped wavefront dislocation, which can be visualized as a helical phase structure

around the center where as a Gaussian beam has a uniform phase and planar wavefront [38, 39]. The phase varies linearly with the azimuthal angle ϕ as described by the phase term $\exp(im\phi)$ provided the vortex is circular and symmetric; where m is called the order or topological charge that defines the number of helices per wavelength or the number of times phase should change by 2π in one complete rotation around the center of the vortex and its direction of rotation decides the sign of topological charge.

The electric field distribution of an optical vortex of order m embedded in a host Gaussian beam of width w can be written as

$$E_m(x,y,z) = E_0(x+\epsilon\, iy)^m \frac{w_0}{(w(z))^{m+1}} \exp\left(-\frac{x^2+y^2}{w(z)^2}\right) \exp\left(ik\frac{x^2+y^2}{2R(z)}\right) \exp\left(ikz - i(m+1)\zeta(z)\right) \tag{1.1}$$

where E_0 is the field amplitude, k is the wave vector and $w(z), R(z)$ and $\zeta(z)$ are the beam parameters. "ϵ" denotes the sign of topological charge or the order which is +1 for positive and -1 for negative.

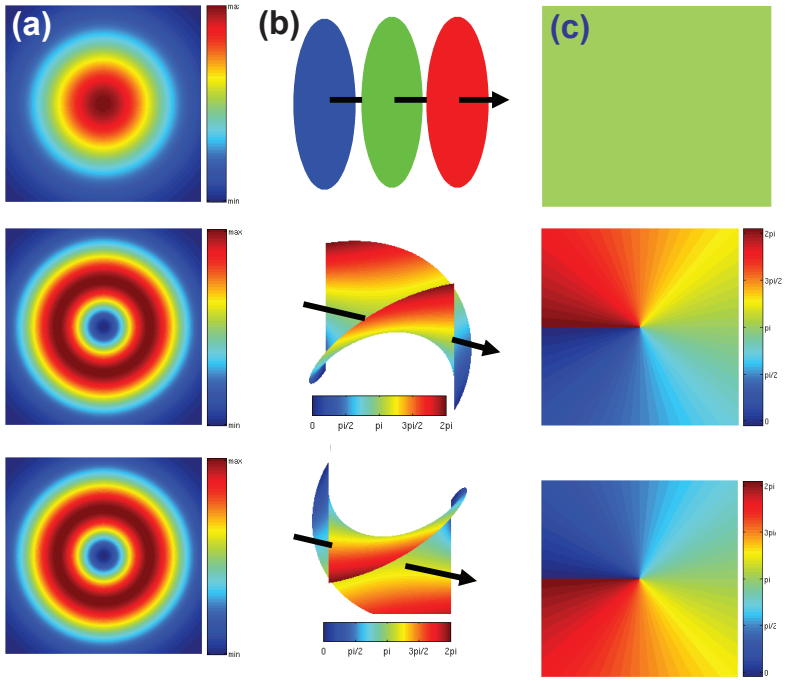

Figure 1.1: The intensity distribution (a), wavefront (b) and the phase (c) of a Gaussian beam (top) and the optical vortices of orders +1 (middle) and -1 (bottom).

The intensity distribution at a given plane, the wavefront and the phase of optical vortices of orders +1 and -1 have been shown in Figure 1.1 along with a Gaussian beam for a

comparison. The Poynting vector of these beams rotates around the center due to the presence of spiral phase distribution that causes an orbital angular momentum (OAM) of $m\hbar$ per photon [17]. This OAM can be used to impart torque to the particles in an optical tweezer set up [40] and, more recently, has served as a better quantity for encoding information in classical and quantum protocols [30–33].

Three of the most common methods for producing optical vortices in the lab are astigmatic mode converter, spiral phase plate and computer–generated holography. Astigmatic mode converter modifies the Hermite Gaussian (HG) modes with a rectangular symmetry to Laguerre Gaussian (LG) modes having circular symmetry [41, 42]. Spiral phase plates directly impose the vortex structure on an incident beam by linearly varying the optical path length around the circumference of the device [43–45]. Computer generated holograms (CGHs) are created by mathematically interfering an oblique plane wave with an optical vortex. The vortices can be obtained by diffracting a plane wave through the CGH [46]. The detailed description of these three techniques is given below.

1.1.1 Astigmatic mode converter

An astigmatic mode converter is formed by a pair of cylindrical lenses which have the same focal length (f) and mounted parallel to each other [41]. This set up is analogous to the birefringent wave plate with zero fast axis orientation that modulates the polarization components according to the optic axis. The separation between the two lenses decides the induced phase difference between two orthogonal Hermite–Gaussian modes. If the separation is $\sqrt{2}f$ ($2f$) then the phase difference is $\frac{\pi}{2}$ (π) analogous to quarter (half) wave plate. Therefore it is also called as $\frac{\pi}{2}$ (π) converter.

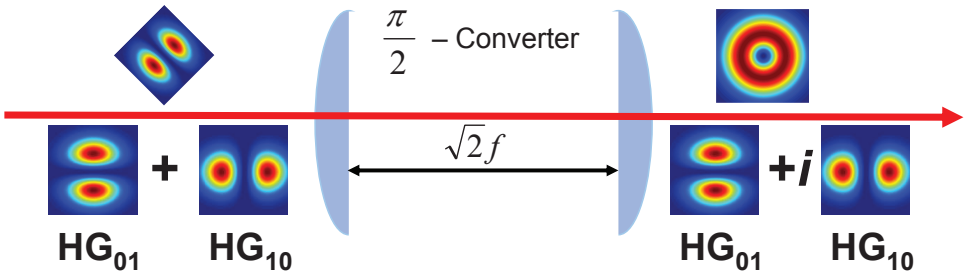

Figure 1.2: The schematic of the input and output spatial modes of an astigmatic mode converter consisting of two cylindrical lenses with a given separation.

In order to transform HG mode to LG mode and vice versa, one should use $\frac{\pi}{2}$ con-

verter. The schematic of astigmatic mode converter is shown in Figure 1.2 in which an input $HG_0^1|_{@45^o}$ mode, superposition of HG_0^1 and HG_1^0 modes which are parallel and perpendicular to the cylindrical lens respectively, converts into LG_0^1 mode. Later on the same mode converter was realized using a cylindrical lens and a mirror [47]. This is the folded version of a basic astigmatic mode converter and by controlling the distance between the lens and the mirror, one can change the induced phase difference between orthogonal HG modes. The astigmatic mode converter changes the rectangular symmetry to circular and vice versa. The polarization controlled OAM CNOT gate and the spatial mode sorter were also implemented using a single lens $\frac{\pi}{2}$ converter [47, 48].

1.1.2 Spiral phase plate or vortex lens

Spiral phase plate (SPP) or vortex lens (VL) is a kind of mode converter that imparts a spiral phase directly to a coherent light beam. SPP has a thickness which varies circumferentially around the center of plate, but is uniform radially [44]. The plate is made of a dielectric material which is transparent. Hence a beam with fundamental Gaussian mode passing

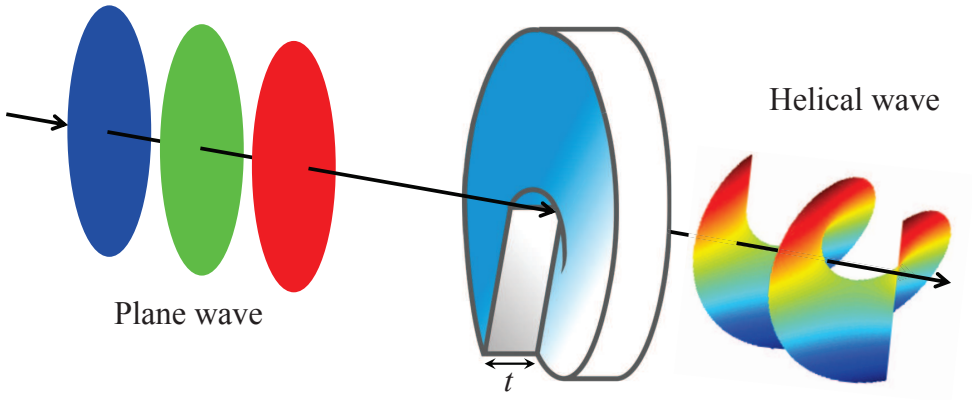

Figure 1.3: Changing the planar wavefronts to helical wavefronts using a spiral phase plate.

though the SPP experiences a spiral element to its phase front. This can be achieved either by changing the thickness around the center or by changing the optical path which is possible with the spatial variation of refractive index.

The schematic and the process of conversion have been shown in Figure 1.3. In order to be effective, SPP must be smooth and accurately shaped to a fraction of wavelength. The conversion efficiency of a SPP to convert a Gaussian beam to a vortex beam is very high and it can be used even with high power lasers. The SPP is generally designed for single

wavelength of light and one topological charge. However, adjustable spiral phase plates work for multi–wavelength and multi–order purpose [49]. The SPP can be realized easily at higher wavelengths which has a significant contribution in wireless communication using radio wave (mm-wave) vortices [21, 50].

1.1.3 Computer generated holography

An object can be generated by illuminating a coherent light beam on a digitally generated hologram. In general, hologram is an interference pattern of an object with a reference [51–54]. To generate the vortex beams, one needs to interfere the spiral function $e^{im\theta}$, m being the order, with planar wavefront e^{ikx}, k being the spatial period. This interference pattern can be obtained through a computer program and looks like a fork. By printing these fork patterns on a transparent sheet using a high quality printer and illuminating the branch point with a laser beam, the required vortex beam of both positive and negative orders can be generated in the first diffraction orders with central order as the host Gaussian beam.

The electric field distribution of an optical vortex (object) of order m embedded in a host Gaussian beam of width w is given by

$$E_o = (x+iy)^m \, e^{-\left(x^2+y^2\right)/w^2} e^{-ik\left(x^2+y^2\right)/2R} e^{-i(kz+\theta)} \tag{1.2}$$

where R is the radius of curvature and θ is the Guoy phase shift. For the sake of simplicity, all the field amplitudes have been considered as unity. In cylindrical coordinate system, the above equation reduces to

$$E_o = r^m e^{\pm im\theta} e^{-r^2/w^2} e^{-ikr^2/2R} e^{-i(kz+\phi)}. \tag{1.3}$$

The electric field distribution for a plane reference beam is

$$E_r = e^{-i(k_x x + k_z z)}. \tag{1.4}$$

The intensity for the interference pattern of m^{th} order optical vortex E_o (say at beam waist, $R \longrightarrow \infty$) with the reference beam E_r at $z = 0$ is given by

$$I = |e^{-ik_x x} + e^{\pm im\theta} e^{-r^2/w^2}|^2. \tag{1.5}$$

By setting w as unity and ignoring all amplitude variations in the above equation, we get the spatially varying transmission function as

$$T = 2\left[1 + \cos\left(k_x x + m\theta\right)\right]. \tag{1.6}$$

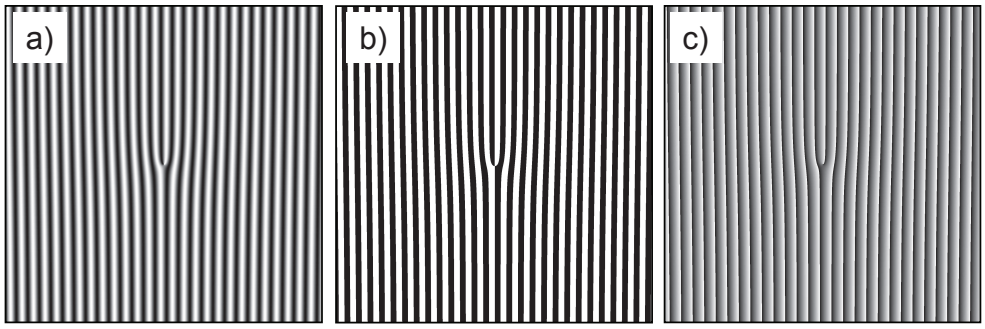

Figure 1.4: The computer generated holograms with sinusoidal (a), binary (b) and blazed (c) transmission functions for making an optical vortex of order +1.

This amplitude transmission function is a fork like grating with sinusoidal [46] optical density as shown in Figure 1.4(a). This is an amplitude hologram which modulates the amplitude of the incident beam. One can make other types of holograms such as binary [55] and blazed [56] holograms whose transmission functions are given by

$$T_{binary} = sign\left[2\left(1+\cos\left(k_x x + m\theta\right)\right)\right] \tag{1.7}$$

$$T_{blazed} = \frac{1}{2\pi} Mod\left(k_x x + m\theta, 2\pi\right). \tag{1.8}$$

where $sign[x] = x/|x|$ and $Mod(\alpha, \beta)$ is the remainder on division of α by β. The binary and blazed holograms for generating an optical vortex of order +1 are shown in Figures 1.4 (b) and (c) respectively. One can also use phase only holograms for the better diffraction efficiency which changes the phase according to the given interference pattern without affecting the amplitude.

By printing these fork patterns on a transparent sheet using a high quality printer and illuminating the branch point with a laser or reference beam, one can obtain the vortex beams.

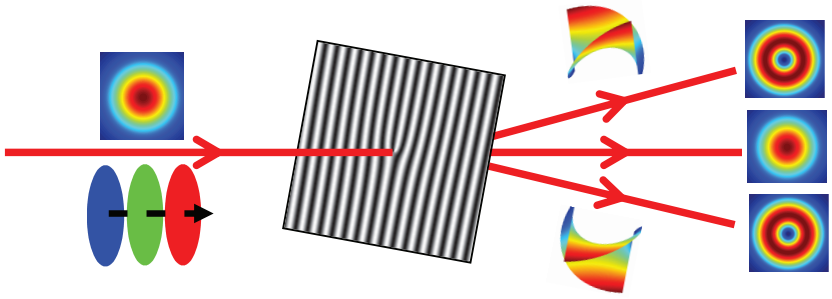

Figure 1.5: The schematic for the generation of optical vortices by passing a Gaussian beam through a branch point of the hologram.

However, one can also transfer these patterns to the liquid crystal based device, spatial light modulator [57, 58], using a computer interface. The schematic for the generation of optical vortices with the use of printed holograms is shown in Figure 1.5. The higher order (order of 100 or above) optical vortices can be generated using special kind of holograms called kinoforms [59].

The interference patterns are used not only for the generation of optical vortices but also for their detection. The interference patterns of a Gaussian beam and optical vortices of orders +1 or -1 with planar (linear fringes) and spherical (spiral fringes) wavefronts have been shown in Figure 1.6. The difference in number of fringes below and above the singu-

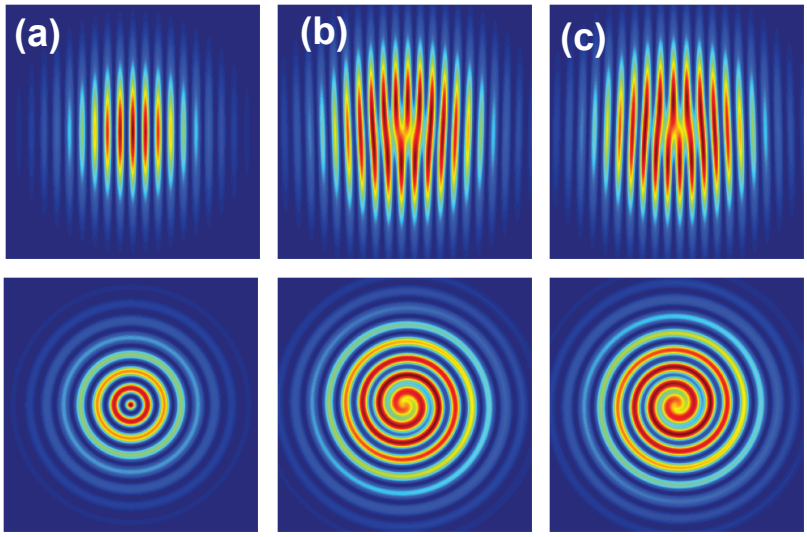

Figure 1.6: The interference patterns of a Gaussian beam (left) and the vortex beams of order +1 (middle) and −1 (right) with planar (top) and spherical (bottom) wavefront.

larity of the fork or the number of spirals indicates the order of vortex beam. There are many other techniques to measure the charge of an optical vortex [60–67] such as applying Fourier transform to its intensity distribution [63], passing it through a tilted lens [60], and a triangular aperture [67].

Optical vortices also exist naturally in speckles [68–71] formed by the scattering of coherent light beams through a rough surface or a ground glass plate (GGP). The number of dark spots present in the speckles are actually first order optical vortices. The probability of getting positive and negative charge optical vortices of order one is same that makes the sum of all the vortex charges is zero when a Gaussian beam scatters through a rough surface [68]. These optical vortices are anisotropic in nature i.e. the azimuthal phase varies non-linearly around the position of singularity. It is also interesting to study the properties of speckles

generated by the scattering of phase singular beams as the scattered beam itself contains the phase singularity.

1.2 Speckle phenomena

The speckles are fine-scale granular structures formed when a coherent light beam reflects or passes through a rough surface [72, 73]. This random intensity distribution is due to the interference of many scattered or reflected wavefronts from randomly distributed microscopic inhomogeneities of the rough surface at the detection plane. We know that the fringe width in an interference pattern is directly proportional to the wavelength and the distance from the source to detection plane. In the same vein, since the speckles are due to the interference, their size is directly proportional to the wavelength and the propagation distance i.e. the

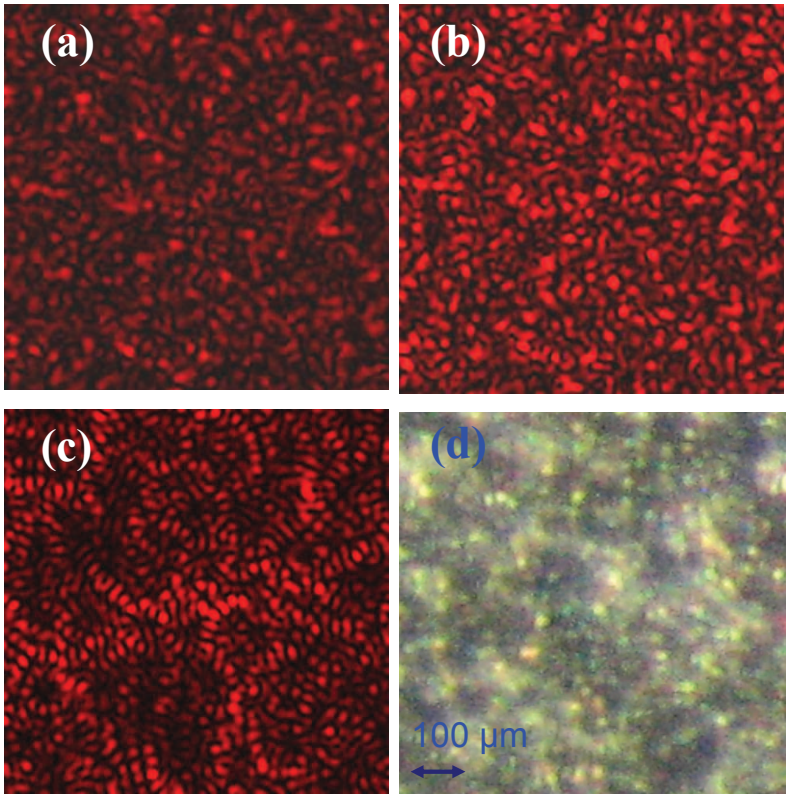

Figure 1.7: The speckle patterns generated by the scattering of a Gaussian (a), optical vortex (b) and perfect optical vortex of order +1 (c) through the ground glass plate (d).

distance between the rough surface and the detection plane. The speckle size is inversely proportional to the square root of the area of illumination. The size of speckles is also

inversely proportional to the size of the inhomogeneities which plays an equivalent role of slit width. The contrast of speckles depends on temporal and spatial coherence of the incident beam which is equal to one for a perfectly coherent beam and zero for a perfectly incoherent beam. The speckles generated by the scattering of a Gaussian beam, an optical vortex and a perfect vortex of order +1 have been shown in Figures 1.7(a), 1.7(b), and 1.7(c) respectively. For generating these speckles, we use a ground glass plate as scatterer whose microscopic image has been shown in Figure 1.7(d).

The speckles play an important role in many technological and scientific applications ranging from the rough surface characterization to stellar speckle interferometry [73–82]. The scattering of light through a disordered media can be used to focus it below the Rayleigh diffraction limit which has been verified experimentally [76]. However, the characterization of speckles generated by the scattering of different spatial modes such as optical vortices has not been studied in detail. In this thesis, we characterize the size and divergence of the speckles generated by optical vortices and their variation with the order. We also study the scattering of perfect optical vortices, whose core size is independent of the order.

1.3 Scattering of optical vortices

The scattering of optical vortices is important in many applications starting from astrophysics to communication. The angular velocity of a rotating object cannot be determined using the linear Doppler shift, however, the rotation of a spinning object induces a frequency shift to the light beam that is proportional to the OAM of a light beam. By measuring this frequency shift (of the order of kHz) due to the scattering of higher order optical vortices with large OAM a small change in the rotation can be measured [83, 84]. Recently, Tamburini et al. showed through a numerical calculations that a rotating black hole emits the radiation containing a spectrum of OAM. It was suggested that a black hole can be observed by detecting this structured light using proper telescopes. However, it is not easy to determine the OAM spectrum because of their scattering effects over a long distance [22, 85]. It has been shown that the intensity correlations of scattered optical vortices can be used to measure the spectrum of OAM [86] which may have implications in detecting the OAM of light coming from the black hole. The scattering of two optical vortices with different orders can also be used to generate coherence vortices, singularities in a cross-correlation function. The order of this singularity is equal to the difference between the two individual topological charges [11, 87].

Recently, the decay of temporal intensity correlation of scattered optical vortices with increase in the order was studied and verified experimentally [88, 89]. Although, the vortices are observed to be robust against the diffraction through a circular aperture, their robustness has not been tested against scattering through random media which finds many applications in the optical transfer of information [90]. This thesis addresses the issue of recovering vorticity of an optical vortex after scattering. We verify the vorticity of a scattered optical vortex using a non-separable state of polarization and OAM.

1.4 Perfect optical vortices

It is well known that optical vortex beams have helical wavefronts due to which they transfer the OAM to dielectric particles in the trapping process. This OAM can also be used for many classical and quantum information protocols. Several techniques for generating the optical vortex beams have been reported during last decade, but all of them exhibit a strong dependence of the vortex radius on the topological charge, making it difficult to obtain a high spatial accuracy and a high orbital angular momentum simultaneously. Recently, a new type of optical vortex, called perfect optical vortex [91], whose radius is independent of topological charge and whose intensity gradient takes an extremely large value was introduced to overcome this limitation. The field distribution of a perfect optical vortex of order m is written as

$$E(\rho, \theta) = \delta(\rho - \rho_0) e^{im\theta} \tag{1.9}$$

where ρ is a transverse coordinate and θ is the azimuthal phase.

The presence of a delta function makes the field to be present along the perimeter of a circle i.e. a circular ring. However, the ideal POV beams cannot be realized in the lab. For their realization, we need to introduce a small and finite width of the ring (say $\Delta\rho$) which makes the delta function as an exponential function. Therefore the field distribution of a POV of order m, ring radius ρ_0, and ring width $\Delta\rho$ becomes [92]

$$E(\rho, \theta) = e^{-\frac{(\rho-\rho_0)^2}{\Delta\rho^2}} e^{im\theta} \tag{1.10}$$

where $\Delta\rho << \rho_0$.

The POV beams can be generated using a number of techniques [93–95]. However, one can simply realize them using the Fourier transform of the Bessel-Gauss beams [94]. The BG beams can be produced using a computer generated hologram obtained by the superposition of axicon ($e^{ia\rho}$) and a spiral ($e^{im\theta}$) functions. The sinusoidal and the blazed axicon holograms

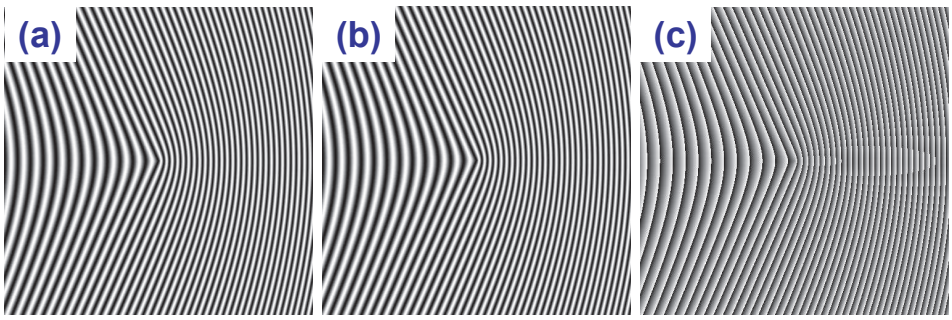

Figure 1.8: The axicon holograms with a (a) sinusoidal, (b) binary and (c) blazed transmission functions. This hologram is used to generate the Bessel–Gauss beams.

to generate the BG beams have been shown in Figure 1.8. By embedding the vortex phase structure into the hologram, one can generate the higher order BG beams. The ring width of a POV beam is inversely proportional to the width of the Gaussian beam falling on the hologram and the ring radius is directly proportional to the axicon parameter. The theoretical intensity distributions of the POV beams of orders 0, 10, 20, 30 at different axicon parameters have been shown in Figure 1.9.

In this thesis, we use the order independent intensity distribution to verify a physical process if the speckle distribution depends on the field mode or the intensity distribution. We also generate the random non-diffracting structured patterns using the speckles produced by the scattering of a POV beam.

1.5 Objective of the thesis

Optical vortices have been used for communication both in classical and quantum domains. Therefore, to study the robustness of optical vortices after scattering through a scattering media and their propagtaion characteristics through different optical systems is very important. In this thesis, we study the intensity distribution of optical vortices and their propagation through free space as well as an astigmatic optical system. We also study the properties of speckles generated by the scattering of optical vortices and confirm the vorticity of scattered optical vortices. Finally, we study the scattering of perfect optical vortices, whose core size is independent of the order, through a ground glass plate. The results are compared with the one obtained for regular optical vortices.

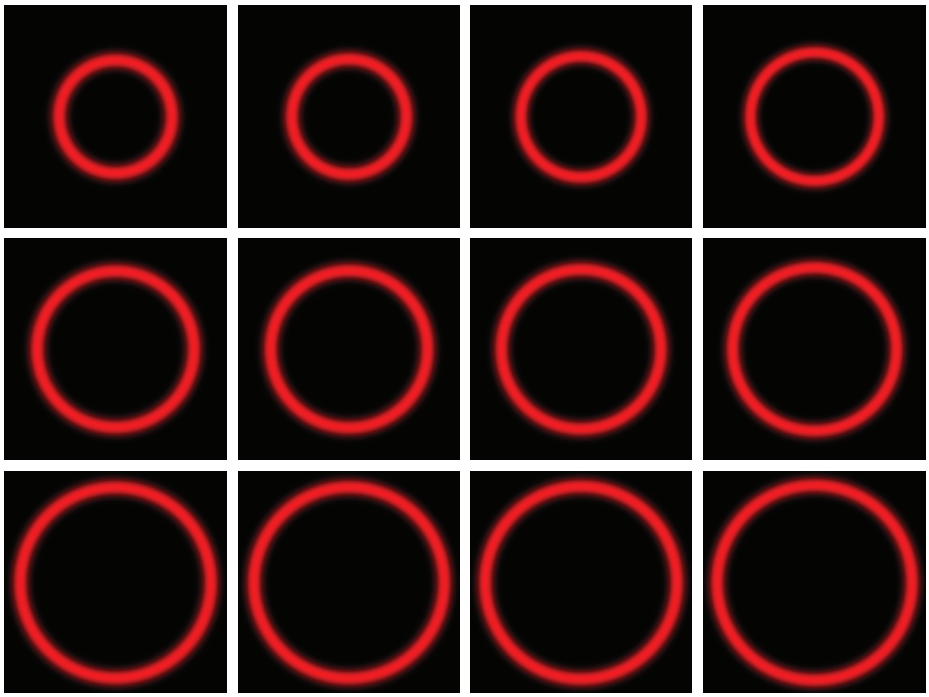

Figure 1.9: Theoretically obtained intensity distributions of the POV beams of orders 0, 10, 20, 30 (from left to right) and at axicon parameters of 10, 13, 16 /mm (from top to bottom).

1.6 Overview of the thesis

Chapter 1 gives the basic introduction towards optical vortices, scattering of light beams and perfect optical vortices. In chapter 2, the spatial intensity profile of optical vortices has been studied using two novel and measurable parameters, inner and outer radii along with their propagation through free space. We show that the propagation characteristics depend only on width of the host Gaussian beam and its intensity profile at the source plane. We also study the variation of divergence of vortex beams with their order. Chapter 3, contains the propagation characteristics of a pair of optical vortices embedded in a host Gaussian beam through an astigmatic optical system - a tilted lens. The propagation dynamics is explained by a closed-form analytical expression and used the intensity distribution at a predicted position past the lens to determine the charges present in the beam.

In chapter 4, We study the scattering of higher order optical vortices through a ground glass plate that results in the formation of speckles. Intensity autocorrelation measurements of speckles show that their size decreases with increase in the order of vortex. We relate

these results with the area of annular bright ring present in the vortex beams. In chapter 5, We experimentally generate the ring-shaped beams by collecting the scattered light of LG and BG beams. We also study the dependence of ring-shaped beams on the speed of rotating ground glass (RGG) plate and the width of incident light beam. We theoretically verify the results using the propagation of partially coherent standard or elegant LG beams. In chapter 6, we show that the scattered light passing through a lens has the same vorticity when probed at the Fourier plane. The vorticity is measured using a non-separable state of polarization and orbital angular momentum of light. The observed vorticity is found to be independent of the amount/direction of scattered light collected which will enhance the use of optical vortices in public communication systems.

In chapter 7, we generate perfect optical vortices (POV), whose intensity distribution is independent of the order, using Fourier transform of Bessel–Gauss (BG) beams and scatter them through a rough surface. We show that the size of produced speckles is independent of the order and their Fourier transform provides the random non-diffracting fields. The size of speckles can be easily controlled by changing the axicon parameter, used to generate the BG beams. Finally, we conclude in chapter 8.

Chapter 2

Propagation Dynamics of Optical Vortex Beams

Optical vortices or phase singular beams are well known due to their orbital angular momentum (OAM) [14–17]. This OAM can be used as an information carrier which enhances the bandwidth as its modes have an infinite dimensional orthonormal basis [19]. It has been shown that communication is possible with radio wave vortices [20] and demonstrated experimentally for wireless communication [21]. To use different OAM states for information processing, one should have both multiplexing and de-multiplexing setups for these modes and the same has been made with the use of fibers specially designed for OAM modes [23–26]. For implementing these protocols with vortices, one should design fibers that support OAM modes in which case one should know the intensity distribution of these OAM modes as well as their divergence. The structure and divergence of Laguerre–Gauss beams were theoretically studied [96, 97]. However, the parameters used for description cannot be measured in lab.

In this chapter, we discuss about the spatial intensity profile of vortices using two novel and measurable parameters (the inner and outer radii) in section 2.1. We study the propagation of vortices in terms of inner and outer radii experimentally as well as theoretically in section 2.2. The divergence of vortices and its variation with the order have been discussed in section 2.3. Finally, we conclude in section 2.4.

2.1 Inner and Outer radii of an optical vortex beam

The field distribution of an optical vortex beam of order m, embedded in a Gaussian host beam of width w_0, is

$$E_m(x,y) = (x+iy)^m \exp\left(-\frac{x^2+y^2}{w_0^2}\right) \tag{2.1}$$

and its intensity

$$I_m(r) = r^{2m} \exp\left(-\frac{2r^2}{w_0^2}\right), \qquad r^2 = x^2+y^2. \tag{2.2}$$

This intensity distribution is shown in Figure 2.1. Here, we are defining two parameters for a vortex beam: inner and outer radii (r_1, r_2).

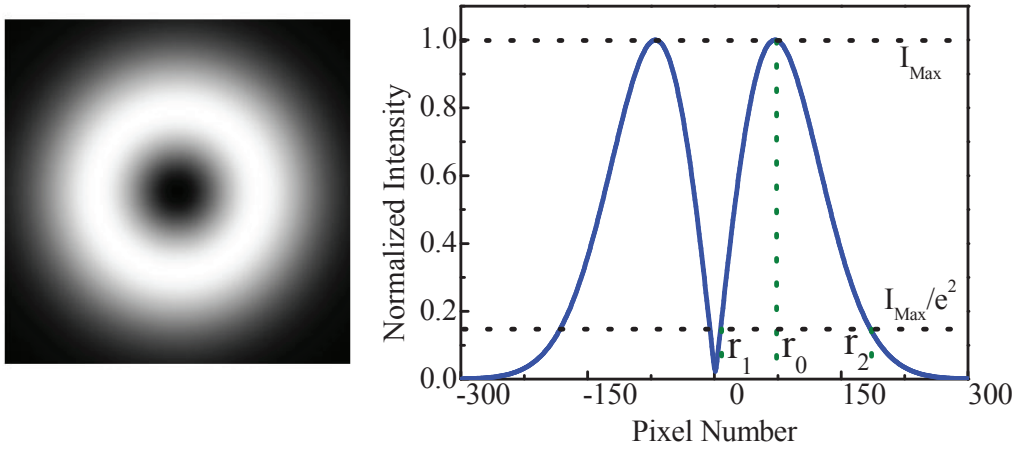

Figure 2.1: The transverse intensity profile of an optical vortex of order 1 and its line profile.

These are the radial distances at which the intensity falls to $1/e^2(13.6\%)$ of the maximum intensity at $r = r_0$ (say). Here, r_1 is the point closer to the origin or the center and r_2 is the point farther from the center. The distances r_i $(i = 0, 1, 2)$ can be obtained as follows. For the sake of convenience, we set $w_0 = 1$, that is, w_0 is the unit of measuring radial distances. We also define $\chi = r^2$ and $\chi_i = r_i^2$ $(i = 0, 1, 2)$ so that $I_m(r) = J_m(\chi) = \chi^m \exp(-2\chi)$. Differentiating $J_m(\chi)$ with respect to χ, one easily obtains $\chi_0 = m/2$ so that the maximum intensity has the value $J_m(\chi_0) = \chi_0^m \exp(-2\chi_0)$. The equations for χ_1 and χ_2 can then be written as

$$\chi_1^m \exp(-2\chi_1) = \chi_0^m \exp(-2\chi_0 - 2), \tag{2.3a}$$

$$\chi_2^m \exp(-2\chi_2) = \chi_0^m \exp(-2\chi_0 - 2). \tag{2.3b}$$

These equations cannot be solved analytically as they are transcendental. We solve these equations numerically for $m > 0$. The numerical values are tabulated in Table 2.1 and plotted in Fig. 2.2.

Remarkably, it is found that to a very good approximation (verified up to the order 200),

$$\chi_2 + \chi_1 = m + 1.3. \tag{2.4}$$

m	χ_1	χ_2	$\chi_2 + \chi_1$
1	0.0262	2.2526	2.2789
2	0.1586	3.1462	3.3048
3	0.3602	3.9538	4.3140
4	0.6034	4.7154	5.3188
5	0.8748	5.4469	6.3216
6	1.1667	6.1569	7.3236
7	1.4746	6.8504	8.3250
8	1.7951	7.5309	9.3260
9	2.1262	8.2006	10.3268
10	2.4662	8.8613	11.3274
11	2.8138	9.5142	12.3280
12	3.1680	10.1605	13.3284
...	.....	.....	.....
20	6.1682	15.1622	21.3304
50	18.5793	32.7529	51.3321
100	40.6553	60.6775	101.3330
200	86.5165	114.8165	201.3330

Table 2.1: Numerical solutions for Eqs. 2.3a and 2.3b

This empirical relationship can now be used to obtain simple expressions for χ_1 and χ_2. Multiplying the left sides of Eqs. 2.3a and 2.3b, using Eq. 2.4 and the formula $(\chi_2 + \chi_1)^2 - (\chi_2 - \chi_1)^2 = 4\chi_1\chi_2$, we get

$$\chi_2 - \chi_1 = \sqrt{q_m}, \qquad q_m = (m + 1.3)^2 - m^2 \exp(-1.4/m). \tag{2.5}$$

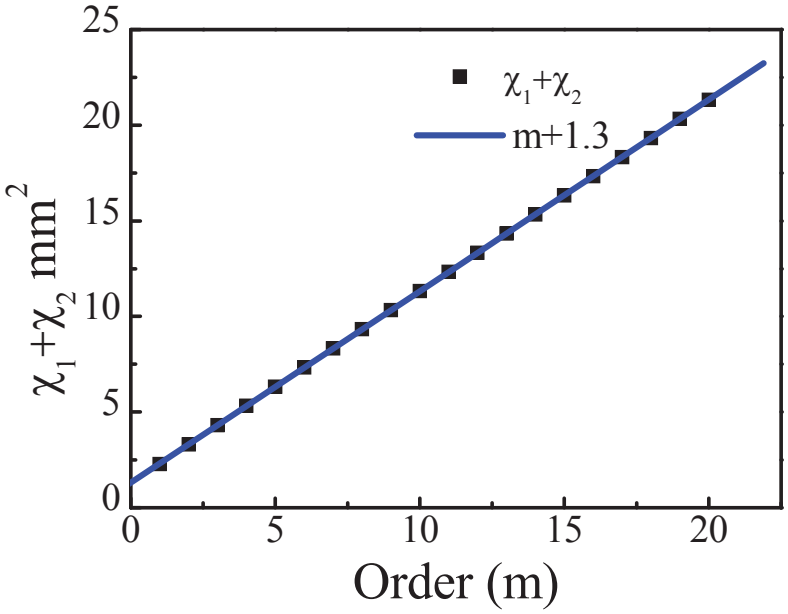

Figure 2.2: Numerically obtained values of $\chi_2 + \chi_1$ (filled squares) and the line $y = m + 1.3$ as functions of m.

Solving Eqs. 2.4 and 2.5, we get χ_1, χ_2 and hence, r_1, r_2:

$$r_1(0) = (m + 1.3 - \sqrt{q_m})^{1/2}/\sqrt{2}, \tag{2.6a}$$

$$r_2(0) = (m + 1.3 + \sqrt{q_m})^{1/2}/\sqrt{2}. \tag{2.6b}$$

'0' represents the source plane at which vortices being generated i.e. zero propagation distance z. Now, the area of the bright region in an optical vortex is given by

$$A_m = \pi(\chi_2 - \chi_1) = \pi\sqrt{q_m} \tag{2.7}$$

which clearly depends on the order (m) of the vortex (see Eq. 2.5). These results can also be used for the geometrical characterization of coherent optical vortices.

We verify experimentally the dependence of the area of the annular bright ring of optical vortices on their orders. For this, we use an intensity stabilised He-Ne laser to generate optical vortex beams using computer generated holography technique. We introduce holograms corresponding to the vortices of different orders to the spatial light modulator (SLM) (Holoeye LCR-2500). We then allow the Gaussian laser beam to be incident normally on the SLM at the branch points of the hologram which gives the vortex beam in the first diffraction order [98, 99]. The vortices of different orders from 1 to 5 have been recorded at closest point at which first diffraction order is separated from the central order and also at different propagation distances starting from 52 cm to 107 cm in steps of 5 cm using an Evolution VF

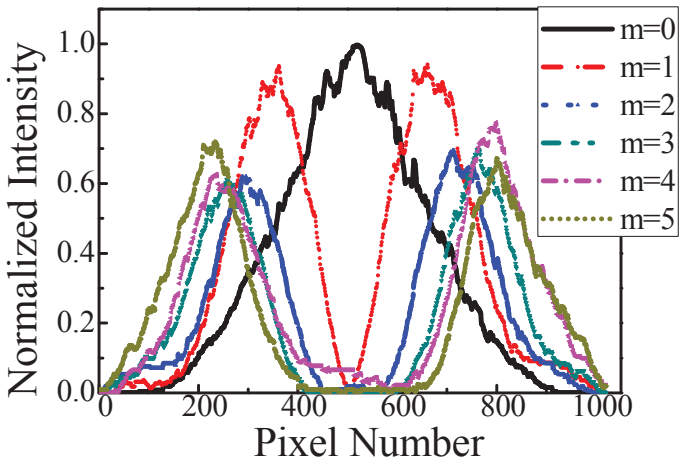

Figure 2.3: Line profiles along the vortex centres of optical vortices for orders 0 to 5 that are produced in the laboratory.

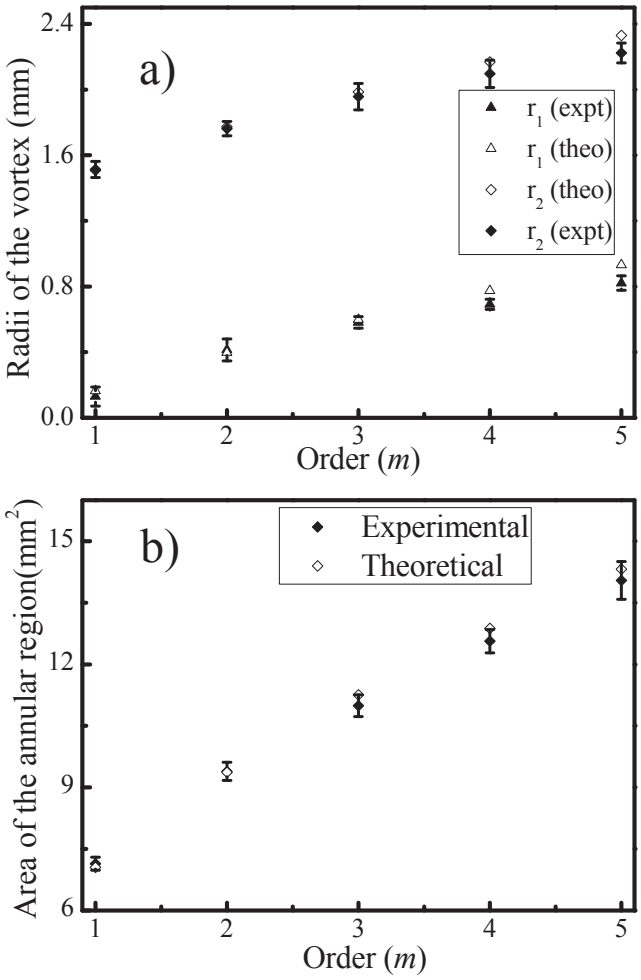

Figure 2.4: Experimental and theoretical results showing the variation of (a) inner and outer radii and (b) area of bright annular region with the order of a vortex.

color cooled CCD camera of pixel size 4.65 μm. We have recorded 20 images for a given order and at a given propagation distance. These images have been further processed to determine the inner and outer radii.

Figure 2.3 shows the line profiles of optical vortices for orders $m = 0$ to 5 produced in the laboratory using computer generated holography technique. We have determined inner and outer radii of the vortex beams from the corresponding line profiles (Fig. 2.3). The variation of inner and outer radii for vortex beams and the area of the annular bright ring with the order are shown in Fig. 2.4. The experimental findings are in good agreement with the theoretical values (obtained from Eqs. 2.6 and 2.7) and prove that area of the annular bright ring increases in proportion to the order.

The small misalignment of the experimental set up being used to generate the optical vortices leads to systematic error that increases with the order. This is because of the small shift in the center of the vortex beam. To avoid this error, we have considered eight different line profiles and determined the corresponding inner and outer radii. The average over eight different line profiles has been considered as actual value and their standard deviation as error.

2.2 Free space propagation of vortex beams

The variation of inner and outer radii with propagation can be studied by propagating the vortex beam through free space. The field distribution of a vortex beam after propagating through a linear ABCD optical system is [88, 89]

$$E_m(u,v) = \left(\frac{ikw_1^2}{2B}\right)^{m+1} (u+iv)^m \exp\left(-\frac{u^2+v^2}{w_2^2}\right) \tag{2.8}$$

where

$$\frac{1}{w_1^2} = \frac{1}{w_0^2} + \frac{ikA}{2B}, \tag{2.9a}$$

$$\frac{1}{w_2^2} = \left(\frac{w_1 k}{2B}\right)^2 + \frac{ikD}{2B}. \tag{2.9b}$$

The corresponding intensity distribution is

$$I_m(u,v) = \alpha_m r^{2m} \exp\left(\frac{-2r^2}{\beta^2}\right) \tag{2.10}$$

where

$$\alpha_m = \frac{k^2 w_1^2 w_1^{*2}}{4B^2}, \qquad r^2 = u^2+v^2, \frac{2}{\beta^2} = \frac{1}{w_2^2} + \frac{1}{w_2^{*2}}. \tag{2.11}$$

Here, α_m is a constant multiplicative factor and will not change the intensity pattern.

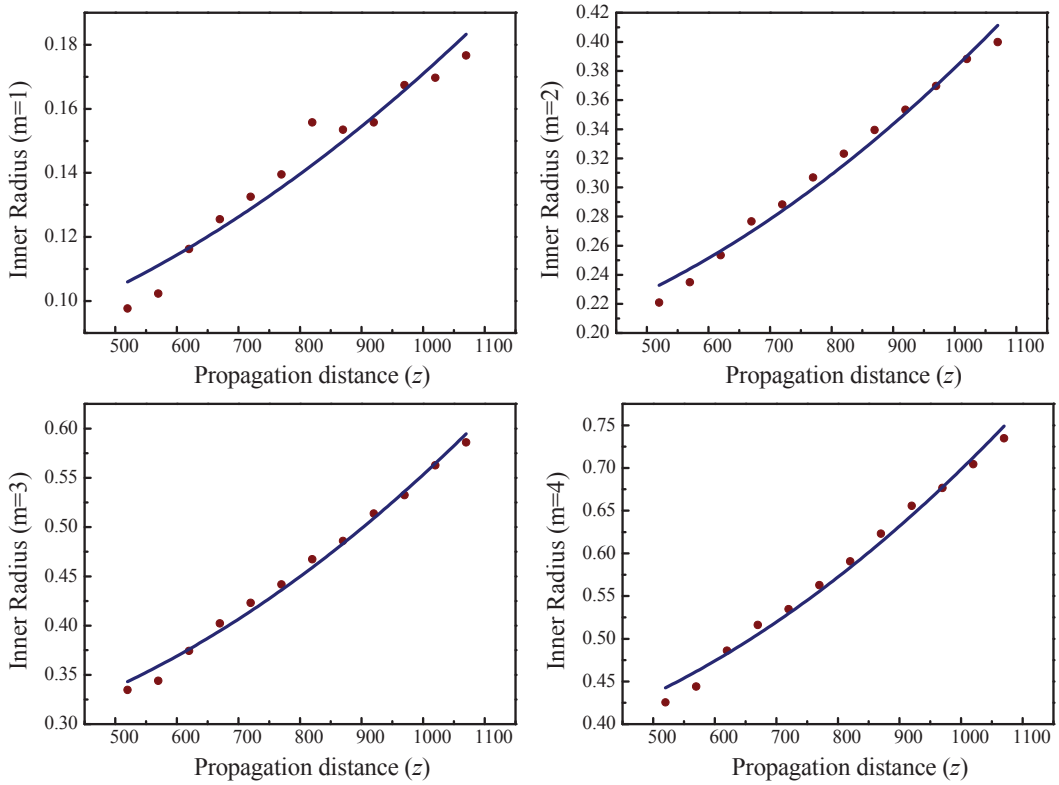

Figure 2.5: The inner radius for vortices of orders $m = 1$ to 4 at different distances.

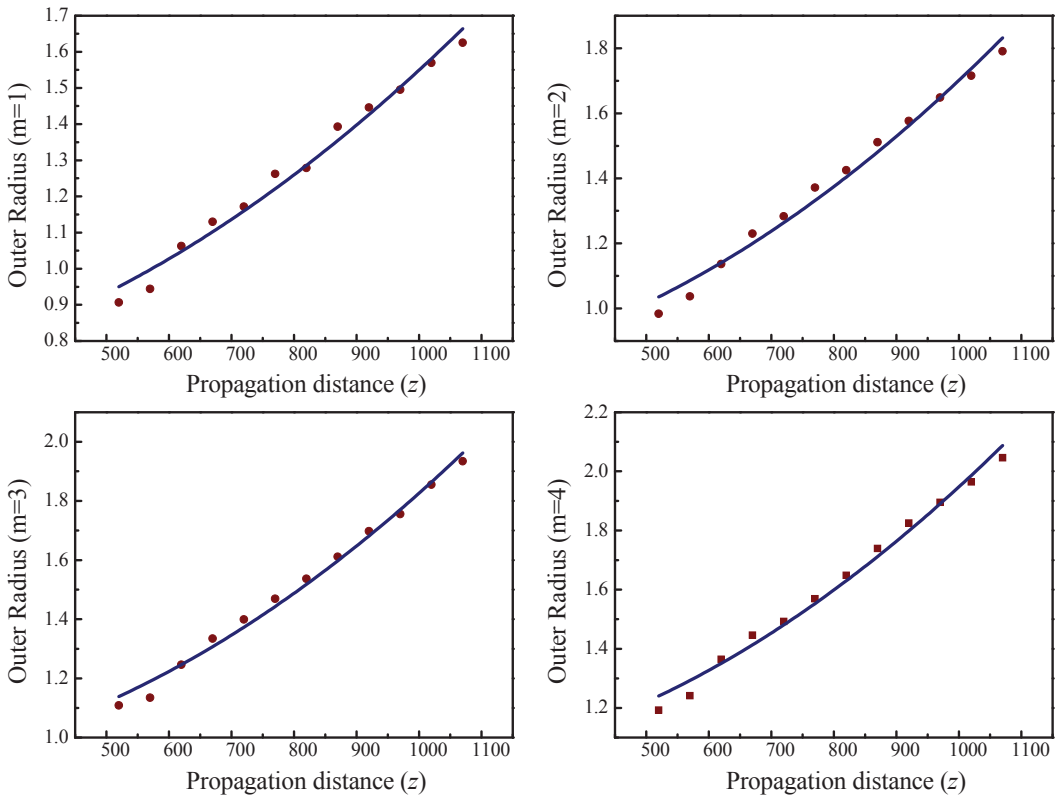

Figure 2.6: The outer radius for vortices of orders $m = 1$ to 4 at different distances.

Defining $\rho = r/\beta$, the above equation can be written as

$$F_m = \frac{I_m}{\alpha_m \beta^{2m}} = \rho^{2m} \exp(-2\rho^2). \tag{2.12}$$

This equation is similar to Eq. 2.2 and have the solutions ρ_1 and ρ_2 which are the same as that of $r_1(0)$ and $r_2(0)$ of Eq. 2.6. Now the inner and outer radii of the vortex beam at a particular propagation distance are given by $\rho_1 = r_1(z) = \beta r_1(0)$ and $\rho_2 = r_2(z) = \beta r_2(0)$ where $r_1(0)$ and $r_2(0)$ are the inner and outer radii at $z = 0$ as expressed in Eq. 2.6.

The expression for β is

$$\frac{2}{\beta^2} = \frac{1}{w_2^2} + \frac{1}{w_2^{*2}} \longrightarrow \beta = w_0 A \left(1 + \frac{4B^2}{k^2 A^2 w_0^4}\right)^{1/2}. \tag{2.13}$$

For free space propagation ($A = 1$ and $B = z$), the above equation becomes

$$\beta = w_0 \left(1 + \frac{4z^2}{k^2 w_0^4}\right)^{1/2} = w_0 \left(1 + \frac{z^2}{z_R^2}\right)^{1/2} = w(z) \tag{2.14}$$

where $z_R = \pi w_0^2/\lambda$ is the Rayleigh range and $w(z)$ is the width of host Gaussian beam at distance z. Now, the inner and outer radii as a function of z can be written as

$$r_1(z) = w(z) r_1(0), \qquad r_2(z) = w(z) r_2(0). \tag{2.15}$$

This relation shows that the defined parameters can describe the vortex beams in a simpler manner as their propagation is similar to the host Gaussian beam.

Figures 2.5 and 2.6 show the variation of inner and outer radii with propagation distance for the optical vortex beams of orders $m = 1$ to 4. Red dots represent the experimental data points and the blue solid lines represent the fitting with Eq. 2.15. From these figures, it is clear that the experimental results are in excellent agreement with the theoretical predictions. The slope of these curves at $z >> z_R$ has been considered as the divergence i.e. the rate of change of inner and outer radii. The experimental results are obtained by taking the average over 20 images and the error bars are too small to be visible in the plot. The width of host Gaussian beam used to fit the experimental data is same for all the curves.

2.3 Divergence of the vortex beam

Now, the divergence of optical vortices has been defined as the rate of change of inner and outer radii r_i, $i = 1, 2$ with respect to the propagation distance z and is given by

$$d_m^i(z) = \frac{\partial r_i(z)}{\partial z} = \frac{w_o r_i(0)}{\left(z^2 + z_R^2\right)^{1/2}} \frac{z}{z_R}, \qquad i = 1, 2. \tag{2.16}$$

The divergence depends mainly on the corresponding radii at $z = 0$. At large z ($z >> z_R$), the divergence is constant and is given by

$$d_m^i = \frac{w_o r_i(0)}{z_R}. \tag{2.17}$$

These results are same for vortex beams generated either by using mode converter or diffrac-

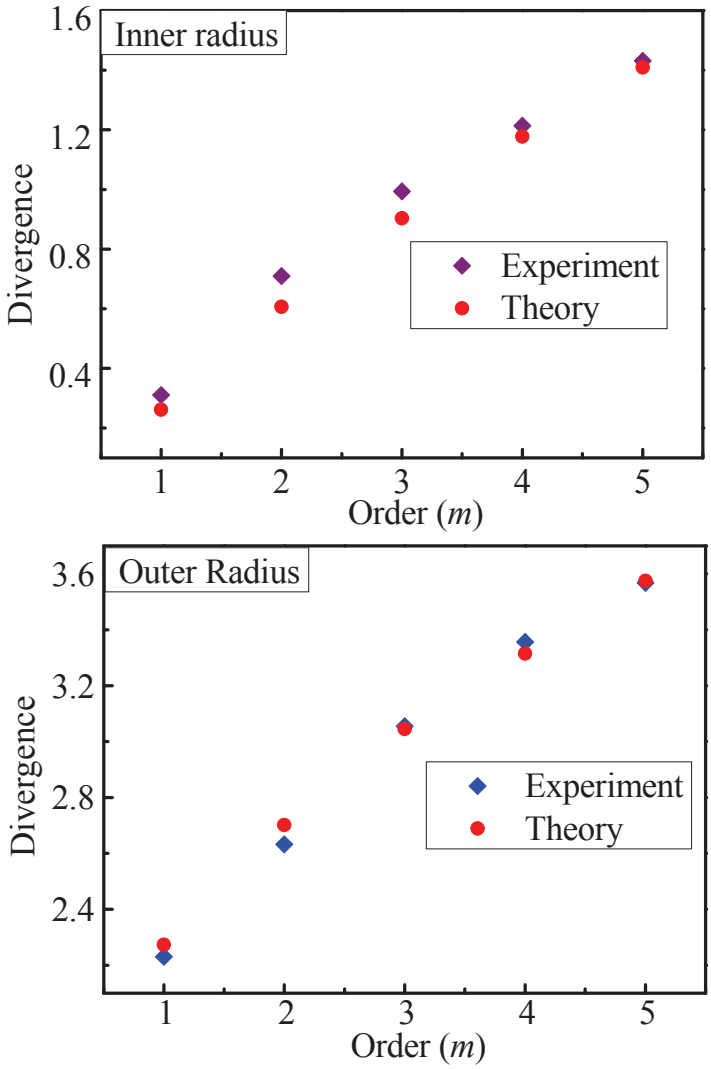

Figure 2.7: The divergence i.e. the rate of change of inner (top) and outer (bottom) radii with the order of vortex beams obtained experimentally (blue diamonds) as well as theoretically (red dots).

tive optical elements since we consider only the intensity distribution and its propagation which is similar to the host Gaussian beam [97].

Figure 2.7 shows the variation of divergence with order of the vortex. The rates of change of inner and outer radii are directly proportional to their value at $z = 0$. The blue diamonds

represent experimentally obtained divergence and the red dots represent the corresponding results obtained from Eq. 2.17. The variation of divergence with order for the inner and outer radii are same as the variation of corresponding radius with order at $z = 0$ as is clear from Eq. 2.17.

2.4 Conclusion

We have described the intensity distribution of optical vortices by using two novel and measurable parameters, the inner and outer radii. The propagation dynamics of vortices can be easily described by its intensity distribution at the source plane and the width of the host Gaussian beam at the plane of observation. We have also studied the rate of change of inner and outer radii, divergence, and their variation with the order. The experimental results are well supported by the analytical results.

Chapter 3

Pair of Vortices through an Astigmatic Optical System

It is known that the two optical vortices interact with each other if they are embedded in a single host Gaussian beam. The relative separation between the two vortices is invariant with the free space propagation if the two vortices are of same sign. If both the vortices are having opposite signs, they will annihilate with each other provided they are of same magnitude otherwise form a single vortex of a charge equal to the difference between the two individual charges [100–106]. The optical beams with a pair of vortices can be generated using a computer generated holography technique [100]. The background phase function at a point where two dipoles annihilate, has a continuous potential which causes the annihilation [103]. The same background phase function is also used to accelerate the annihilation process [104].

In this chapter, we consider a pair of vortices with arbitrary topological charges embedded in a Gaussian beam and study its evolution through an astigmatic optical system, a tilted lens. Section 3.1 starts with the theory for propagation of a pair of vortices through an astigmatic optical system. Section 3.2 describes the experimental set up used to generate a pair of vortices as well as its propagation through a tilted lens. Section 3.3 contains the experimental results for various conditions of the input beam as well as theoretical predictions. Finally we will conclude the chapter with section 3.4.

3.1 Theory

Consider a pair of optical vortices embedded in a Gaussian beam, one with topological charge $\epsilon_1 m$ ($\epsilon_1 = \pm 1$) located at $x_1 = -x_0$, $y_1 = 0$ and another with topological charge $\epsilon_2 n$ ($\epsilon_2 = \pm 1$) at $x_1 = x_0$, $y_1 = 0$. The complex field distribution of the vortex pair at the waist plane of the host Gaussian beam, with waist size w_0, is given by

$$E_1(x_1, y_1) = (x_1 + x_0 + i\epsilon_1 y_1)^m (x_1 - x_0 + i\epsilon_2 y_1)^n \times \exp\left[-\left(\frac{x_1^2 + y_1^2}{w_0^2}\right)\right]. \tag{3.1}$$

The tilted lens is placed at a distance z_0 from the waist plane. The vortex passes through the lens and travels a further distance z. The overall ray transfer matrix $\mathbf{M_{tot}}$ is given by [39, 60]

$$\mathbf{M_{tot}} = \begin{pmatrix} \mathbf{A} & \mathbf{B} \\ -\mathbf{C}/f & \mathbf{D} \end{pmatrix} \tag{3.2}$$

where $\mathbf{A}$, $\mathbf{B}$, $\mathbf{C}$ and $\mathbf{D}$ are 2×2 diagonal matrices with diagonal elements given by a_j, b_j, c_j and d_j respectively. Explicitly,

$$\begin{aligned} c_1 &= \sec\theta,\ c_2 = \cos\theta,\ a_j = 1 - zc_j/f, \\ d_j &= 1 - z_0 c_j/f, \qquad b_j = z_0 + z d_j, j = 1, 2. \end{aligned} \tag{3.3}$$

Next, we define two column vectors $\mathbf{r_1}$, $\mathbf{r_2}$ so that their transposes are given by row vectors $\mathbf{r_i}^T = (x_i, y_i),\ i = 1, 2$. The field $E_2(x_2, y_2)$ at a distance z past the lens is given by the generalized Huygens-Fresnel integral [39]:

$$E_2(x_2, y_2) = \frac{i/\lambda}{|B|^{1/2}} \iint dx_1\, dy_1\, E_1(x_1, y_1) e^{-(i\pi/\lambda)\phi(\mathbf{r_1}, \mathbf{r_2})} \tag{3.4}$$

where $|B| = |b_1 b_2|$ is the determinant of $\mathbf{B}$ and

$$\begin{aligned} \phi(\mathbf{r_1}, \mathbf{r_2}) &= \mathbf{r_1}^T \mathbf{B}^{-1} \mathbf{A} \mathbf{r_1} + \mathbf{r_2}^T \mathbf{D} \mathbf{B}^{-1} \mathbf{r_2} - 2\mathbf{r_1}^T \mathbf{B}^{-1} \mathbf{r_2} \\ &= x_1^2 a_1/b_1 + y_1^2 a_2/b_2 + x_2^2 d_1/b_1 + y_2^2 d_2/b_2 - 2(x_1 x_2/b_1 + y_1 y_2/b_2). \end{aligned} \tag{3.5}$$

The integration over x_1 and y_1 are carried out by writing $E_1(x_1, y_1)$ as

$$E_1(x_1, y_1) = \lim_{\substack{t \to 0 \\ t' \to 0}} \left[\frac{\partial^m}{\partial t^m} \frac{\partial^n}{\partial t'^n} \exp\left\{f\left(t, t'\right)\right\}\right], \tag{3.6a}$$

$$f(t, t') = t(x_1 + x_0 + i\epsilon_1 y_1) + t'(x_1 - x_0 + i\epsilon_2 y_1) - \frac{x_1^2 + y_1^2}{w_0^2}. \tag{3.6b}$$

Using the definition of Hermite polynomial and a recurrence relation

$$H_n(x) = \frac{\partial^n}{\partial t^n} \exp(2xt - t^2)|_{t=0} \tag{3.7a}$$

$$\frac{d^j}{dx^j} H_n(x) = \frac{2^j n!}{(n-j)!} H_{n-j}(x), \tag{3.7b}$$

we finally get

$$E_2(x_2,y_2) = \frac{kw_1w_2(i/2)^{m+n+1}\gamma^{m+n}}{(b_1b_2)^{1/2}} \times \exp\left[-\left(\beta_1 x_2^2 + \beta_2 y_2^2\right)\right] F_{m,n}(x_2,y_2); \tag{3.8a}$$

$$F_{m,n}(x_2,y_2) = \sum_{j=0}^{\min(m,n)} \binom{m}{j}\binom{n}{j} \Delta^j j! H_{m-j}[f_1(x_2,y_2)] H_{n-j}[f_2(x_2,y_2)] \tag{3.8b}$$

where, $k = 2\pi/\lambda$,

$$\frac{1}{w_j^2} = \frac{1}{w_0^2} + i\frac{ka_j}{2b_j}, \tag{3.9a}$$

$$\gamma = (w_1^2 - w_2^2)^{1/2}, \tag{3.9b}$$

$$\Delta = -2(w_1^2 - w_2^2\epsilon_1\epsilon_2)/\gamma^2, \tag{3.9c}$$

$$\alpha_j = \frac{kw_j^2}{2b_j}, \tag{3.9d}$$

$$\beta_j = \left(\frac{kw_j}{2b_j}\right)^2 + i\frac{kd_j}{2b_j}, \tag{3.9e}$$

and

$$\begin{aligned}\begin{bmatrix} f_1(x_2,y_2) \\ f_2(x_2,y_2) \end{bmatrix} &= \frac{1}{\gamma}\begin{bmatrix} \alpha_1 x_2 + i(\epsilon_1\alpha_2 y_2 - x_0) \\ \alpha_1 x_2 + i(\epsilon_2\alpha_2 y_2 + x_0) \end{bmatrix} \\ &= \frac{1}{\gamma}\begin{bmatrix} \phi_1(x_2,y_2) \\ \phi_2(x_2,y_2) \end{bmatrix}\end{aligned} \tag{3.10}$$

Eqs. 3.8-3.10 form one of our main results. It generalizes previous work [106] on the propagation dynamics of a vortex pair through an astigmatic system. In that the topological charges m and n need not be the same and can have arbitrary integer values.

Before proceeding further, we note that the above general result includes the following special cases:

(1) For $m = n$, we get the propagation dynamics of (a) an isopolar vortex pair if $\epsilon_1\epsilon_2 = 1$ and (b) a vortex dipole if $\epsilon_1\epsilon_2 = -1$;

(2) For $n = 0$, the j-sum reduces to the $j = 0$ term only, and we get the propagation dynamics for an off-center single vortex given by

$$E_2(x_2,y_2) = \frac{kw_1w_2(i/2)^{m+1}}{(b_1b_2)^{1/2}} \exp\left[-\left(\beta_1 x_2^2 + \beta_2 y_2^2\right)\right] \times \gamma^m H_m[(\alpha_1 x_2 + i\epsilon_1\alpha_2 y_2 - ix_0)/\gamma]; \tag{3.11}$$

(3) Setting $x_0 = 0$ in the above result, one immediately recovers our previous result [60] for a single vortex at the origin.

The sum $F_{m,n}$ can be evaluated formally as follows. We introduce the 2-variable Hermite-Kampé de Fériet polynomials $H_n(x,y)$ as [107]

$$H_n(x,y) = n! \sum_{r=0}^{[n/2]} \frac{x^{n-2r}y^r}{(n-2r)!r!} \tag{3.12}$$

in terms of which the classical Hermite polynomials $H_n(x)$ are given by

$$H_n(x) = H_n(2x, -1). \tag{3.13}$$

Next, we consider the 4-variable 2-index 1-parameter Hermite polynomials $H_{m,n}(x, z; y, w|\tau)$ defined as [107–109]

$$H_{m,n}(x, z; y, w|\tau) = \sum_{s=0}^{\min(m,n)} \tau^s s! \binom{m}{s} \binom{n}{s} \times H_{m-s}(x, z) H_{n-s}(y, w). \tag{3.14}$$

It is then easy to show that

$$F_{m,n} = H_{m,n}(2f_1, -1; 2f_2, -1|\Delta) \tag{3.15}$$

which has the following generating function

$$\exp[-(u^2 + v^2) + 2(f_1 u + f_2 v) + \Delta uv] = \sum_{m,n=0}^{\infty} \frac{u^m v^n}{m!n!} H_{m,n}(2f_1, -1; 2f_2, -1|\Delta) \tag{3.16}$$

3.1.1 Determination of net topological charge

As noted earlier [60], the modulations due to the Hermite polynomial become most prominent when $w_2 = w_1^*$. This happens at a certain value $z = z_c$, say critical plane. To determine z_c and *also* the distance z_0 between the waist plane and the lens, we impose the following conditions:

$$\frac{ka_1}{2b_1}|_{z=z_c} = -\frac{ka_2}{2b_2}|_{z=z_c} = \frac{1}{w_0^2} \tag{3.17}$$

Solving Eq. 3.17 and introducing the Rayleigh range $z_R = kw_0^2/2$, we get

$$\begin{aligned} z_0 &= z_R \left(1 + \frac{2f\cos\theta}{z_R \sin^2\theta}\right)^{1/2} \\ z_c &= \frac{z_R(1 + \cos^2\theta) + z_0 \sin^2\theta}{2(z_R/f)\cos\theta - \sin^2\theta} \end{aligned} \tag{3.18}$$

The first equality in Eq. 3.18 ensures that $w_2 = w_1^*$ at $z = z_c$ (see Eq. 3.9a) whereas the last equality makes many expressions appearing in Eqs. 3.8-3.10 considerably simpler at $z = z_c$. Thus, at $z = z_c$,

$$\begin{aligned} \Delta &= \begin{cases} -2 & \text{if } \epsilon_1\epsilon_2 = 1, \\ -2i & \text{if } \epsilon_1\epsilon_2 = -1; \end{cases} \\ \begin{pmatrix} w_1^2 \\ w_2^2 \end{pmatrix} &= \frac{w_0^2}{\sqrt{2}} \begin{pmatrix} \exp(-i\pi/4) \\ \exp(i\pi/4) \end{pmatrix}; \\ \gamma &= w_0 \exp(-i\pi/4); \\ f_1 &= \delta_1 x_2 - \epsilon_1\delta_2 y_2 + (x_0/w_0)\exp(-i\pi/4) \\ f_2 &= \delta_1 x_2 - \epsilon_2\delta_2 y_2 - (x_0/w_0)\exp(-i\pi/4) \end{aligned} \tag{3.19}$$

where

$$\delta_j = \frac{kw_0}{2\sqrt{2}b_i} \tag{3.20}$$

3.1.1.1 Vortices with topological charges of the same sign

Suppose $\epsilon_1 = \epsilon_2 = 1$. Then, $f_1 = \theta_- + \theta_0$ and $f_2 = \theta_- - \theta_0$ where,

$$\begin{aligned} \theta_- &= \delta_1 x_2 - \delta_2 y_2 \\ \theta_0 &= (x_0/w_0)\exp(-i\pi/4). \end{aligned} \tag{3.21}$$

Note that the dependence on x_2 and y_2 is in the form θ_- only.

For a small separation between the vortices, one can expand the Hermite polynomials appearing in Eq. 3.8 as functions of x_0/w_0 by using the formula

$$H_n(x+y) = H_n(x) + 2nyH_{n-1}(x) + O(y^2). \tag{3.22}$$

Substituting in Eq. 3.8 and using the summation rule [109]

$$\sum_{r=0}^{\min(m,n)} (-2)^r r! \binom{m}{r} \binom{n}{r} H_{m-r}(x) H_{n-r}(x) = H_{m+n}(x), \tag{3.23}$$

we get

$$F_{m,n} = H_{m+n}(\theta_-) + 2\theta_0(m-n)H_{m+n-1}(\theta_-) + O(\theta_0^2). \tag{3.24}$$

For $\epsilon_1 = \epsilon_2 = -1$, θ_- will change to $\theta_+ = \delta_1 x_2 + \delta_2 y_2$ in the above expressions.

3.1.1.2 Vortices with topological charges of opposite signs

Suppose $\epsilon_1 = 1$, $\epsilon_2 = -1$. In this case,

$$\begin{aligned} f_1 &= \theta_- + \theta_0 \\ f_2 &= \theta_+ - \theta_0. \end{aligned} \tag{3.25}$$

Note that in this case, the dependence on x_2 and y_2 is in the form $\theta_\pm = \delta_1 x_2 \pm \delta_2 y_2$.

For a small separation between the vortices, we can proceed as in the previous section, to get

$$\begin{aligned} F_{m,n} &= H_{m,n}(2\theta_-, -1; 2\theta_+, -1| -2i) + 2m\theta_0 H_{m-1,n}(2\theta_-, -1; 2\theta_+, -1| -2i) \\ &\quad -2n\theta_0 H_{m,n-1}(2\theta_-, -1; 2\theta_+, -1| -2i) + O(\theta_0^2). \end{aligned} \tag{3.26}$$

This equation can be used describe the propagation of a pair of vortices with opposite signs and embedded in a Gaussian beam.

3.1.2 Propagation dynamics away from the critical plane ($z > z_c$)

As $|z - z_c|$ increases, the absolute value of $|\gamma|$ falls off rapidly and the modulations due to the Hermite polynomials fade away quickly. Using the limiting form $\lim_{\gamma\to 0} H_m(x/\gamma) = (2x/\gamma)^m$, we can write $E_2(x_2, y_2)$ in terms of incomplete two-variable Hermite polynomials $h_{m,n}(x, y|\tau)$, which are defined as [107, 110]

$$\begin{aligned} h_{m,n}(x,y|\tau) &= m!n! \sum_{j=0}^{\min(m,n)} \frac{\tau^j x^{m-j} y^{n-j}}{j!(m-j)!(n-j)!} \\ &= \begin{cases} m!\tau^m x^{n-m} L_m^{(n-m)}(-xy/\tau), & n > m, \\ n!\tau^n y^{m-n} L_n^{(m-n)}(-xy/\tau), & m > n. \end{cases} \end{aligned} \tag{3.27}$$

Thus $E_2(x_2, y_2)$ reduces to

$$\begin{aligned} E_2(x_2,y_2) &= \frac{kw_1w_2 i^{m+n+1}}{2(b_1b_2)^{1/2}} \exp\left[-\left(\beta_1 x_2^2 + \beta_2 y_2^2\right)\right] \\ &\times \begin{cases} m!\tau^m \phi_1^{n-m} L_m^{(n-m)}(-\phi_1\phi_2/\tau), & n > m, \\ n!\tau^n \phi_2^{m-n} L_n^{(m-n)}(-\phi_1\phi_2/\tau), & m > n. \end{cases} \end{aligned} \tag{3.28}$$

where ϕ_j are defined in Eq. 3.10 and $\tau = -(w_1^2 - w_2^2\epsilon_1\epsilon_2)/2$. To the best of our knowledge, this is the first time one encounters with these polynomials in experimental optics.

3.1.3 Propagation dynamics when the lens is not tilted

For $\theta = 0$, the j-dependence of the parameters in Eq. 3.3 and Eq. 3.9a disappear. Thus,

$$\begin{aligned} c_j &= 1,\ a_j = a = 1 - z/f, \\ d_j &= d = 1 - z_0/f,\ b_j = b = z_0 + zd, \\ \frac{1}{w_j^2} &= \frac{1}{w^2} = \frac{1}{w_0^2} + i\frac{ka}{2b}, \\ \alpha_j &= \alpha = \frac{kw^2}{2b}, \beta_j = \beta = \left(\frac{kw}{2b}\right)^2 + i\frac{kd}{2b}, \\ \Delta &= -2w^2(1 - \epsilon_1\epsilon_2)/\gamma^2, \text{and} \qquad \gamma \to 0. \end{aligned} \tag{3.29}$$

First, we take the limit $\gamma \to 0$ as in the previous section and use the definitions in Eq. 3.29 to get

$$E_2(x_2,y_2) = \frac{ikw^2}{2b} \exp[-\beta(x_2^2 + y_2^2)] \times \sum_{j=0}^{\min(m,n)} \binom{m}{j} \binom{n}{j} \Gamma^j j! \Delta_1^{m-j} \Delta_2^{n-j} \tag{3.30}$$

where

$$\begin{aligned}\Delta_1 &= x_0 + \frac{ikw^2}{2b}(x_2 + i\epsilon_1 y_2)\\ \Delta_2 &= -x_0 + \frac{ikw^2}{2b}(x_2 + i\epsilon_2 y_2)\\ \Gamma &= \frac{w^2}{2}(1 - \epsilon_1\epsilon_2).\end{aligned} \tag{3.31}$$

For isopolar vortices ($\epsilon_1\epsilon_2 = 1$), only the $j = 0$ term survives in Eq. 3.30, and we get

$$E_2(x_2, y_2) = \frac{ikw^2}{2b}\exp[-\beta(x_2^2 + y_2^2)]\Delta_1^m\Delta_2^n. \tag{3.32}$$

For dipolar vortices ($\epsilon_1\epsilon_2 = -1$), we use Eq. 3.27 to get

$$\begin{aligned}E_2(x_2, y_2) &= \frac{ikw^2}{2b}\exp[-\beta(x_2^2 + y_2^2)]\\ &\times \begin{cases} m!w^{2m}\Delta_1^{n-m}L_m^{(n-m)}(-\Delta_1\Delta_2/w^2), & n > m,\\ n!w^{2n}\Delta_2^{m-n}L_n^{(m-n)}(-\Delta_1\Delta_2/w^2), & m > n.\end{cases}\end{aligned} \tag{3.33}$$

We present the experimental observations that validate our theoretical predictions in the following sections.

3.2 Experimental set-up

The experimental set up is shown in Figure 3.1. Suitable phase masks for creating vortex pairs are produced by using computer generated holography (CGH) technique [46] and sent to a spatial light modulator (SLM) (Holoeye LCR 2500) via a computer. The SLM is illuminated by an intensity stabilized He-Ne laser (Spectra-Physics, Model 117A) of power 1 mW and wavelength 632.8 nm to produce the desired vortex pair. The vortex pair is selected with an aperture (A) and passed through a spherical bi-convex lens of focal length 50 cm which is tilted by an angle 6°.

The tilting of the lens has been done with a rotational stage with least count of 0.1°. The aperture is at a distance $z_1 = 90$ cm in front of the SLM. We use the method described in [111], to find that the Gaussian laser beam hosting the selected vortex pair has a beam waist 0.186 mm at a virtual point which is at a distance of $z_2 = 60.8$ cm *behind* the SLM. The distance between the lens and the aperture is $z_3 = 245$ cm. Thus the total distance traveled by the vortex pair from the waist plane to the lens is $z_0 = z_1 + z_2 + z_3 = 395.8$ cm. The resultant intensity patterns are recorded by a CCD camera (MediaCybernetics, Evolution VF cooled Color Camera) placed at a distance z past the lens.

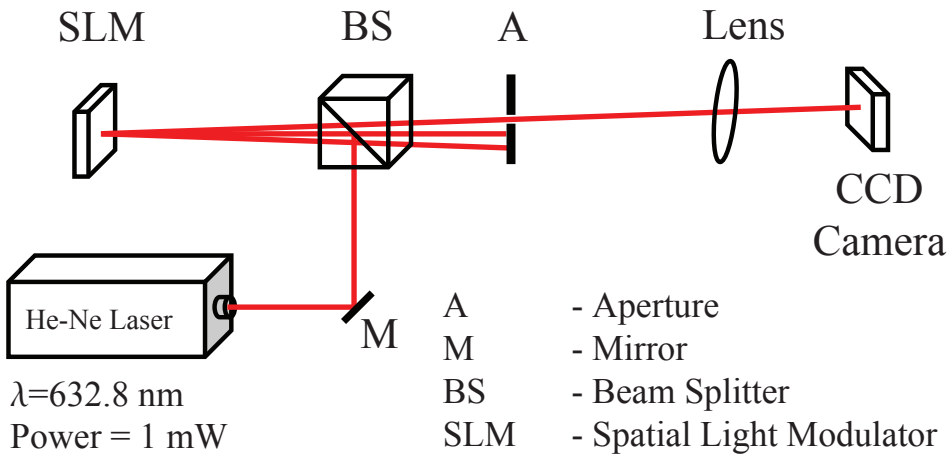

Figure 3.1: Experimental set-up for the determination of the net charge of an arbitrary vortex pair embedded in a Gaussian beam.

We start the experiment by taking the intensity distributions of a pair of isopolar vortices and the corresponding interference patterns at two planes as shown in Figure 3.2. One of the planes is at 96 cm from the SLM, the nearest plane where the diffraction orders can be separated with an aperture and another after freely propagating a distance 147 cm from the SLM. In our experiments where intensity distributions have been recorded after the tilted lens, the aberrations due to the SLM have been neglected as they will be insignificant compared to the astigmatism introduced by the lens.

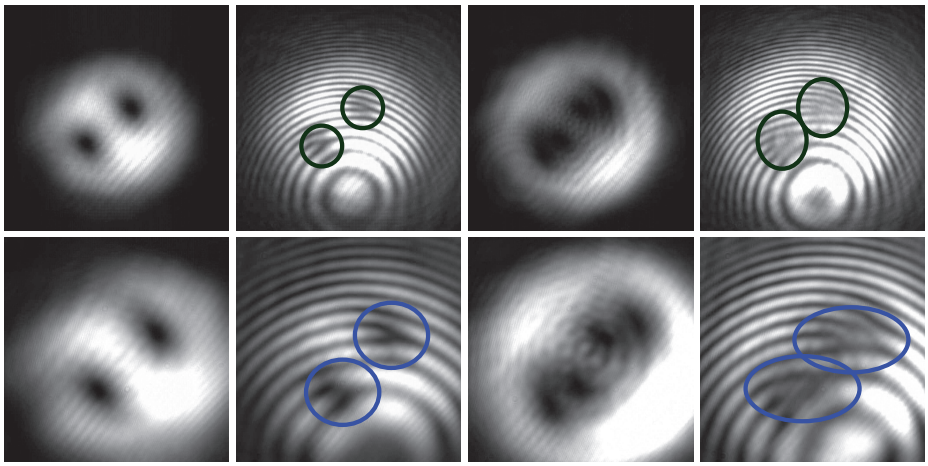

Figure 3.2: The intensity distributions of a vortex pair embedded in a Gaussian beam and the corresponding interferograms at 96 cm (left) and 147 cm (right) from the SLM with the orders (top) m=n=1; (bottom) m=n=2.

3.3 Experimental results

In this section, we determine the net topological charge of the vortex pair from its intensity distribution at $z = z_c$. The predicted value of z_c from Eq. **??** is 57.2 cm which is close to the experimentally observed value of 56.3 cm. In the intensity patterns, with reference to Eq. 3.1, the vortex on the left ($x_1 = -x_0$) has a charge $\epsilon_1 m$ and the vortex on the right ($x_1 = x_0$) has a charge $\epsilon_2 n$. The corresponding Figure is labelled as ($\epsilon_1 m$, $\epsilon_2 n$).

3.3.1 Intensity distribution at the critical plane ($z = z_c$)

Figure 3.3 shows the theoretical (first two rows) and experimental (last two rows) images for the intensity patterns of a pair of vortices with the same sign ($\epsilon_1 = \epsilon_2 = 1$) but different magnitudes m and n with the separation parameter set at $x_0 = 0.1w_0$.

For small separation x_0, these patterns can be explained by Eq. 3.24. Since the first term in Eq. 3.24 is the leading term, one can obtain the net charge $m + n$ by noting that there are $m + n + 1$ bright stripes in the intensity distribution. These stripes are parallel to one another and lie along a line that is neither horizontal nor vertical, but tilted in a clockwise direction almost along a diagonal as the dependence on x and y is through a single variable $\theta_- = \delta_1 x_2 - \delta_2 y_2$ and $\delta_1 \sim \delta_2$. However, interference with the second term will lead to a slightly asymmetric distribution of brightness among the stripes. As is clear from the second term in Eq. 3.24, this asymmetry depends on the difference between the magnitude of charges and the separation between them. Additionally, when the vortices swap their positions as in (4,1) and (1,4), the lower half of the pattern becomes the mirror image of the upper half and vice-versa. For $m = n$ as in (2,2), (3,3) and (4,4), the two halves have identical intensity patterns. In this special case, the net charge is even and the charge of each vortex is half of the net charge. If the charge of each vortex were negative ($\epsilon_1 = \epsilon_2 = -1$), then θ_- would be replaced by $\theta_+ = \delta_1 x_2 + \delta_2 y_2$ and the bright stripes would be tilted in an anti-clockwise fashion (not shown).

Figure 3.4 shows theoretical results corresponding to asymmetry of the intensity distributions (at $z = z_c$) with the separation between two vortices and the difference between their topological charges. This asymmetry increases with the separation provided there is a difference in their topological charges as shown in Figure (3.4) (top). These results are for m=4, n=1 at separations from $0.1w_0$ to $0.5w_0$. If there is no difference in the charges of the two vortices (m=n=2) then there is no asymmetry in lobes as shown in Figure 3.4 (bottom). The corresponding experimental results are given in Figure 3.5. A line profile of the intensity

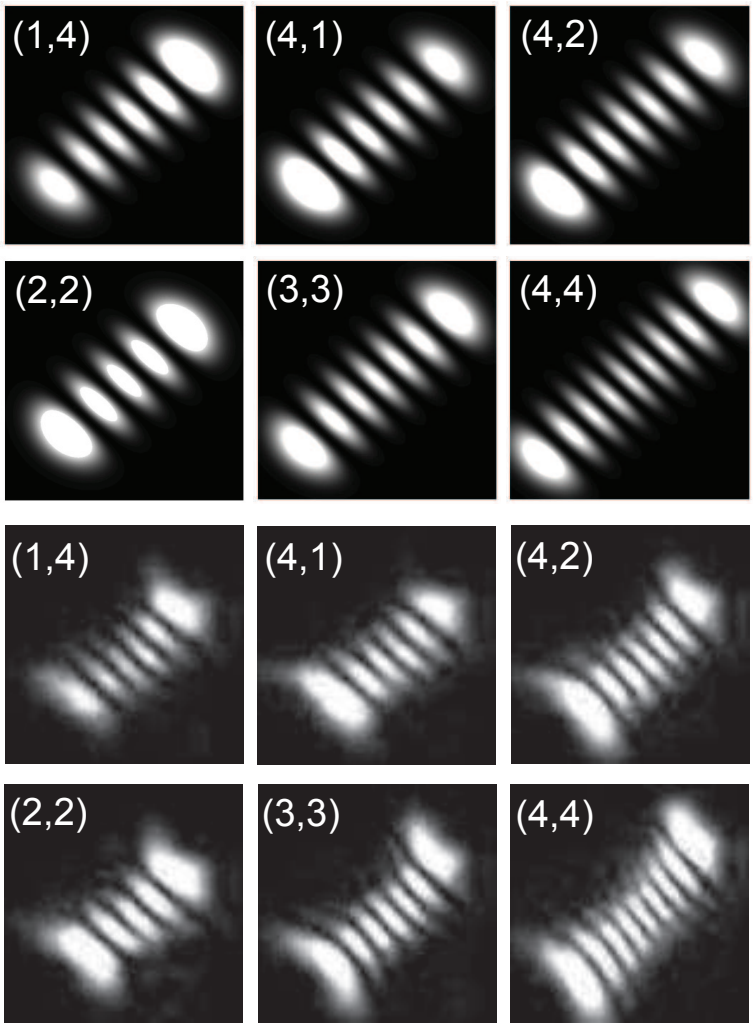

Figure 3.3: The theoretical (first two rows) and experimental (last two rows) results for the intensity patterns of a vortex pair with topological charges of the same sign, at $z = z_c$ for $x_0 = 0.1w_0$.

along the center of the lobes as shown in Figure 3.6 makes it more clear.

To investigate the effect of the separation parameter x_0, we have also studied the propagation of an off-axis vortex of charge 2 through the tilted lens. The corresponding theoretical (first two rows) and experimental (last two rows) results for the intensity patterns at $z = z_c$ are shown in Figure 3.7. From the images, it is clear that the intensity of one of the outer lobes increases as the vortex moves farther away from the center and the remaining lobes lose their intensity. In the notation of this section, this off-axis vortex can be labelled as (2,0) for $x_0 = |x_0|$. Consequently, when x_0 becomes negative, the vortex is identically described as (0,2) with $x_0 = |x_0|$ and the pattern flips diagonally. The situation is analogous to the case of (4,1) and (1,4) as described in the previous paragraph.

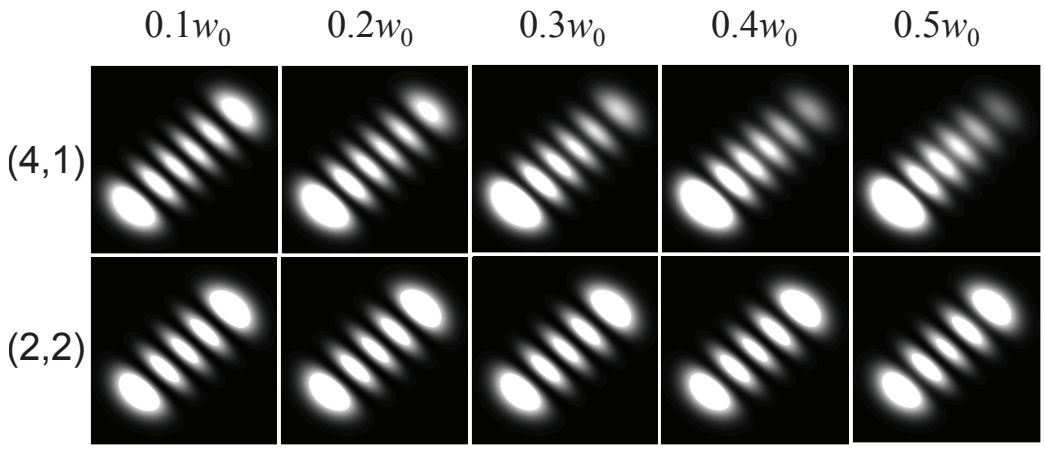

Figure 3.4: The theoretical results for the intensity patterns of a vortex pair with topological charges of the same sign with varying separation at $z = z_c$, (top) m=4, n=1; (bottom) m=n=2.

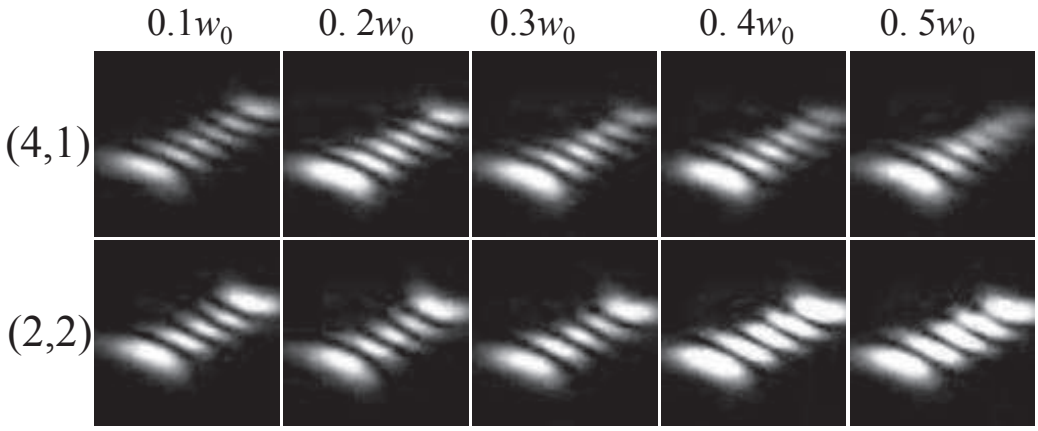

Figure 3.5: The experimental images corresponding to Figure 3.4.

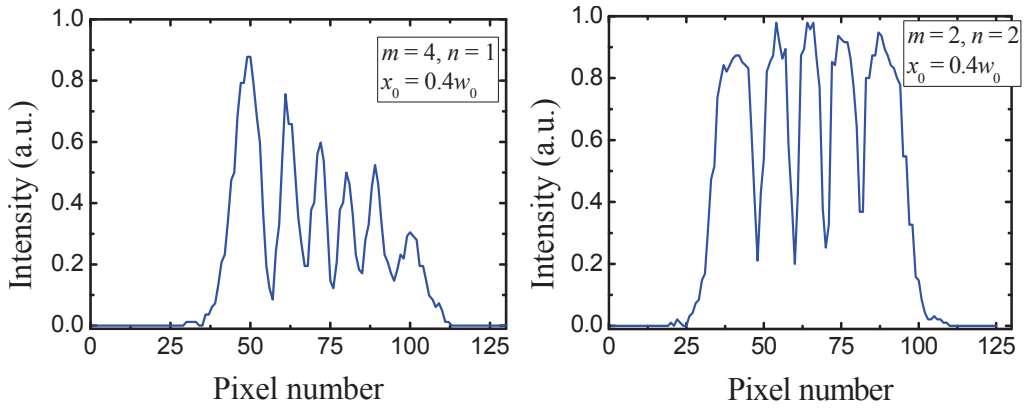

Figure 3.6: The line profiles of intensity distributions along the center of the lobes corresponding to Figure 3.5 at $x_0 = 0.4w_0$, (left) m=4, n=1; (right) m=n=2.

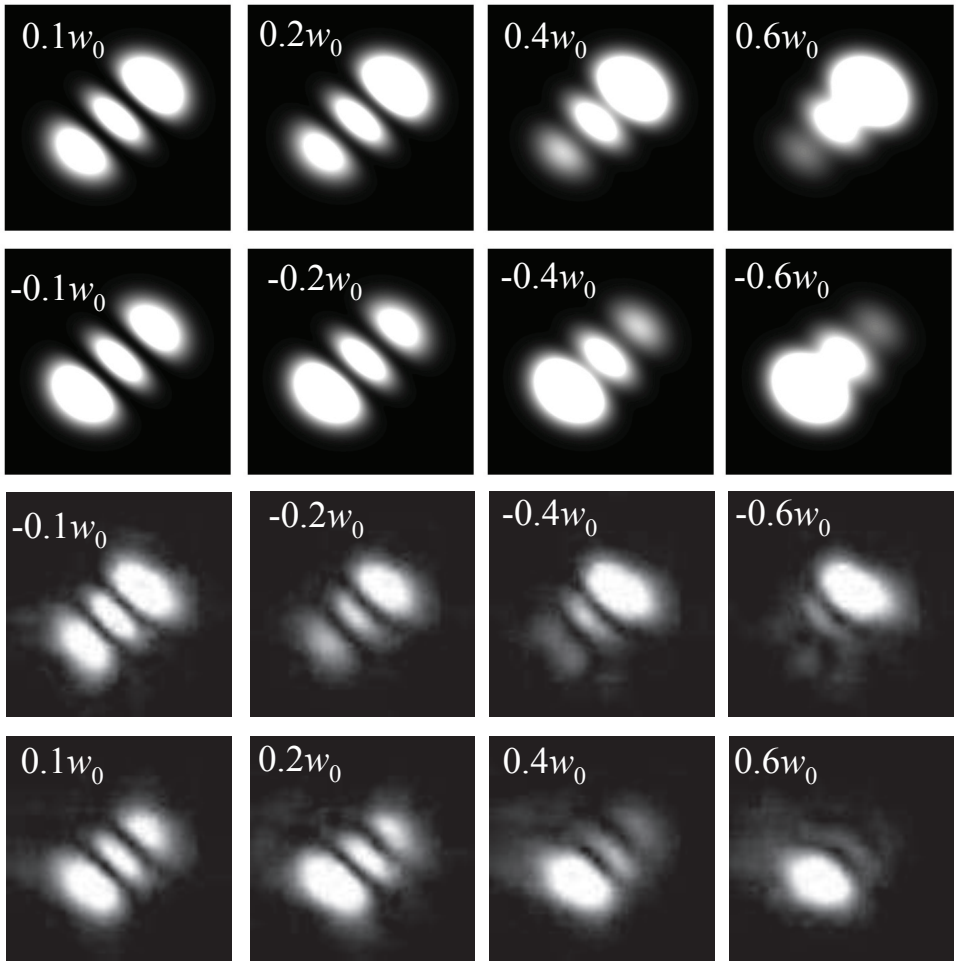

Figure 3.7: The theoretical (first two rows) and experimental (last two rows) results for the intensity patterns of an off-axis vortex of charge 2, at $z = z_c$ for different values of x_0 as labelled in the insets.

Figure 3.8 shows the theoretical (first two rows) and experimental (last two rows) images corresponding to opposite singularities ($\epsilon_1\epsilon_2 = -1$) for separation parameter $x_0 = 0.1w_0$ and topological charges as shown in the images.

For small values of m and n, these patterns can be explained by expanding the Hermite polynomials in power series. The calculation would be long and tedious. Instead, we make the following empirical observation. If $m \neq n$ and $m \geq 2$, $n \geq 2$ the pattern has a rectangular 'razor-blade' structure which is tilted clockwise (anti-clockwise) if the net charge is positive (negative). On closer observation, we note that there are m bright spots on two parallel sides and n bright spots on the remaining two parallel sides. Thus, for vortex dipoles ($m = n$) the pattern is square with its corners in the east, west, north and south directions, each side having $m = n$ bright spots. Clearly, for vortices of opposite signs with $m \geq 2$ *and* $n \geq 2$, we

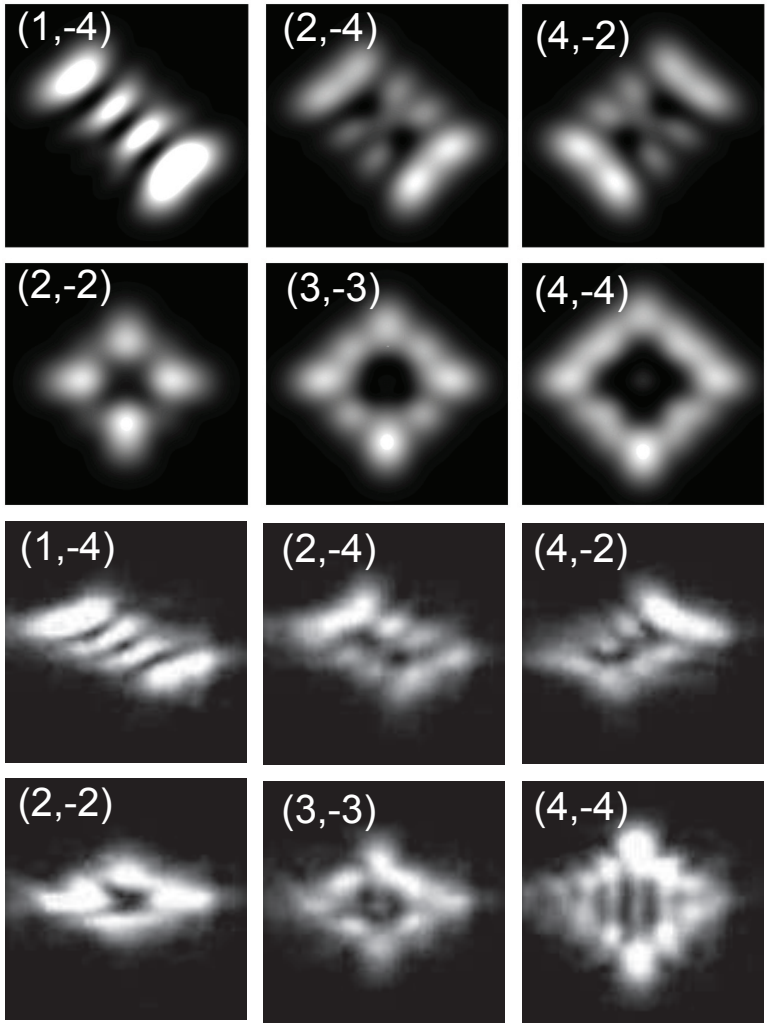

Figure 3.8: The theoretical (first two rows) and experimental (last two rows) results for the intensity patterns of a vortex pair with topological charges of opposite signs, at $z = z_c$ for $x_0 = 0.1w_0$.

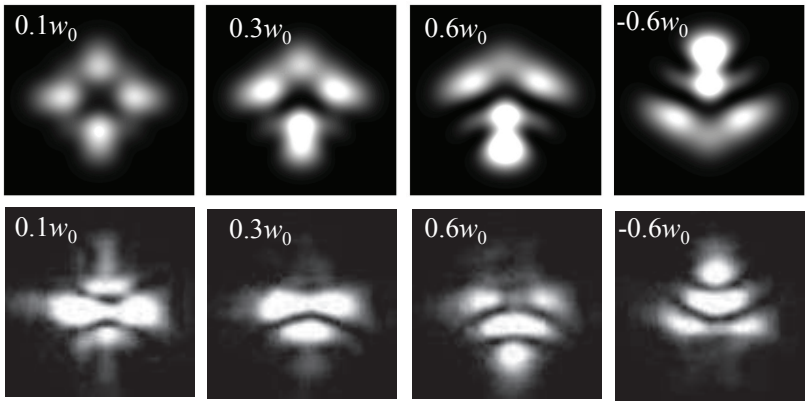

Figure 3.9: The theoretical (top row) and experimental (bottom row) results for the intensity patterns of a dipole vortex of charge (2,-2), at $z = z_c$ for different values of x_0 as labelled in the figures.

can determine the individual charges as well (see, for example, Figures for (2,-4) and (4,-2)).

As far as we know, Figure 3.8 represents *the first optical realization* of the 4-variable 2-index 1-parameter Hermite polynomials $H_{m,n}(x, z; y, w|\tau)$ modulated by an elliptical Gaussian beam (see Eqs. 3.8, 3.15 and 3.26).

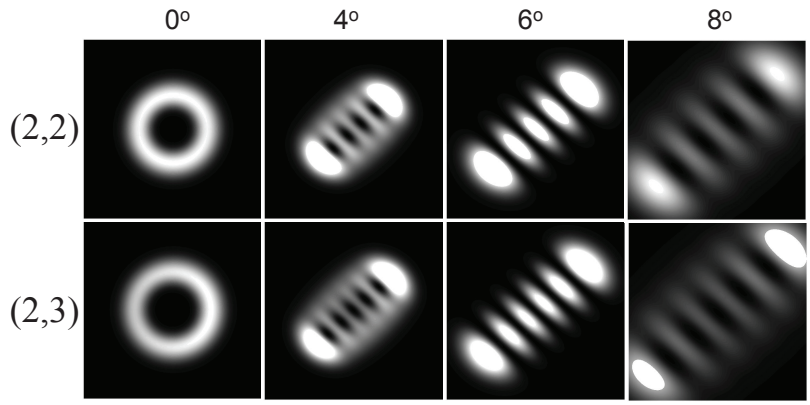

Figure 3.10: Theoretical results for the intensity patterns of a vortex pair with topological charges (top) m= n=2; (bottom) m=2, n=3, at $z = z_c$ corresponding to the tilt angle $\theta = 6°$. As the tilt angle moves away from 6°, the sharpness of the patterns decreases, as expected.

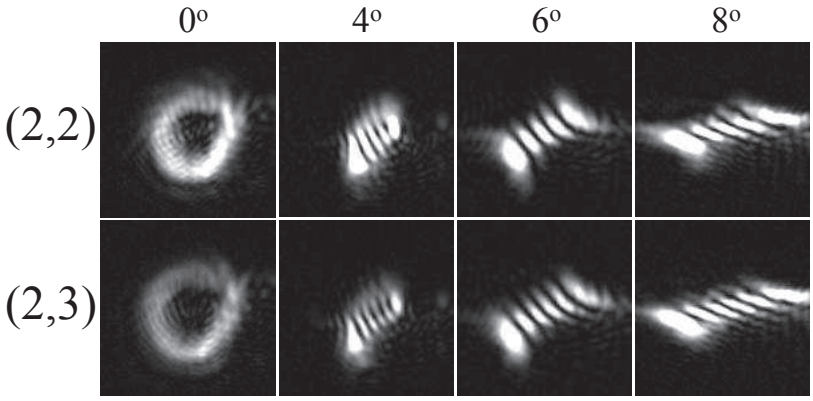

Figure 3.11: The experimental images corresponding to Figure 3.10 at $z = z_c$.

In Figure 3.9, we show the evolution of a dipole vortex of charge $(2, -2)$ as a function of separation between the two vortices. For small separation, the intensity distribution is symmetric in both the transverse directions. As the separation is increased, the pattern becomes asymmetric. When the separation parameter x_0 becomes negative, the vortex is identically described as $(-2, 2)$ with $x_0 = |x_0|$ and the pattern flips vertically.

We have also studied the variation in the intensity distribution at a particular plane

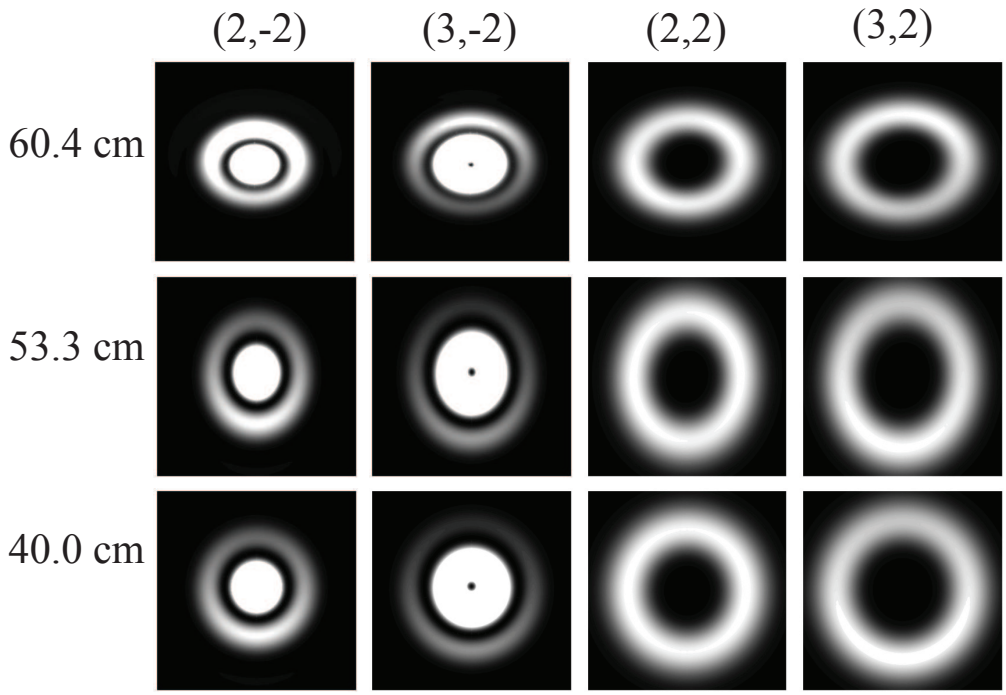

Figure 3.12: Theoretical intensity patterns of a vortex pair of different charges (as given on the top) at various values of the propagation distance z (as given on the left).

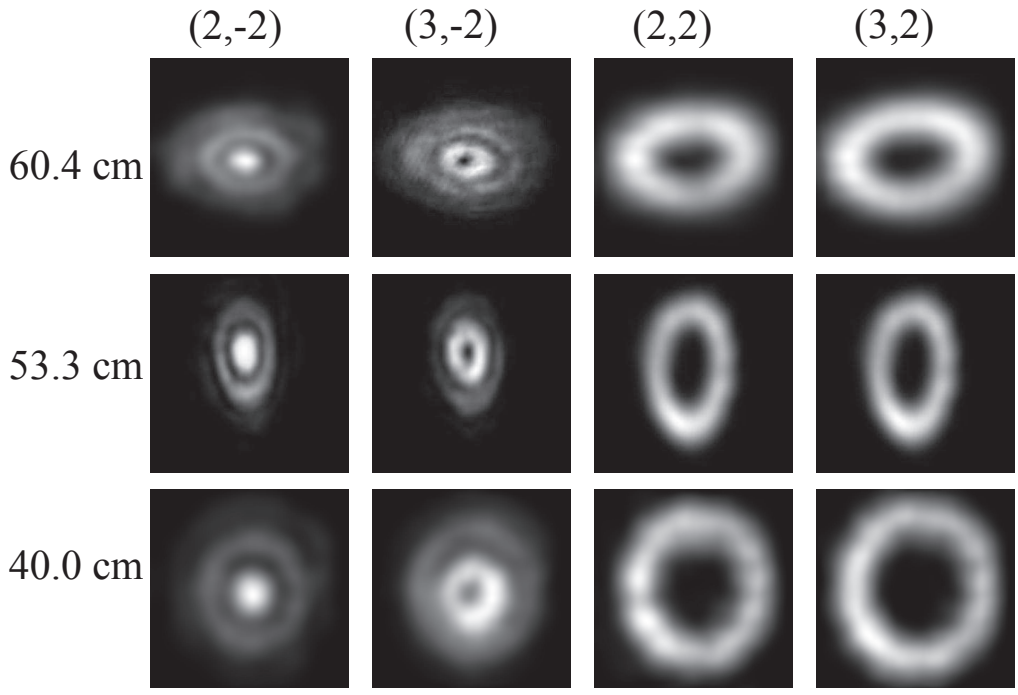

Figure 3.13: The experimental images corresponding to Figure 3.12.

($z = 56.3$ cm corresponding to the experimentally observed value of z_c for a tilt angle $\theta = 6°$) by changing the tilt angle of the lens. As z_0 and z_c depend on θ, the bright or dark lobes with highest contrast are obtained only at $\theta = 6°$ in this case. The theoretical as well as experimental results have been shown in Figures 3.10 and 3.11 respectively. Using Eq. 3.32, we have also obtained the intensity patterns when the lens is not tilted to highlight the dramatic impact a tilted lens makes.

3.3.2 Evolution of vortices beyond the critical plane

As we move away from the point $z = z_c$, the modulations due to the Hermite polynomials disappear quickly. The propagation dynamics is now governed by Eq. 3.28. The theoretical and corresponding experimental intensity patterns for various values of z are shown in Figures 3.12 and 3.13 respectively. The intensity patterns are, in general, elliptical. Far away from z_c, all patterns become circularly symmetric as $\alpha_1 \to \alpha_2$ and $\beta_1 \to \beta_2$ [60].

3.4 Conclusion

We have studied, both analytically and experimentally, the propagation of a Gaussian beam carrying a vortex pair of arbitrary topological charges through a tilted lens. We have also demonstrated a method to find the net topological charge of the vortex pair. Moreover, for vortices with topological charges of opposite signs and magnitudes $m \geq 2$, $n \geq 2$, we can determine the individual charges as well. Our method is easy to implement in the laboratory as it needs just a single tilted lens except the tilt has to be small for paraxial approximation to be valid. Vortices being generic to all the waves, this study can be extended for other systems like acoustic and matter waves.

Chapter 4

Scattering of Optical Vortices and Formation of Speckles

Speckle pattern is a random intensity distribution observed when a coherent light beam passes through a rough surface. The formation of speckles is due to the interference of many scattered waves having random phases which are induced by inhomogeneities of the rough surface. The study of speckles have contributed significantly both in science and the technology [73–82].

In this chapter, we discuss about the scattering of vortex beams through a rough surface (ground glass plate in the present case). Section 4.1 discusses about the experimental set up used to generate the speckles and quantification of their size using autocorrelation is discussed in section 4.2. We describe the GGP using a δ-correlated Gaussian function in section 4.3 and verify the experimentally obtained results. We also study the spatial intensity correlations of scattered optical vortices and compare them with the temporal intensity correlations in section 4.4. We discuss about the shift in focal point with the change in distance between the GGP and the imaging lens as well as incident beam width in section 4.5. Finally we conclude in section 4.6.

4.1 Experimental set up

The experimental set up for generating the optical vortices and the corresponding speckles is shown in Figure 4.1. An intensity stabilized He-Ne laser (Spectra Physics 117A) of wavelength 632.8 nm, power 1 mW and beam waist 0.3 mm is used to generate the optical vortices. The optical vortex beams are produced using computer generated holograms displayed on a spatial

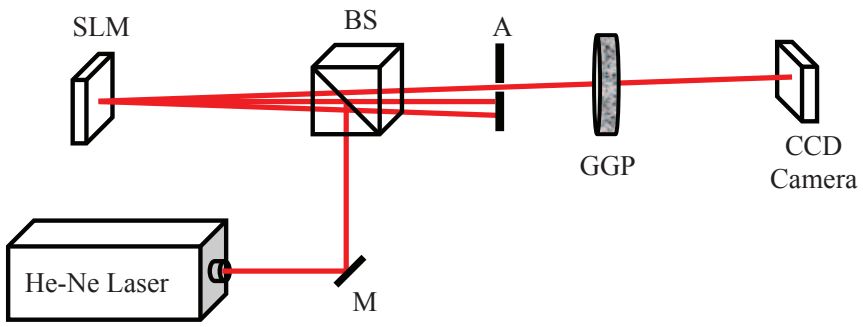

Figure 4.1: The experimental set-up for generating the speckles by scattering the optical vortex beams. Here, A–Aperture, M–Mirror, BS–Beam splitter, SLM–Spatial light modulator, and GGP–Ground glass plate.

light modulator (SLM) (Holoeye LCR 2500). Different computer generated holograms are introduced to the SLM through a computer for generating vortices of different order in the first diffraction order. The required beam is selected with an aperture A, and passed through the GGP. The scattered light from the GGP forms a granular pattern of intensity maxima and minima or speckles, as shown in Figure 4.2. These speckles are recorded with an Evolution VF colour cooled CCD camera with pixel size 4.65 μm. The SLM is placed at a distance of 60 cm from the laser and the GGP is at a distance of 66 cm from the SLM. The CCD camera is placed at a distance of 18 cm from the GGP.

4.2 Speckle patterns of vortex beams

Figure 4.2 shows the recorded speckle patterns produced by the scattering of optical vortices of orders $m = 0$ to 5 through the same GGP; where $m = 0$ corresponds to the host Gaussian beam. The speckles are recorded at a distance of 18 cm from the GGP. It is clear from the figure that the speckle size (S_m) decreases with the increase in order (m). We quantify this decrease in speckle size using the intensity auto-correlation method.

4.2.1 Auto-correlation for finding the speckle size

The size of recorded speckles can be determined by using auto-correlation method [72, 73] which calculates the correlation of speckle pattern with itself. In this method, we fix one image of the speckles and observe its correlation numerically with a number of images shifted in position. These shifts can be made pixel by pixel in both the transverse directions. We

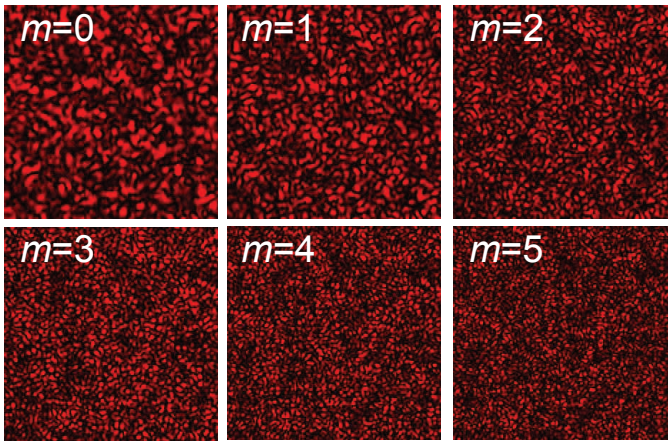

Figure 4.2: The speckle patterns formed by the scattering of optical vortices with orders $m = 0 - 5$ at a given plane.

plot the obtained results as a function of the shift. The correlation factor is maximum if two speckle distributions are completely overlapped and it decreases with the decrease in overlap. The correlation factor becomes zero if their overlap is less than the speckle size as any two speckles are independent of each other due to the random nature of speckles. The correlation curve has a Gaussian distribution whose full width at half maximum (FWHM) gives the speckle size in any of the transverse directions.

Here, we have considered the normalized speckle patterns to determine the speckle size as they are overfilling the CCD camera. Figure 4.3(a) shows the speckle pattern formed by the scattering of a first order vortex through the GGP. The dimensions of autocorrelation function is always twice the considered dimensions of speckle pattern as we are observing correlation along both the positive and negative directions. The speckle patterns recorded for finding the speckle size and its autocorrelation function are shown in Figures 4.3(a) and 4.3(b) respectively. The distributions of the autocorrelation function in two transverse directions have been shown in Figures 4.3(c) and 4.3(d). The FWHM of these two distributions provide the speckle size in corresponding transverse directions.

4.2.2 Speckle size vs order

We show the dependence of speckle size (S_m) on the area of the bright annular vortex ring (A_m) (as discussed in chapter 2). In Figure 4.4, we plot $ln(S_m)$ with $ln(A_m)$. From this graph also, it is clear that the speckle size decreases as the order of vortex increases. The curve is a straight line with slope equal to the exponent of A_m on which S_m depends. With the best

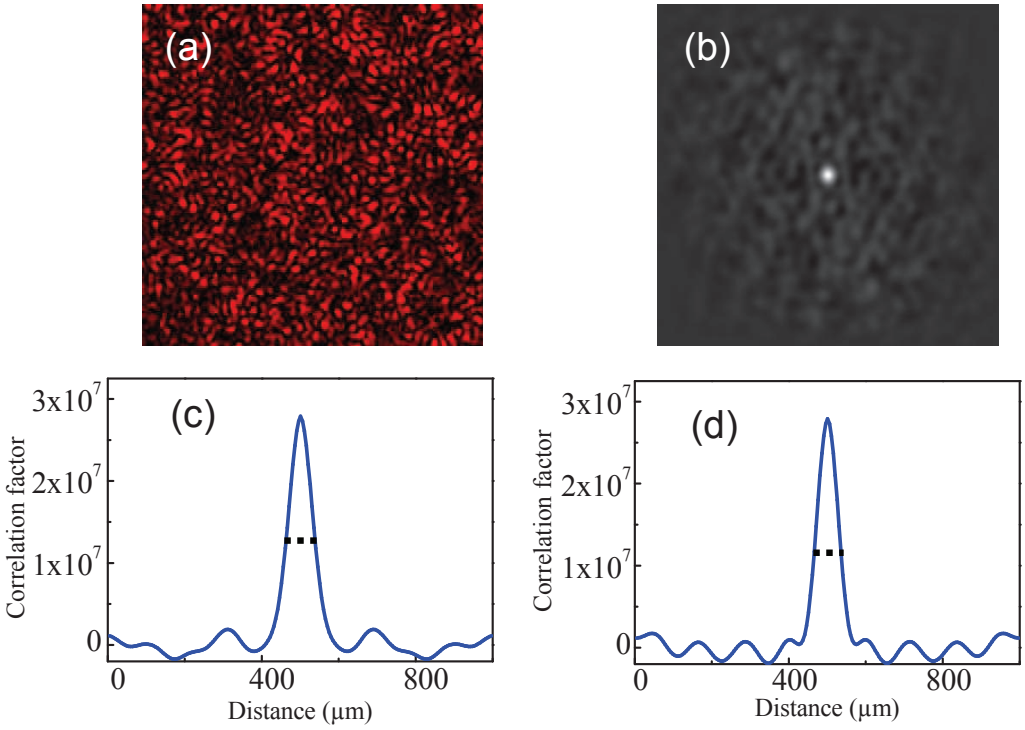

Figure 4.3: (a) The obtained speckle pattern of first order optical vortex, (b) the distribution of auto correlation function, (c) and (d) are the variation of autocorrelation function in transverse directions X and Y respectively.

fit to our experimental data, we have found that the speckle size is directly proportional to $A_m^{-0.612\pm0.021}$. In Figure 4.4, we present the experimental data along with the best fit curve, which is different from the corresponding result for a Gaussian beam. For a Gaussian beam scattered through the ground glass plate, one expects a Brownian distribution, and in fact one gets speckle size as proportional to $A^{-0.50}$ [72, 73]. We have verified this experimentally by using different beam sizes of a Gaussian beam and shown in inset of Figure 4.4. This suggests the non-Gaussian statistics of the speckles generated by the scattering of optical vortex beams. We know that the size of speckles, the lowest length scale at which light is correlated, plays a crucial role in astronomy. By finding the size of speckles (S), one can determine the angular diameter (W) of the stars from the relation $W = L\lambda/S$ where L is the distance of star from the observation plane and λ is the wavelength. Taking an analogy, our experimental results show a decrease in speckle size with order implying an increase in the angular diameter of source generating these speckles i.e. optical vortices. Therefore, we attribute the decrease in speckle size to the increase in area of illumination with the order as shown in Figure 2.4(b).

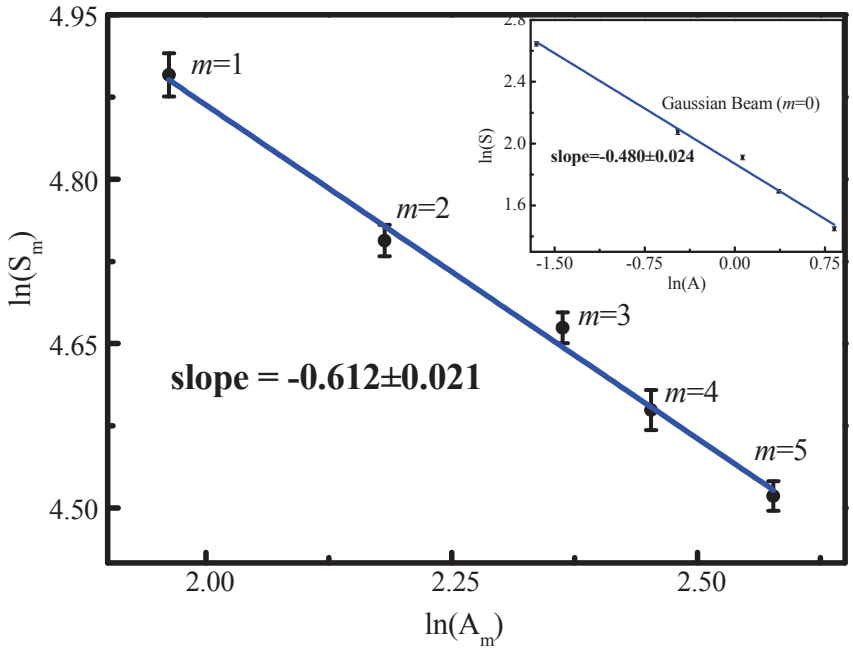

Figure 4.4: The plot of $\ln S_m$ versus $\ln A_m$ where S_m and A_m are the experimentally obtained speckle size and area of bright region of optical vortices respectively, (Inset, the same plot for a Gaussian beam with different sizes/areas). The solid line is the best fit to our experimental data.

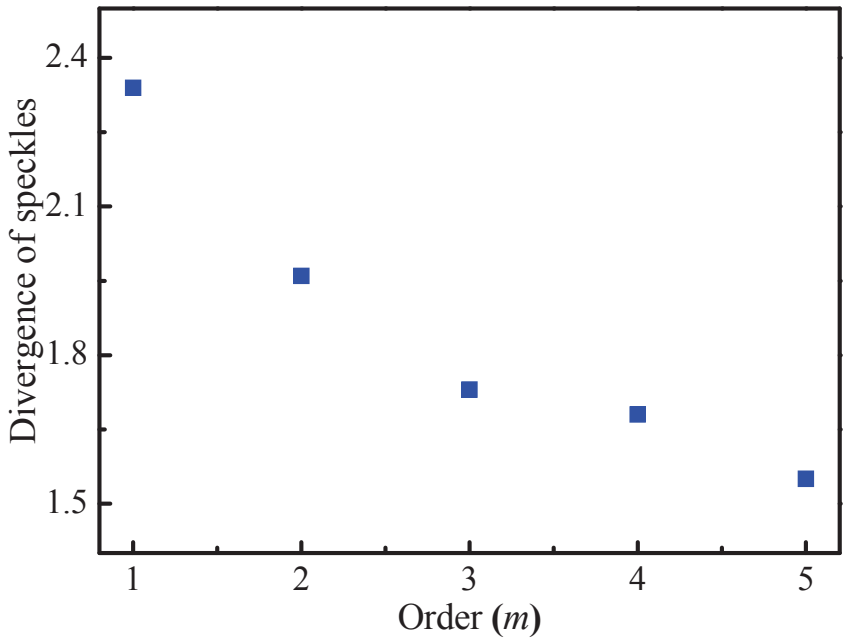

Figure 4.5: The plot of speckle divergence vs order of the vortex.

We also study the rate of change of speckle size with propagation distance, namely divergence of speckles. For this, we have recorded speckles at seven different planes separated by a distance of 2 cm from each starting at 11 cm from the GGP and found their size. The slope of line obtained for speckle size vs propagation distance gives the divergence of speckles. We found that the divergence decreases with increase in the order as shown in Figure 4.5.

4.3 Theoretical modelling

Rough surface of a ground glass plate serves as a good source for generating the speckles. The goal is to study the variation of size and intensity correlation properties of speckles generated by the scattering of vortex beams. Here, we work in the strong scattering zone for which the wavelength λ is comparable to the average size of inhomogeneities or the separation between two nearest neighbour inhomogeneities. At this condition, the localization effects are stronger and speckles can be observed easily.

For modelling the GGP, we need to consider the absence of correlations between any two inhomogeneities i.e. the phase introduced to the beam at that spatial point. This can be well described using a δ–correlation function; however, the finite size of the inhomogeneities makes it a δ–correlated Gaussian function. The mathematical form of this correlation function can be written as

$$\phi(x,y) = \delta\left(x_1 - x_2, y_1 - y_2\right) \times e^{-((x_1-x_2)^2+(y_1-y_2)^2/\sigma^2)} \tag{4.1}$$

where σ is the correlation length. In numerical calculations, it can be realized by replacing the δ function with a 2-D spatial random function Rand(x, y) and above equation becomes

$$\phi(x,y) = e^{-((x_1-x_2)^2+(y_1-y_2)^2/\sigma^2)} * \mathrm{Rand(x,y)} \tag{4.2}$$

where $*$ represents a 2-D convolution between the two functions.

Now, the electric field of an optical vortex after scattering through a GGP plate is given by [112]

$$E'(x,y) = E(x,y)e^{i\phi(x,y)} \tag{4.3}$$

where $E(x, y)$ is electric field of an optical vortex and $\phi(x, y)$ is random phase introduced by GGP to the vortex.

To verify the experimentally obtained results (Figure 4.2), we numerically simulate the speckles corresponding to the scattering of optical vortices of order m=0–5 as shown in Figure 4.6. The results show that the size of speckles decreases with increase in the order of vortex which is same as of our experiment.

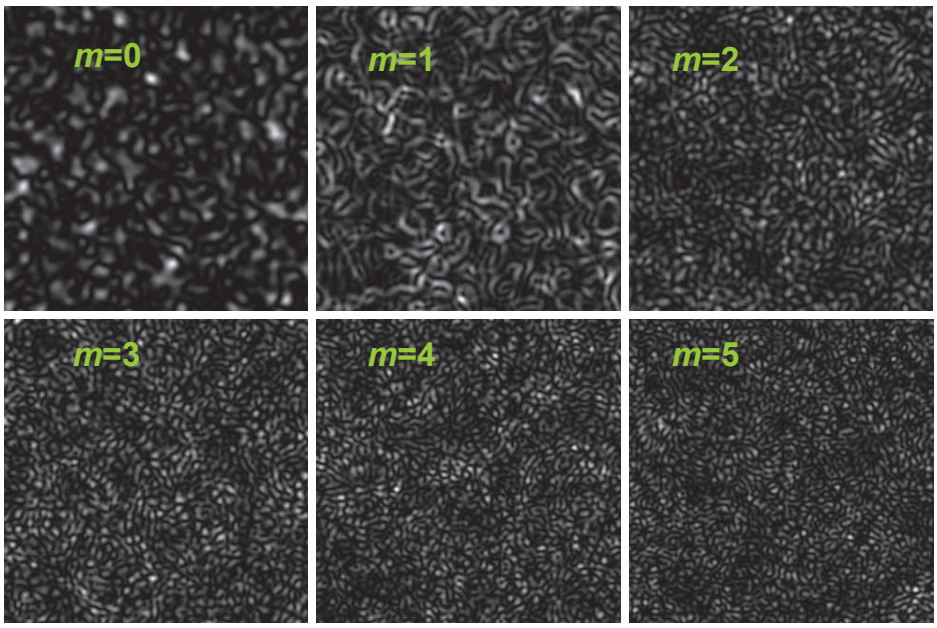

Figure 4.6: The numerically obtained speckle patterns for optical vortices with orders m=0–5.

4.4 Intensity correlation vs order of the vortex

In the 1950s, Robert Hanbury Brown and Richard Q. Twiss performed a series of intensity correlation experiments to measure the correlation between intensity fluctuations in the light beams from different sources of light [113]. The objective of these experiments was to calculate the size of radio stars through the coherence of the observed radiation measured with an intensity correlation experiment. Later, the concept of intensity correlation heralded the birth of modern quantum optics [114, 115]. Although the original HBT experiments were conducted half a century ago, these experiments still carry their importance in many branches of science [116–127]. The observation of bunching (anti-bunching) effect in HBT experiments with bosons (fermions) reveals the direct existence of symmetric (antisymmetric) wave function for bosons (fermions) [124]. The anti-correlation between the arrival times of the free electrons [121], anticipated due to Pauli's exclusion principle, is also observed in HBT experiment with free electrons. Recently, Bromberg et al. [127] performed HBT-type experiments with interacting bosons. The photons in their experiments are made to interact through a non-linear medium [123, 125]. It has been shown that the interaction among the propagating photons strongly affects the intensity correlation measurements. A large number of HBT type experiments have also been performed with Bose–Einstein condensates and

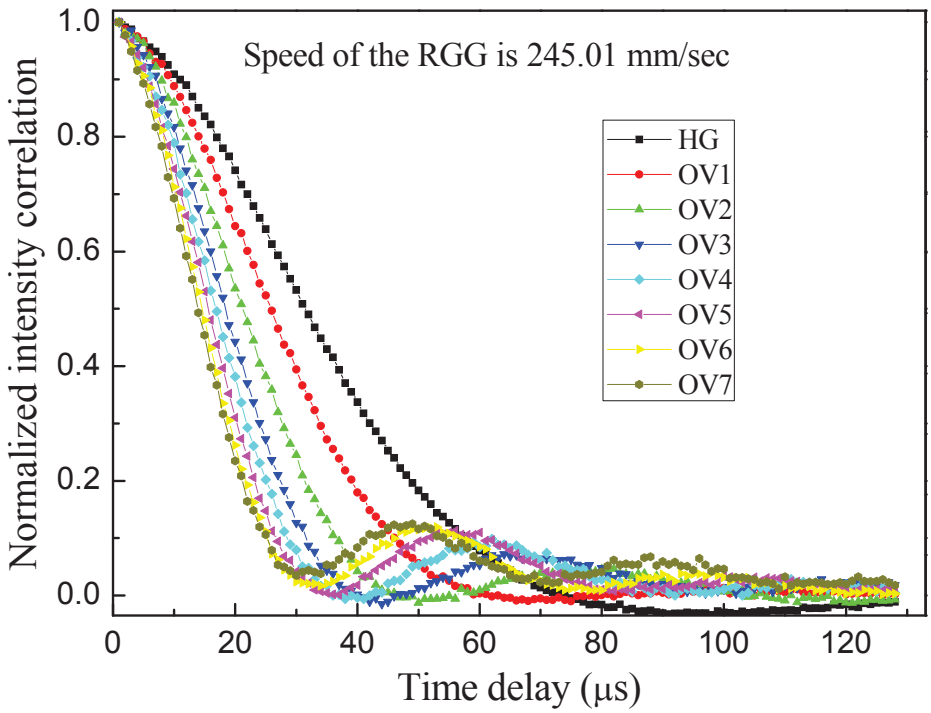

Figure 4.7: The experimentally obtained temporal intensity correlation curves for the optical vortices of orders m=0–7.

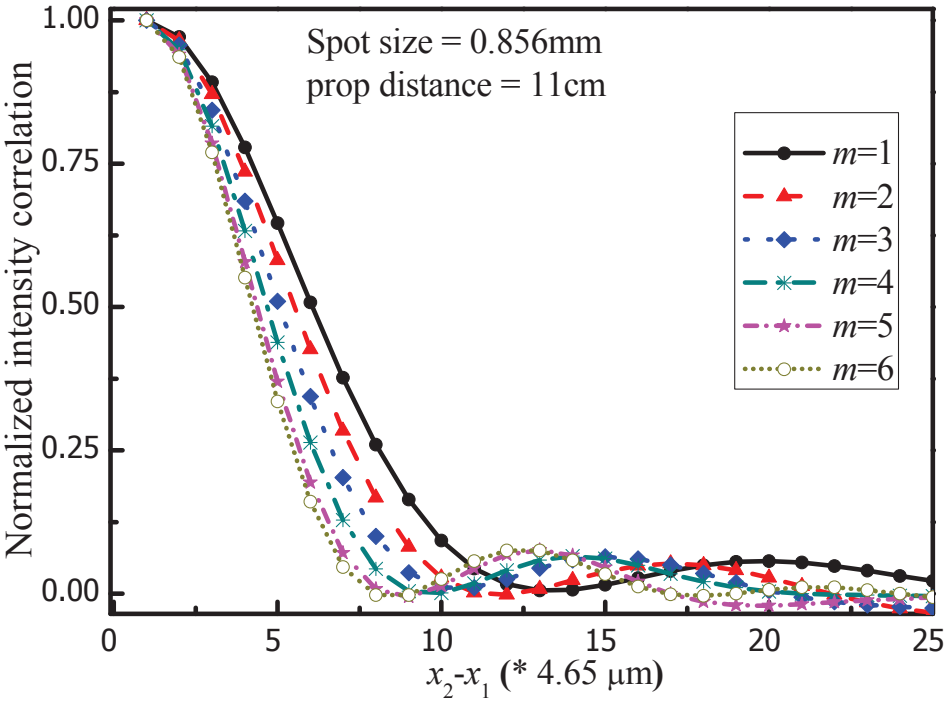

Figure 4.8: The experimentally obtained spatial intensity correlation curves for the optical vortices of orders m=1–6.

ultra-cold quantum gases. The results from these experiments show the analogy between the behaviour of photons and atoms.

We have performed HBT type experiments for optical vortices and those scattered through a rotating ground glass (RGG) plate. It has been found that the intensity correlation function for optical vortices behaves similar to that of the Gaussian laser beams. However, on scattering, intensity correlation curves for vortices show features which are very much different from that of the scattered Gaussian beam of the laser. Along with faster decay of intensity correlation for vortices, we observe partial revival of their correlations at longer time delays or larger separations, a feature that is absent for the Gaussian beam.

For measuring the temporal intensity correlations, we have collected the scattered optical vortices using a photomultiplier tube (PMT). This signal is given to the digital correlator in which the HBT-type of experiments are performed and obtained the correlation curves. These curves have been shown in Figure 4.7. It is clear that the decay of correlation is sharper for higher order vortices.

We have also determined the spatial intensity correlations of the recorded speckles. The results have been shown in Figure 4.8. It is clear from the figure that spatial correlation properties are similar in behaviour as of temporal correlation as the decay of correlation becomes sharper with the increase in order.

It is known in the context of imaging that the spatial noise due to the speckles decreases if more number of speckles are present [72, 73]. We have shown that the speckle size decreases with the order of vortex which effectively increases the number of speckles present in a given area. Therefore, one can use higher order vortices to reduce the spatial noise in speckle imaging. The results may find use in ghost imaging with vortices [128–130] and in stellar intensity interferometry.

4.5 Scattering and the focal plane

In the course of our study on the scattering of optical vortices, we observed a shift in the focal plane of the lens when it was moved away or towards the GGP. A plot between the position of focal plane (focal shift) and the distance of lens from the GGP has been shown in Figure 4.9. It is clear, when the lens moves towards the GGP, the focal plane shifts away from the lens and vice versa. Similar results have been obtained by changing the aperture size placed in front of the lens for the Gaussian Schell model (GSM) beams[131, 132]. In both the cases, the focal plane moves towards the lens when we collect less amount of partially

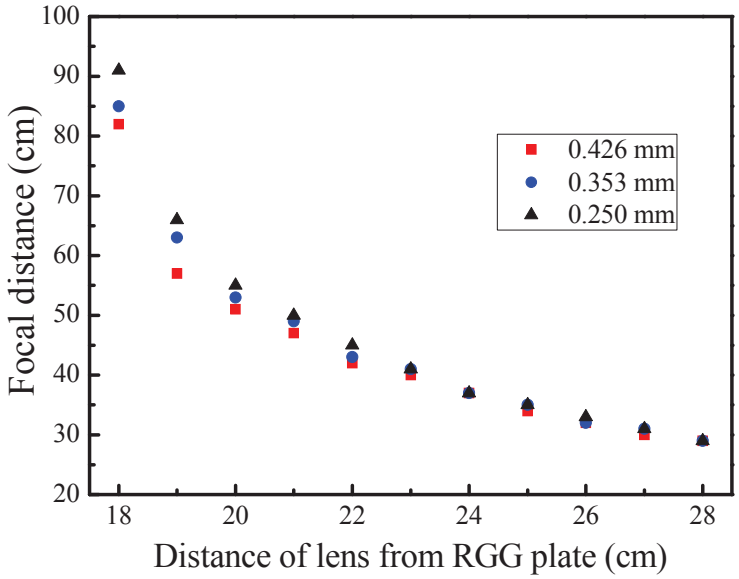

Figure 4.9: Plot showing the shift in focal plane with the position of lens from the GGP for different beam widths.

coherent light or effectively decrease the aperture size. The effect of incident beam width on the focal shift has also been studied. We have observed that at a given distance of the lens from the GGP, the focal point shifts towards the lens with decrease in the beam width, which effectively decreases the amount of light collected. The controlled focal shift obtained here may be useful in changing the trapping planes. In inverted optical tweezer set up, the focal plane shifts due to the refractive index mismatch between the immersion oil and cover slip; such shifts may be compensated with controlled focal shifts in the path of trapping beams.

4.6 Conclusion

We have studied the variation of size and divergence of the speckles with the order of an optical vortex. We have also quantified their size using the intensity auto-correlation method. The GGP has been simulated with a δ-correlated Gaussian function for the verification of experimental results. We have shown that the spatial intensity correlation properties are similar to the temporal properties for scattered optical vortices. It is obtained that the geometrical focus of lens changes with the amount of light collection that depends on the distance between the GGP and the lens as well as spot size of the incident beam.

Chapter 5

Speckles and Formation of Ring Shaped Beams

Ring shaped or dark hollow beams have found applications in guiding cold atoms [133] and trapping of low refractive index particles [134]. Such beams can be generated through multi-mode light wave guides, multi-mode fibers [135], spiral phase plates [43–45], and computer generated holograms (CGH) [46]. The Laguerre-Gaussian (LG) beams with zero radial index have attracted a great deal of attention due to their applications in optical manipulation, optical communication and quantum information [16, 19]. We have considered LG beams with zero radial index throughout the chapter. Along with the LG beams, Bessel beams owing to their interesting properties of propagation without an apparent spreading due to diffraction have also been a subject of study since more than two decades [136]. Usually in a laboratory the Bessel beams are generated using a Gaussian laser beam and termed as Bessel-Gauss (BG) beams.

The scattered light of a Gaussian laser beam through a rotating ground glass (RGG) plate can be modeled as a Gaussian Schell-model (GSM) beam [137]. This GSM beam is partially coherent light which has Gaussian intensity distribution and Gaussian spectral degree of coherence. Recently, a lot of applications of partially coherent beams have been suggested in diverse areas [138]. Wang et al. [139] have introduced the partially coherent LG beams of all orders. The temporal coherence properties of partially coherent beams generated by the scattering of optical vortices through a RGG plate have also been studied [88, 89]. It has been shown that the decay of coherence becomes sharper with increase in the order of LG beam. A similar type of behavior has been observed theoretically in the Fourier transform of the spatial correlation function of the LGSM and the BGSM beams [140]. It has been

stated that the beams having a rotational symmetry in the Fourier transform of their spatial correlation function and zero value on the beam axis can generate a dark core in the far field intensity distribution. Mie and Korotkova [140] generated ring shaped beams with an arbitrary beam (including Gaussian beam) by introducing LG correlation function through a phase screen. We have experimentally generated ring shaped beams with LG beams by introducing Gaussian correlation function through a RGG plate. The obtained experimental results are simulated by using the expression of cross spectral density of the partially coherent beams generated by a Schell model source, and at $z = 0$ it is given by [139]

$$W(x_1, y_1, x_2, y_2, 0) = \sqrt{I_1(x_1, y_1, 0) I_2(x_2, y_2, 0)} \times g(x_1 - x_2, y_1 - y_2, 0). \tag{5.1}$$

where $I_1(x_1, y_1, 0)$ and $I_2(x_2, y_2, 0)$ are the intensity distributions at the positions $(x_1, y_1, 0)$ and $(x_2, y_2, 0)$ respectively; $g(x_1 - x_2, y_1 - y_2, 0)$ is the spectral degree of coherence.

In this chapter, we generate ring shaped beams using the speckles obtained by scattering Laguerre Gaussian (LG) and Bessel-Gaussian (BG) beams of non-zero topological charge. Although, the phase of a LG beam completely randomized by the rough surface, we are able to recover the dark core by probing the field at Fourier plane of a plano convex lens. We discuss the experimental set up in section 5.1 and the corresponding results in section 5.2. We simulate the same far field intensity distributions using partially coherent standard LG beams in section 5.3. Finally, we conclude in section 5.4.

5.1 Experimental set up

Our experimental set up for the generation of ring-shaped beams is shown in Figure 7.1. An intensity and frequency stabilized He-Ne laser (Spectra Physics 113A) beam of maximum power 1 mW and beam waist 0.3 mm is used to generate LG and BG beams. These beams are produced with the computer generated holography technique using a spatial light modulator (SLM). Different computer generated holograms for generating different LG and BG beams are introduced to the SLM through a computer. The required beam is selected with an aperture A, and passed through the lens (L1) of focal length 25 cm and the RGG plate. The RGG plate is translated along the direction of incident beam to change the width of the beam falling on the plate. We have done experiment for four positions of the RGG plate by translating in steps of 2.5 cm starting from 15 cm. The scattered light from the RGG can be approximated as the corresponding Schell-model beam which is focused with a plano convex lens (L2) of focal length 10 cm. The images corresponding to the different input beams are recorded with an Evolution VF color cooled CCD camera of pixel size 4.65 μm. The SLM

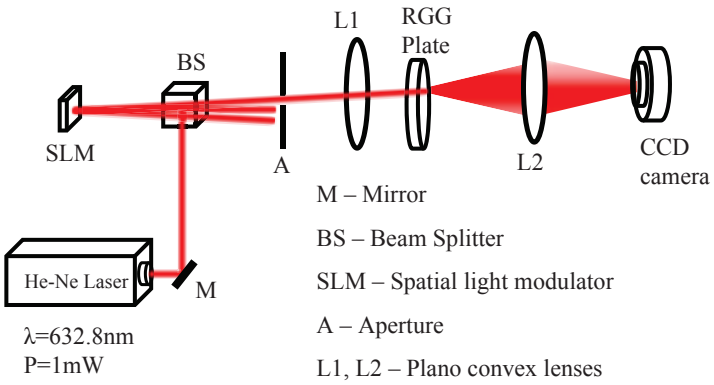

Figure 5.1: Experimental set up for the generation of ring shaped beams.

is placed at a distance of 63 cm from the laser and the lens L1 is placed at 56 from the SLM. The lens L2 is kept at a distance of 24 cm from the RGG plate and the CCD camera is placed 37 cm from the lens. Position of the lens L2 is adjusted to get a clear far field intensity distribution for an optimum diameter of the ring shaped beams that could be captured with the CCD camera being used by us.

5.2 Results and discussion

We start our experiment with the recording of the images of scattered second order LG and BG beams (azimuthal index 2) from the static ground glass plate. The images are captured at the distance of 5 cm from the plate and also at the 18 cm from the focusing lens (L2);

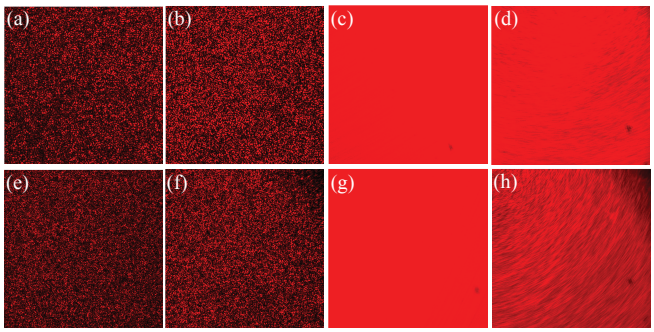

Figure 5.2: Images showing the intensity distributions of scattered second order LG (a-d) and BG (e-h) beams; (a, e) are recorded after the ground glass and (b, f) after the lens, while (c, g) and (d, h) are recorded at same places when the ground glass is rotating (linear speed 72.1 cm/sec).

both for a incident beam of width 1.1 mm. The same are also recorded with the rotating ground glass plate. These images are shown in Figure 5.2. One can notice that the recorded images do not show any intensity distribution like original LG and BG beams i.e. there is no trace of dark core. The random intensity distributions obtained for static ground glass (Figures 5.2(a,b,e,f) gets averaged out in case of the RGG plate (Figures 5.2(c,d,g,h)).

Although the phase of vortices gets completely randomized by the GGP, the dark core of vortices can be revived using a single plano-convex lens. We have seen that the far field intensity distributions form ring shaped beams with dark core for incident beams with non-zero azimuthal index. To study the effect of width of incident beam falling on the GGP

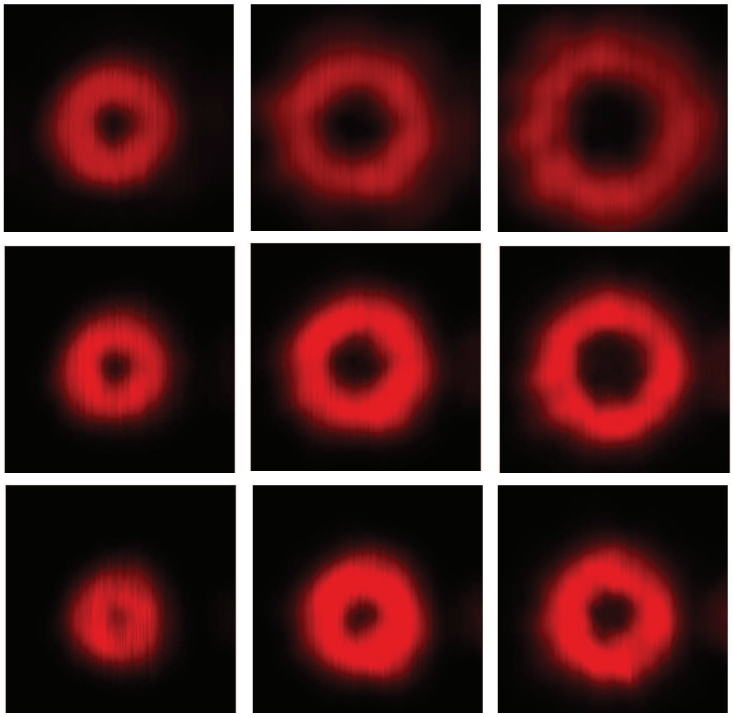

Figure 5.3: Far field intensity distribution of the scattered LG beams of different azimuthal indices ($l = 2, 4, 6$) through a RGG plate for different widths of the incident beam, 0.496 mm (top), 0.412 mm (middle) and 0.321 mm (bottom).

on far-field intensity distributions, we record at four different widths obtained using the lens (L1). The far field intensity distributions of the scattered LG and BG beams have respectively been shown in Figures 5.3 and 5.4. We have shown the far field intensity distributions of scattered LG and BG beams with azimuthal indices 2, 4 and 6 (radial index is zero for all images) for a speed 34.3 cm/s of the RGG plate. The presented results correspond to the different widths of the (taken as width of host Gaussian beam) incident beam falling on the

GGP. It is clear from the Figures 5.3 and 5.4 that the diameter of dark core increases with increase in the azimuthal index for both the LG and the BG beams and decreases with the decrease in incident beam width. The darkness of core decreases gradually with the decrease in width and finally gets disappears if the beam width is less than 0.140 mm for first order scattered vortex.

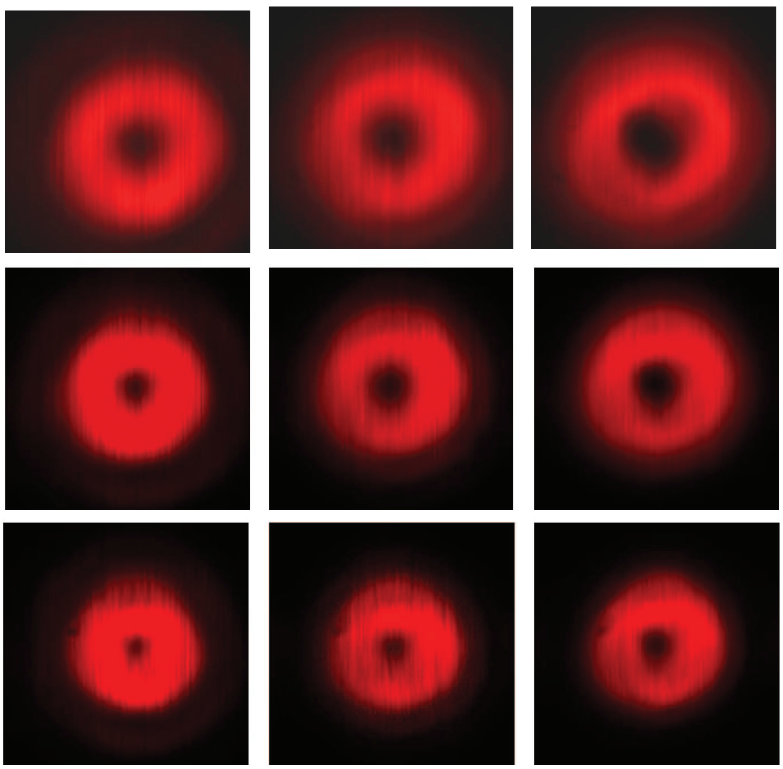

Figure 5.4: Far field intensity distribution of the scattered BG beams for same conditions as in Figure 5.3

We have studied the effect of speed of the GGP and observed that the diameter and darkness (measured by the dip in its line profile) of dark core is independent of the speed of the RGG plate i.e. temporal coherence of the scattered light. This has been shown by drawing the line profiles along the dark core of the far field intensity distributions of scattered second order LG (left) and BG (right) beams at different speeds of the RGG plate for incident beam width of 1.1 mm and shown in Figure 5.5 (top). We also verify the disappear of dark core using the line profiles as shown in Figure 5.5 (bottom). It is clear that the darkness (dip of the curve) of the core decreases gradually with the decrease in width.

We have also studied the effect of azimuthal index on the size of dark core of ring shaped beams at a given temporal and spatial coherence. We have plotted the line profiles through

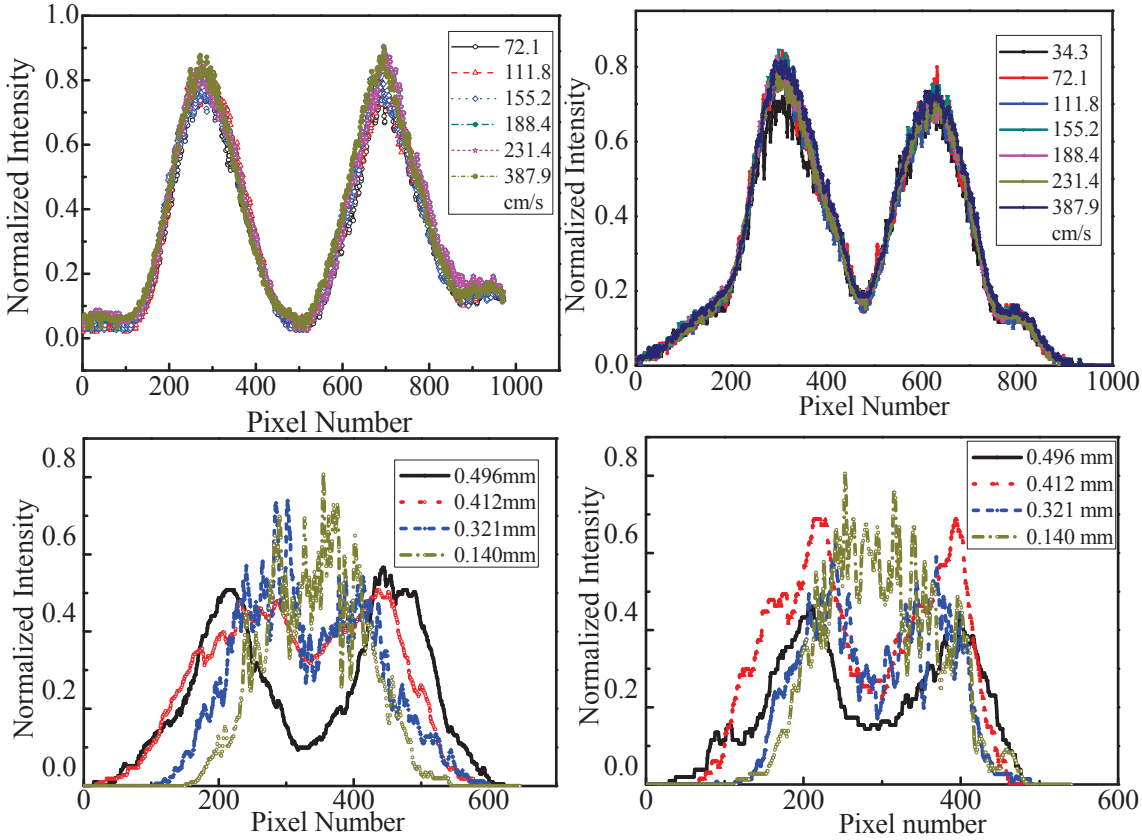

Figure 5.5: The line profiles along the core of ring shaped beams generated from scattered second order LG (left) and BG (right) beams at different speeds of the RGG plate (top) and for different incident beam widths. (bottom)

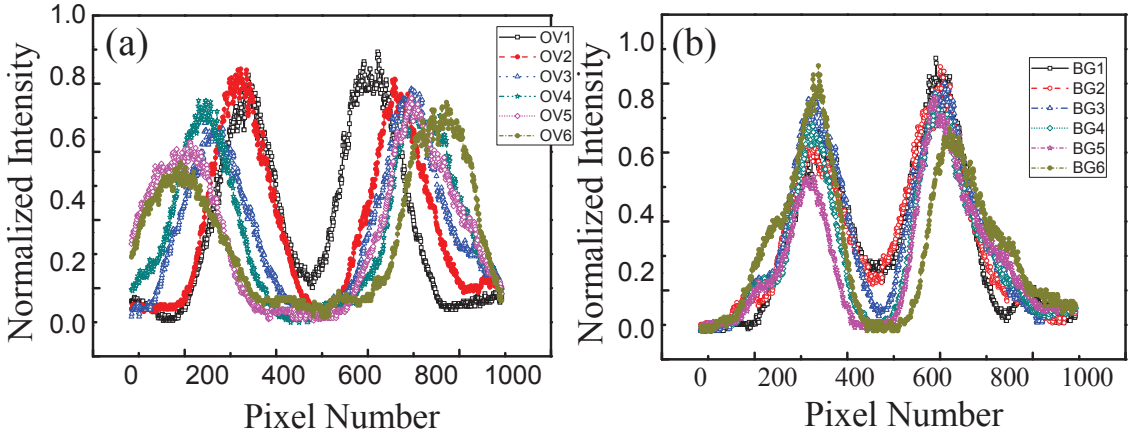

Figure 5.6: The line profiles (intensity distribution) along the centers of far field intensity distributions of scattered LG (a) and BG (b) beams for l = 1-6

.

the centers of ring shaped beams formed by scattered LG and BG beams with different azimuthal indices (l = 1–6) for the incident beam size of 1.1 mm and the RGG speed of 34.3 cm/sec; shown in Figure 5.6. The dark cores of the ring shaped beams are quite prominent and as the azimuthal index increases it becomes broader.

5.3 Theoretical analysis

For the theoretical analysis, we start with the electric field of a standard LG beam at the source plane ($z = 0$) which can be written as

$$E_{pl}\left(r,\phi;0\right) = \left(\frac{qr}{w_0}\right) L_p^l \left(\frac{q^2r^2}{w_0^2}\right) \exp\left(\frac{r^2}{w_0^2}\right) \exp\left(il\phi\right) \tag{5.2}$$

where r and ϕ are the radial and azimuthal coordinates, L_p^l denotes the Laguerre polynomial with radial mode p and azimuthal index l and $q = \sqrt{2}$. w_0 is the host Gaussian beam width. The corresponding cross-spectral density can be obtained by substituting the Eq. 5.2 in the Eq. 5.1, and is given by

$$\begin{aligned} W\left(x_1,y_1,x_2,y_2,;0\right) \;=\; & \frac{1}{2^{4p+2l}(p!)^2} \sum_{m=0}^{p}\sum_{n=0}^{l}\sum_{h=0}^{p}\sum_{s=0}^{l} 1(i^n)^* i^s \begin{pmatrix} p \\ m \end{pmatrix}\begin{pmatrix} l \\ n \end{pmatrix}\begin{pmatrix} p \\ h \end{pmatrix}\begin{pmatrix} l \\ s \end{pmatrix} \\ & \times H_{2m+l-n}\left(\frac{qx_1}{w_0}\right) H_{2h+l-s}\left(\frac{qx_2}{w_0}\right) H_{2p-2m+n}\left(\frac{qy_1}{w_0}\right) H_{2p-2h+s}\left(\frac{qy_2}{w_0}\right) \\ & \times \exp\left(-\frac{x_1^2+y_1^2+x_2^2+y_2^2}{w_0^2}\right) \exp\left(-\frac{\left(x_1-x_2\right)^2+\left(y_1-y_2\right)^2}{2\sigma^2}\right) \end{aligned} \tag{5.3}$$

where σ is coherence length. when $\sigma \longrightarrow \infty$, the above equation represents the electric field of a coherent LG beam. The cross-spectral density of any partially coherent beam after passing through a linear and aligned optical system is given by

$$\begin{aligned} W(u_1,v_1,u_2,v_2) = & \left(\frac{1}{\lambda|B|}\right)^2 \iiiint W(x_1,y_1,x_2,y_2) \\ & \times \exp\left[\frac{-ik}{2B}\left\{\left(Ax_1^2 - 2x_1u_1 + Du_1^2\right)\right.\right. \\ & - \left(Ay_1^2 - 2y_1v_1 + Dv_1^2\right) + \left(Ax_2^2 - 2x_2u_2 + Du_2^2\right) \\ & \left.\left. - \left(Ay_2^2 - 2y_2v_2 + Dv_2^2\right)\right\}\right] dx_1dx_2dy_1dy_2 \end{aligned} \tag{5.4}$$

where x_i, y_i and u_i, v_i are the position co-ordinates in the input and output planes. A, B, C, D are the transfer matrix elements of the optical system and $k = 2\pi/\lambda$ where λ is the wavelength. By substituting the cross-spectral density (Eq. 5.3) in the above equation, we

get [139]

$$
\begin{aligned}
W(u_1,v_1,u_2,v_2) &= \left(\frac{1}{\lambda|B|}\right)^2 \frac{1}{2^{4p+2l}(p!)^2}\frac{\pi^2}{M_1M_2}\left(\frac{1}{2M_2}-\frac{q^2}{2M_1M_2w_0^2}\right)^{(2p+l)/2} \\
&\times \exp\Big[-\frac{ikD^*}{2B^*}u_1^2+\frac{ikD}{2B}u_2^2\Big]\exp\frac{k^2u_2^2}{4M_1B^2} \\
&\times \exp\Big[-\frac{k^2}{4M_2}\left(\frac{u_1}{B^*}-\frac{u_2}{2M_1\sigma^2B}\right)\Big]\exp\Big[-\frac{ikD^*}{2B^*}v_1^2+\frac{ikD}{2B}v_2^2\Big] \\
&\times \exp\frac{k^2v_2^2}{4M_1B^2}\exp\Big[-\frac{k^2}{4M_2}\left(\frac{v_1}{B^*}-\frac{v_2}{2M_1\sigma^2B}\right)\Big] \\
&\times \sum_{m=0}^{p}\sum_{n=0}^{l}\sum_{c_1=0}^{(2m+l-n)/2}\sum_{e_1=0}^{(2p-2m+n)/2}\sum_{h=0}^{p}\sum_{s=0}^{l}\sum_{d=0}^{(2h+l-s)}\sum_{c_2=0}^{d/2}\sum_{d_1=0}^{(2p-2h+s)/2}\sum_{e_2=0}^{d_1/2} \\
&\times \binom{p}{h}\binom{l}{s}\binom{2h+l-s}{d}\binom{2p-2h+s}{d_1}(-1)^{c_1+c_2+e_1+e_2} \\
&\times \frac{(2m+l-n)!}{c_1!(2m+l-n-2c_1)!}\frac{d!}{c_2!(d-2c_2)!}\frac{(2p-2m+n)!}{e_1!(2p-2m+n-2e_1)!} \\
&\times \frac{d_1!}{e_2!(d_1-2e_2)!}(2i)^{2c_1+2c_2+2e_1+2e_2-d-d_1-2p-l} \\
&\left(\frac{1}{\sqrt{M_2}}\right)^{d+d_1-2c_1-2c_2-2e_1-2e_2} \\
&\times \left(\frac{2q}{w_0}\right)^{-2c_1-2e_1}\left(\frac{2q}{\sqrt{2}\sigma^2\sqrt{M_1^2w_0^2-q^2M_1}}\right)^{d+d_1-2c_2-2e_2} \\
&\times H_{2p-2h+s-d}\left(-\frac{iqku_2}{\sqrt{2}B\sqrt{M_1^2w_0^2-q^2M_1}}\right) \\
&\times H_{2m+l-n+d-2c_1-2c_2}\left(\frac{ku_2}{4M_1\sqrt{M_2}\sigma^2B}-\frac{ku_1}{2\sqrt{M_2}B^*}\right) \\
&\times H_{2p-2h+s-d_1}\left(-\frac{iqkv_2}{\sqrt{2}B\sqrt{M_1^2w_0^2-q^2M_1}}\right) \\
&\times H_{2p-2m+n+d_1-2e_1-2e_2}\left(\frac{kv_2}{4M_1\sqrt{M_2}\sigma^2B}-\frac{kv_1}{2\sqrt{M_2}B^*}\right) \qquad (5.5)
\end{aligned}
$$

where

$$
\begin{aligned}
M_1 &= 1/w_0^2+1/\left(2\sigma^2\right)-ikA/(2B) \\
M_2 &= 1/w_0^2+1/\left(2\sigma^2\right)-ikA^*/(2B^*)-1/\left(4M_1\sigma^4\right). \qquad (5.6)
\end{aligned}
$$

We plot the far field intensity distributions of partially coherent LG beams by propagating it through through free space of distance z_1, lens of focal length f and free space of distance z_2 using Eq. 5.5. We have used the following ABCD matrices for the propagation of partially coherent LG beams beam

$$A=1-\frac{z_2}{f},\quad B=z_1(1-\frac{z_2}{f}),\quad C=\frac{-1}{f},\quad D=\frac{-z_1}{f}. \qquad (5.7)$$

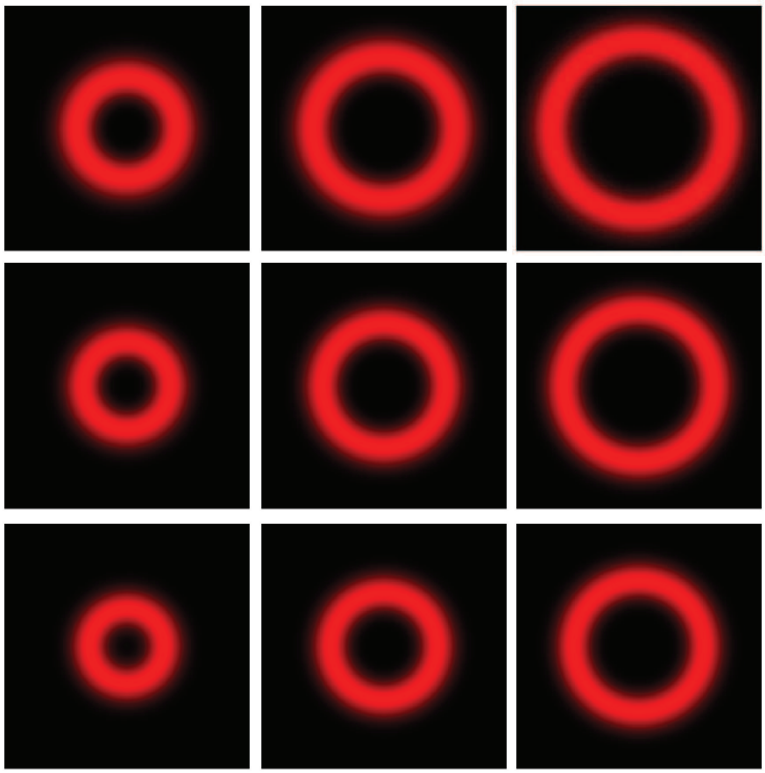

Figure 5.7: Theoretical results for far field intensity distribution of the scattered LG beams of different azimuthal indices ($l = 2, 4, 6$) through a RGG plate for different w_0 values 0.496 mm (top), 0.412 mm (middle) and 0.321 mm (bottom).

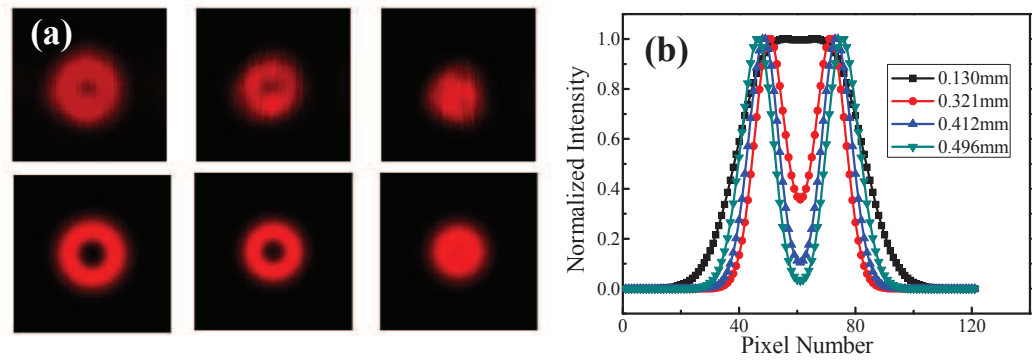

Figure 5.8: (a) The experimental (top) and theoretical (bottom) far field intensity distributions of the scattered LG beam of azimuthal index ($l = 1$) through a RGG plate for different w_0 values, 0.496 mm (left), 0.412 mm (middle) and 0.140 mm (right). (b) The line profiles of theoretical far field intensity distributions of scattered first order vortex for different incident beam widths.

The simulated intensity distributions for LG beams of azimuthal indices $m = 2$, 4, 6 and at different widths of the incident beam are shown in Figure 5.7. The results are in good agreement with the experimental results shown in Figure 5.3.

To quantify the disappearance of the dark core with the decreasing width of incident LG beam in our theoretical plots, we have given the intensity distributions for first order scattered vortex for different incident beam widths in Figure 5.8 (a) and shown that the dark core completely disappears if the beam width is less than 0.140 mm. The line profiles of far field intensity distributions for first order scattered vortex shown in Figure 5.8 (b). From these line profiles also, it is clear that the dark core disappears if incident beam width is less than 0.130 mm. One can obtain the similar results for the scattered BG beams also, as BG beams can be represented by shifted Hermite-Gaussian beams.

5.4 Conclusion

We have experimentally generated the ring-shaped beams by collecting the scattered light of LG and BG beams. We have also studied the dependence of ring-shaped beams on the speed of the GGP and the width of incident light beam. We theoretically verify the results using the propagation of partially coherent standard or elegant LG beams. The generated ring-shaped beams may be of importance in optical trapping experiments. The use of these beams for optical trapping experiments were preferable at higher speeds of the RGG plate as the beams get more and more smooth.

Chapter 6

Vorticity of the Scattered Optical Vortices

Optical vortices are the twisted light beams recognized by their helical wave fronts due to azimuthal phase variation around the point of darkness [14, 29]. They carry an orbital angular momentum (OAM) of $m\hbar$ per photon where m is order of the vortex [16, 64, 141]. The spin angular momentum of light is related to polarization that has two dimensional basis whereas the OAM is related to the spatial mode and forms an infinite dimensional basis. This kind of multi-dimensionality offers a realization of d-dimensional qudits that increases the channel capacity in quantum communication [18, 142]. In the case of classical communication once again, the number of spatial modes available have been utilized to enhance the data capacity in fibers [23, 24, 26]. They have also been used for free space communication [30, 143]. However for communication, it is desirable to encode the information in a variable whose value remains unaffected by the scattering. Therefore, the effect of scattering on coherence for single-photon communication using orbital angular momentum states has been investigated theoretically [32] along with their propagation through a Kolmogorov type of atmospheric turbulence [144].

In this chapter, we experimentally as well as theoretically show that the ring shaped beams formed by the speckles of scattered optical vortices have the same vorticity as the incident optical vortex [139]. To confirm their vorticity, we try the traditional interferometric technique and the obtained results are discussed in section 6.1. However, we cannot assure the vorticity just by seeing these fringes. As an alternative, we use the properties of a classical non-separable state of polarization and OAM [145, 146] to confirm the vorticity. A brief introduction to classical entanglement is given in section 6.2. Our experimental set up,

the confirmation of vorticity and the theoretical analysis are discussed in sections 6.3, 6.4 and 6.5 respectively. Finally, we conclude in section 6.6

6.1 Interferometry of a scattered optical vortex

We start our experiments with the scattering of a vortex beam and vortex-vortex interferometry for both the coherent and the collimated scattered optical vortex beams in a Mach-Zehnder interferometer. First, we scatter a vortex beam embedded in a host Gaussian beam of width $w_0 = 1.92$ mm through a ground glass plate (GGP) and collimate the scattered light using a lens combination as shown in Figure 6.1.

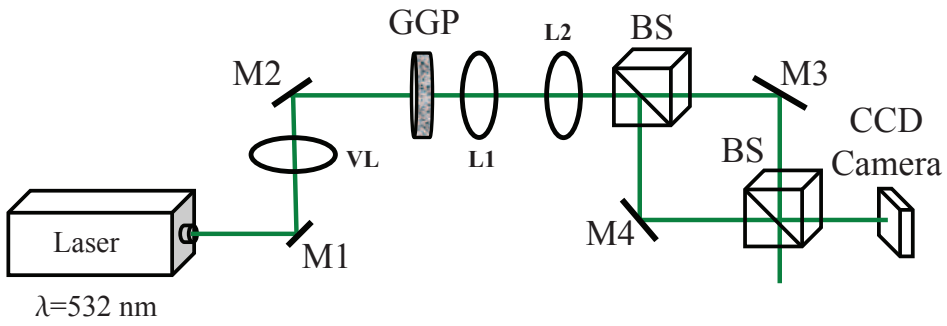

Figure 6.1: The experimental set up for scattering the vortex beam and to observe the vortex-vortex interference fringes. M1, M2, M3, M4 - mirrors; VL - Vortex lens; BS - Beam Splitter; L1, L2 - Plano-convex lenses.

Figure 6.2 shows the intensity distributions of a scattered optical vortex of order 2 at different positions from the scattering plane i.e. after the GGP, immediately after the lens placed at a distance from the GGP, and at the Fourier plane respectively from left to right for zero and non-zero speeds of the GGP. It can be seen that there is no trace of the vortex beam after the GGP as well as immediately after the lens as the phase of the beam gets completely randomized. The speckles got averaged out at the non-zero speed of GGP and provide flat intensity distribution. However, when probed at the Fourier plane, we observe a ring shaped beam.

The collimated scattered beam interferes with itself and produce a fringe pattern when phases are matched from speckle to speckle and then, the GGP is removed to observe the fringes for a coherent vortex beam. The corresponding interference fringes for both, coherent and scattered vortex beams of orders 0–3 have been shown in Figure 6.3. One needs to

match every speckle with its copy present in another arm of the interferometer to get the macroscopic fringes with scattered light. It is clear from the figure that there is a vast similarity in interferograms of coherent and scattered light beams. In both the cases, the number of fringes with discontinuity are equal to the order of the vortex. However, one cannot

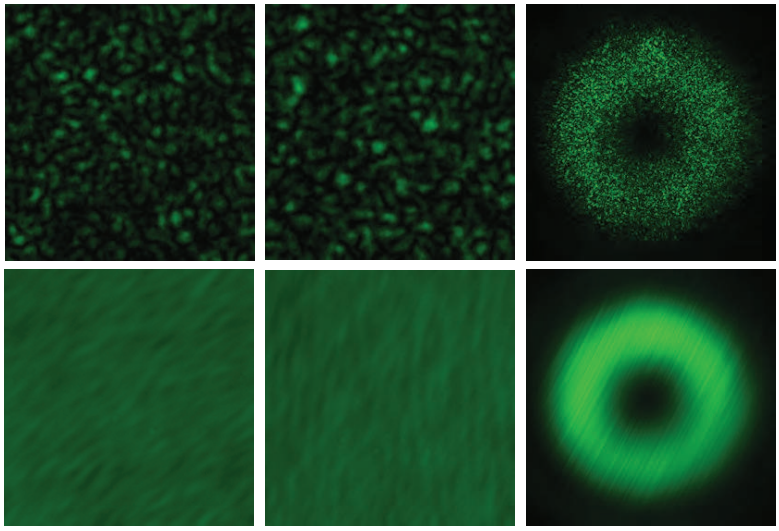

Figure 6.2: The intensity distributions of a scattered optical vortex of order 2 after the GGP (left), immediately after the lens (middle) and the Fourier plane (right) correspond to different speeds of the GGP (top) 0 cm/s and (bottom) 194.7 cm/s.

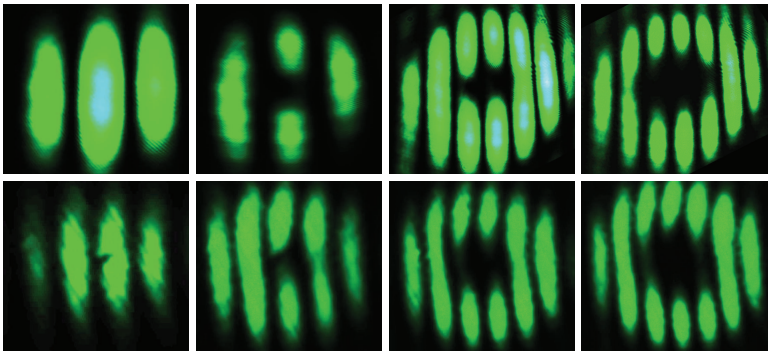

Figure 6.3: Experimentally obtained interference fringes for coherent (top) and scattered (bottom) optical vortex beams of order $m = 0$–3 (from left to right).

confirm the vorticity with these results as the fringe separation and shape change rapidly with a small spatial shift between the two beams of the interferometer. In the case of coherent beam, the fringe pattern changes to oppositely oriented fork fringes, a characteristic of vortex-

vortex interferometry while for the collimated scattered light, it completely disappears due to mismatch from speckle to speckle. Therefore, we look for an alternative method that uses the properties of a non-separable state of polarization and OAM to find the azimuthal phase structure in the scattered optical vortices.

6.2 Entanglement in classical optics

Before we go for the experimental results let us describe briefly about the classical non-separable state of light. A combined system is said to be entangled when its state cannot be expressed as a product of states corresponding to the individual sub systems [147]. One generally uses the entanglement between two spatially separated particles in the same degree of freedom such as spin or polarization. However, one can also have hybrid entanglement in which two degrees of freedom of a single particle or two particles are entangled [148]. This arises due to the non-separability of two degrees of freedom. However, it is not an exclusive property of a quantum system. Similar kind of non-separability can be seen in classical optics, for example radially polarized light beams [149]. This quantum like classical entanglement has been receiving a lot of attention in recent years [145, 150–153]. These non-separable states of light are shown to violate Bell like inequality [154, 155]. Furthermore, they find applications in polarization metrology and ultra sensitive angular measurements [156, 157]. A classical light beam with a non-separable state of polarization and OAM [145] can be represented as

$$E(x,y) = \hat{e}_x LG_0^m(x,y) + \hat{e}_y LG_0^{-m}(x,y) \tag{6.1}$$

where $\hat{e}_x$ and $\hat{e}_y$ are horizontal and vertical polarization states of the light. $LG_0^{\pm m}(x,y)$, Laguerre-Gaussian modes with azimuthal index m and radial index 0 correspond to the field distributions of two equal and oppositely charged optical vortices. This kind of non-separability is also called non-quantum hybrid entanglement [145, 146]. These LG modes, which are OAM states of light can be represented on an OAM Poincaré sphere [158, 159]. All points on this Poincaré sphere can be realized by projecting the above non-separable beam to corresponding polarizations. The projection to horizontal (vertical) polarization gives an optical vortex of order m $(-m)$ while to diagonal and anti-diagonal polarizations will give the superposition of two vortices with the same order but opposite in sign, and can be written as

$$E_D(x,y) = (\hat{e}_x + \hat{e}_y)(LG_0^m(x,y) + LG_0^{-m}(x,y)), \tag{6.2}$$

$$E_A(x,y) = (\hat{e}_x - \hat{e}_y)(LG_0^m(x,y) - LG_0^{-m}(x,y)). \tag{6.3}$$

This superposition of states contains the characteristic of azimuthal phase in their intensity distribution with $2m$ number of petals for the vortex of order m. We follow the same logic in our experiment. We scatter a non-separable state through the GGP and collect part of the light with a plano-convex lens. We get two speckle patterns corresponding to two vortices having orthogonal polarizations which generate ring shaped beams in the Fourier plane. If these partially coherent beams with dark core have azimuthal phase, their superposition must give the petals provided the polarization of both the beams is same. These petals help us in measuring the order of scattered vortex that is half of the number of petals. The

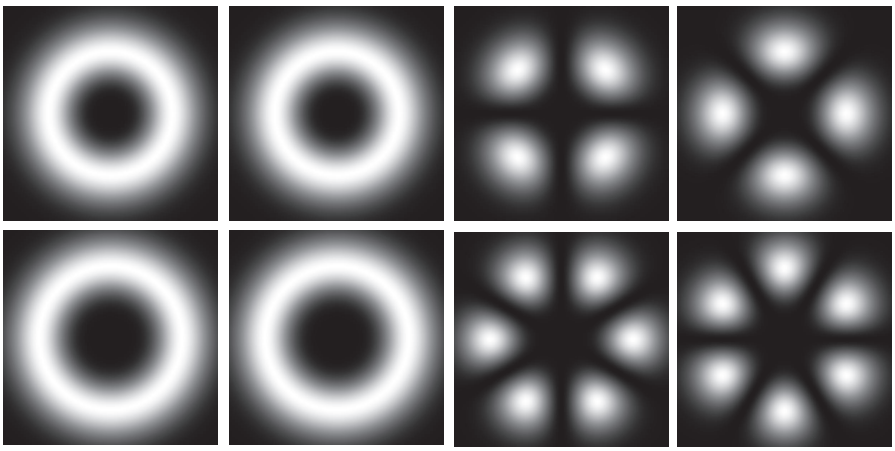

Figure 6.4: The theoretical intensity distributions of a non separable state of polarization and OAM for the different projections – horizontal, vertical, anti–diagonal and diagonal from left to right of $m = 2$ (top) and 3 (bottom).

theoretical intensity distributions corresponding to projections to the different polarizations for a non-separable state have been given in Figure 6.4. The experimental set up and the corresponding results have been explained below.

6.3 Experimental set up

Our experimental set up for the observation of vorticity in scattered optical vortices is shown in Figure 6.5. We have used a diode pumped solid state laser (Verdi 10) of wavelength 532 nm. The light beam passes through a half wave plate whose fast axis is oriented at 22.5° that converts the polarization from vertical to diagonal. Then it passes through a modified polarizing Sagnac interferometer [10] containing a vortex lens of order $m = 1$, 2 & 3. The beam coming out of the interferometer is a non-separable state of the polarization and the

spatial mode. This beam is scattered through a ground glass plate rotating at a constant speed of 194.7 cm/s. The constant rotation of GGP helps in averaging out the speckles and

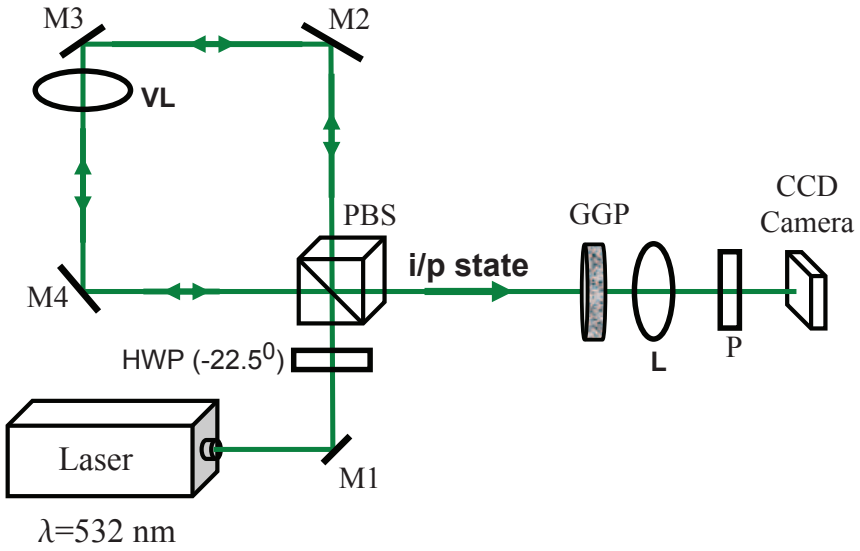

Figure 6.5: The experimental set up for observing the vorticity in scattered optical vortex. M1, M2, M3, M4 - mirrors; HWP - half wave plate; PBS - polarizing beam splitter; VL - vortex lens; i/p state - non–separable state; GGP - ground glass plate; P - polarizer; L - plano convex lens.

reduces the noise while imaging them [72, 73]. The scattered light consists of two orthogonally polarized speckle patterns corresponding to the two oppositely charged vortices. It is focused with a plano-convex lens (L) of focal length 20 cm. Before recording the far field intensity distributions with a CCD camera, we have used a polarizer P to project the output state in different polarizations. The lens is placed at a distance of 22 cm from the GGP and the position of camera has been adjusted to get the geometrical focus. One should note that the geometrical focus of lens shifts towards the lens with decrease in the amount of light collected [140, 160]. We have collected the scattered light with a lens of aperture 2.5 cm to observe the intensity distribution at the Fourier plane.

6.4 Confirmation of vorticity

Figure 6.6 shows the experimentally observed far field intensity distributions of the projections in different polarizations for a light beam obtained by the scattering of a non-separable beam with vortices of orders 2 (top) and 3 (bottom). Since the two orthogonally polarized

speckle patterns never interfere, the far field intensity distribution of the scattered non-separable beam is similar to an optical vortex beam. If we project on horizontal (vertical) polarization, it looks like a vortex beam of order $m(-m)$ (first and second columns). While

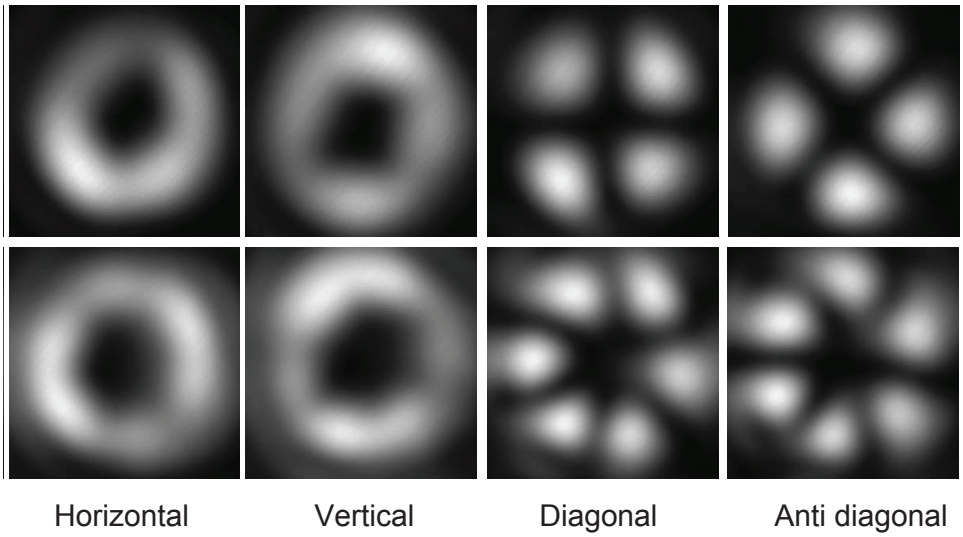

Figure 6.6: Experimentally obtained far field intensity distributions for different projections in polarization after scattering through a ground glass plate. These results correspond to the non-separable states with $m = 2$ (top), 3 (bottom) for w_0=1.92 mm.

projection to any arbitrary polarization results into conversion of two orthogonal polarization states to non-orthogonal and the two vortices start interfering with each other. This superposition gives the petal structures in the far field intensity distributions (third and fourth columns). The petal structures are very clear and look similar to the theoretical intensity distribution for coherent beams as shown in Figure 6.4. These petals confirm the presence of azimuthal phase in the scattered beam.

6.5 Theory

For theoretical analysis, we start with the electric field of an optical vortex of azimuthal index m embedded in a host Gaussian beam of width w

$$E(x, y) = (x + iy)^m e^{-\frac{x^2+y^2}{w^2}}. \tag{6.4}$$

The random medium introduces δ-correlated Gaussian random function to the beam passing through it. This can be achieved numerically by taking the convolution between a 2-D spatial

random function Rand(x, y) and a Gaussian correlation function $C(x, y)$ [72, 73]:

$$\phi(x, y) = C(x, y) * \text{Rand(x, y)} \tag{6.5}$$

where $*$ represents the 2-D convolution between the two functions. The Gaussian correlation function is defined as

$$C(x, y) = e^{-((x_1-x_2)^2+(y_1-y_2)^2/\sigma^2)} \tag{6.6}$$

where σ is the correlation width. Now, the electric field of an optical vortex after scattering through a GGP plate is given by [112]

$$E'(x, y) = E(x, y)e^{i\phi(x,y)} \tag{6.7}$$

where $\phi(x, y)$ is random phase introduced by the GGP to the vortex. The results have been simulated using this random phase distribution.

Figure 6.7 shows the far field intensity distributions for the superposition of two equal and oppositely charged scattered vortices with $m = 2$ and 3 corresponding to the projections on different polarization states. The constant rotation of the GGP has been taken into account by the incoherent addition over 100 frames. The results are in good agreement with the experimental results shown in Figure 6.6. We have used the non-separable beam of polarization and OAM in order to make superposition of two scattered vortices in our experiment. These results confirm the presence of vorticity in the scattered vortex beams.

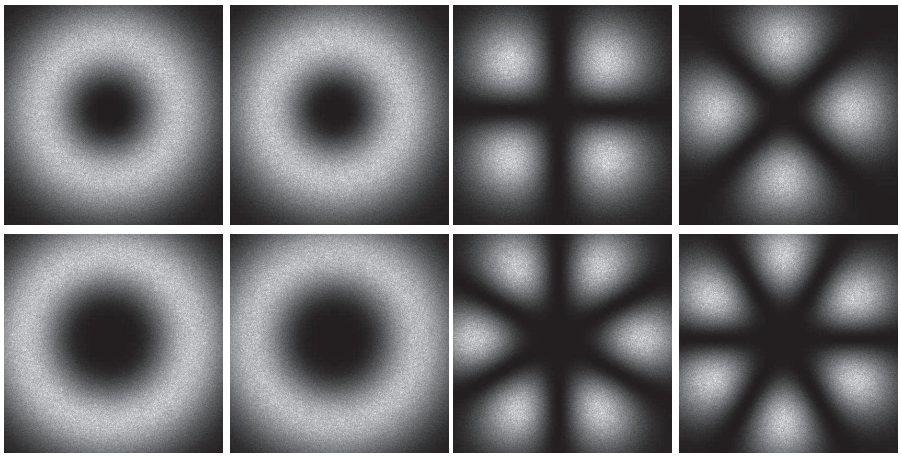

Figure 6.7: The theoretical far field intensity distributions that correspond to the images shown in Figure 6.6.

We also study the effect of speed of rotating GGP on the recovered vorticity. The corresponding results have been shown in Figure 6.8 along with the simulated intensity distributions. The speckles get disappeared with the increase in speed of the GGP due to the

averaging of speckles. For the averaging to occur, one should consider the exposure time of CCD camera used for the imaging that should be much greater than the time required for the GGP to complete one rotation (t_{rot}). The number of frames over which the incoherent addition should be done for a given exposure time (t_{expo}) of the CCD camera is given by $N = t_{expo}/t_{rot}$. It can be seen from the non-varying intensity distributions in a given plane with the speed.

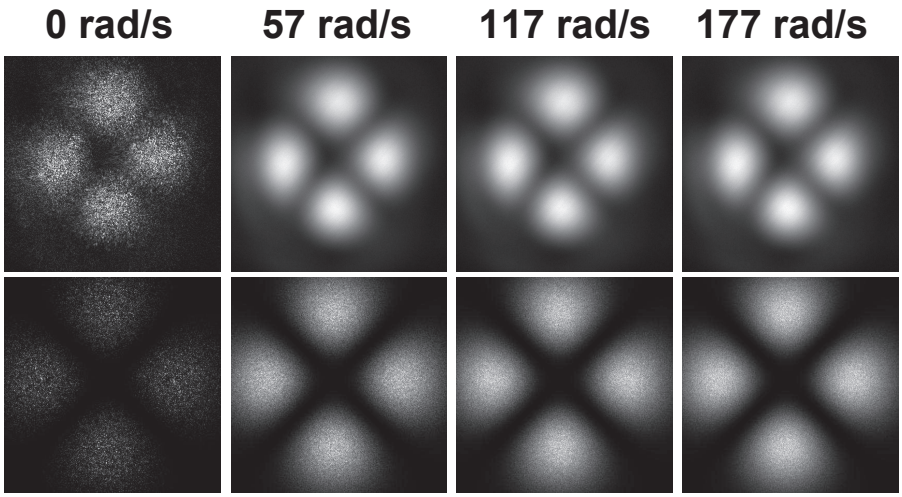

Figure 6.8: The experimental (top) and simulated (bottom) far field intensity distributions for the projection on diagonal polarization of a scattered non-separable light beam of $m = 2$ at different speeds of the GGP given at top of the figure.

We also observe that the topological charge of scattered light is independent of the amount/direction of scattered light collected by the lens. Thus the topological charge or vorticity can serve as a better information carrier due to its robust nature against the scattering. One can also make a number of copies by collecting different parts of the scattered light. This may increase the use of topological charge in public communication systems.

6.6 Conclusion

We have experimentally demonstrated the recovery of vorticity present in the scattered vortices using the properties of a non-separable state of light. The experimental results have been verified with the theoretical analysis by taking into account random phase introduced by the GGP. These results may boost the application of the optical vortex beams as information carriers.

Chapter 7

Perfect Optical Vortices and the Non-Diffracting Speckles

An optical vortex beam is characterized by a doughnut–shaped intensity distribution with a phase singularity, and hence zero field amplitude, at the center. These beams carry an orbital angular momentum (OAM) of $l\hbar$ per photon due to which they found variety of applications in both the science and the technology such as particle manipulation and information theory [18, 20, 23, 27, 30]. The size of vortex beams strongly depends on the topological charge. The intensity distribution of vortex beams has been studied using two measurable parameters, inner and outer radii as it looks like an annular ring and described in chapter 2. We have also studied their variation theoretically as well as experimentally with the order [99].

In order to control the intensity distribution of vortices, perfect optical vortex (POV) beams have been introduced [91]. These beams have a topological charge independent intensity distribution and contain an annular ring of constant radius [92]. The POV beams can be generated using a special kind of holographic phase masks [91]. However, one can generate these beams easily with the use of spatial light modulator (SLM) [93]. Recently, POV beams were generated using the Fourier transform of non-diffracting Bessel-Gauss (BG) beams [94, 95]. POV beams have been used to study the dynamics of micro-sized particles trapped in them [93]. These beams are also known as annular vortices and radius of the annular ring can be controlled simply by changing the axicon parameter while the width can be controlled by changing the host Gaussian beam size. Apart from this, the invariant intensity distribution allows the researchers to verify that whether a physical process is due to the field mode or because of the intensity distribution. Recent study on the scattering of optical vortex beams shows that the speckle size decreases with the order which may be due

to increase in the area of illumination on the rough surface [99, 161] as discussed in chapter 4. Here, we show that the speckle distribution follows the intensity distribution rather than the field mode by quantifying the size of speckles obtained after the scattering of POV beams.

The generation and the evolution of random non-diffracting fields are getting a lot of attention in recent years [162–165]. Here, we generate these fields by the Fourier transform of speckles obtained by the scattering of POV beams through a ground glass plate (GGP). We also study their non-diverging nature i.e. diffraction free propagation by quantifying the speckle size. In this chapter, we describe the generation of POV beams in section 7.1 and their scattering in sections 7.2 and 7.3. Finally we conclude the chapter in section 7.4.

7.1 Generation of perfect optical vortices

We start with the electric field amplitude of a POV beam of topological charge m and ring radius r_r [94, 95]

$$E(r,\theta) = A_0 \exp(im\theta) \exp\left(-\frac{r^2}{w_0^2}\right) I_m\left(\frac{2r_r r}{w_0^2}\right) \tag{7.1}$$

where A_0 is the field amplitude and I_m is the modified Bessel function of first kind of order m. This field can be generated by taking the Fourier transform of a BG beam whose field amplitude in the cylindrical coordinate system (ρ, ϕ, z) is given by [166, 167]

$$E(\rho,\phi,z) = J_m(k_r\rho) e^{im\phi + ik_z z} e^{\left(-\rho^2/w_g^2\right)} \tag{7.2}$$

where $w_0 = 2f/kw_g$ and w_g is the width of a Gaussian beam used to generate the BG beam. k_r and k_z are radial and longitudinal wave vectors. k_r controls the ring radius of the POV beam through $r_r = k_r f/k$, k being the total wave vector and f being the focal length of the lens used to take the Fourier transform of BG beam. The BG beams can be generated in the laboratory using a phase mask formed by the interference of axicon (e^{iar}) and spiral ($e^{im\theta}$) functions, where $a = k\tan^{-1}(\mathrm{k_r/k_z}) = k\sin^{-1}(\mathrm{k_r/k}) = k\cos^{-1}(\mathrm{k_z/k})$ is the axicon parameter. This axicon parameter controls the radius of the ring present in POV beams. The width of annular ring corresponding to POV beams is inversely proportional to the size of host Gaussian beam (w_g) used to generate the BG beams.

Our experimental set up for the generation of POV beams is shown in Figure 7.1. We have used an intensity and frequency stabilized He-Ne laser (Spectra Physics 117 A) of wavelength 632.8 nm and power 1 mW. The laser beam has been propagated in free space before reaching to the spatial light modulator (SLM) (Holoeye LCR-2500) to increase the beam width to 1.5 mm which is required for better intensity modulation. Different computer

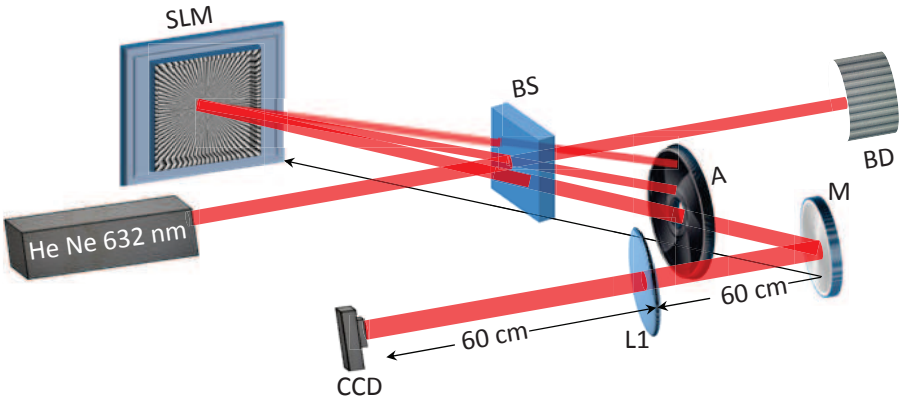

Figure 7.1: The experimental set up for the generation of POV beams using the Fourier transform of BG beam. Here, M-Mirror, SLM-Spatial light modulator, BS-Beam splitter, BD-Beam dumper used to block the unwanted beams, L1-plano convex lens of focal length $f_1 = 60$ cm.

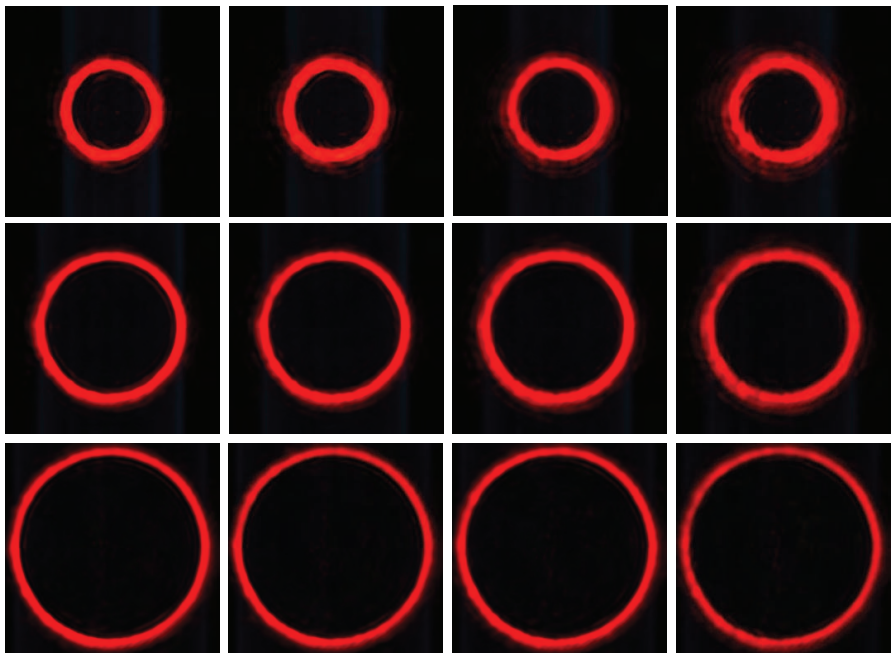

Figure 7.2: Experimentally obtained intensity distributions for POV beams of orders $m = 0, 2, 4, 6$ (from left to right) at different axicon parameters of 7.29 /mm (top), 10.93 /mm (middle) and 14.58 /mm (bottom).

generated holograms corresponding to the BG beams of different orders are introduced to the SLM through a computer. The generated BG beam in the first diffraction order is selected with an aperture (A). Its Fourier transform using a lens (L1) of focal length 60 cm placed at a distance of 60 cm from the SLM produces the POV beam of the same order. For generating ideal BG beams, one needs to have a Gaussian beam of infinite width and very high axicon parameter that gives POV beams of all orders. However, the ring radius of POV beams increases with the increase in axicon parameter. Thus, we have to compromise between the size of POV beams and the maximum order upto which they can be generated. We have used axicon parameters a = 14.58, 17.01, 21.87 /mm for scattering the POV beams through a GGP. The generated POV beams have been recorded using an Evolution VF color cooled CCD camera.

Figure 7.2 shows the intensity distributions of POV beams of different orders m =0, 2, 4, 6 for various axicon parameters (a =7.29, 10.93, 14.58 /mm) obtained by taking the Fourier transform of the BG beams, generated by a phase mask used with the SLM. For a better comparison, we have considered the same scale for all the images. One can clearly see from the figure that the intensity distribution is invariant with order and increases with increase in axicon parameter. It can also be observed that the POV beams are almost covering the entire CCD camera at a =14.58 /mm, which didn't allow us to record them at higher axicon parameters.

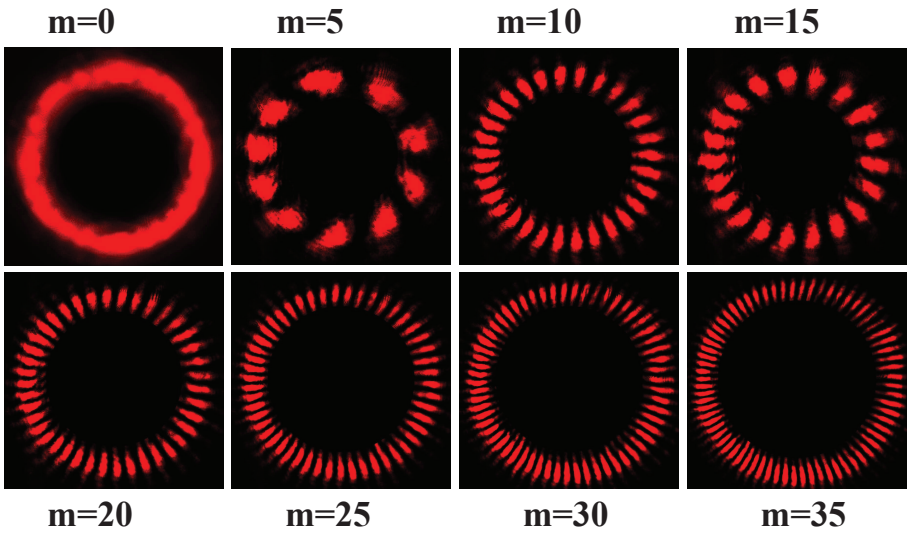

Figure 7.3: The experimentally observed lobes due to the superposition of two equal and oppositely charged POV beams of given orders.

The vorticity of POV beams has been verified using the interferometry of two equal

and oppositely charged vortices. We have aligned the POV beams in a Mach-Zehnder interferometer with a dove prism in one of the arms to invert the charge. The two outputs of interferometer contain superposition of two equal and oppositely charged POV beams of order m and give $2m$ number of lobes due to the presence of azimuthal phase [168]. These lobes have been collected with a lens of focal length 50 cm after the interferometer in order to record them within the CCD camera and shown in Figure 7.3. These images also show that the size of the POV beam is invariant up to the order m =20 and increased slightly when we increase m from 20 to 35. This implies that for a given axicon parameter, we can generate the POV beams upto the order of 20.

7.2 Scattering of POV beams: a comparison with ordinary vortices

After the generation of POV beams, a ground glass plate (GGP) is placed at the plane of generation to study their scattering [72, 73] as shown in Figure 7.4. Figure 7.5 shows the

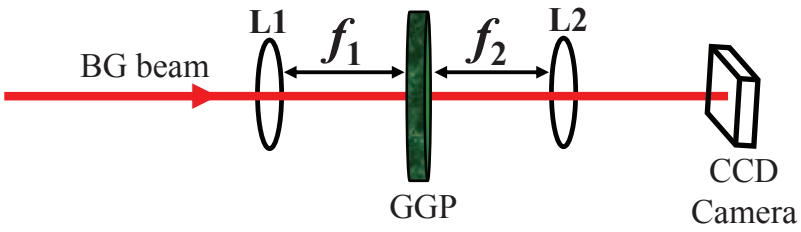

Figure 7.4: The experimental set-up for the scattering of POV beams through the ground glass plate and to generate the non-diffracting speckles. Here, L1 and L2 are plano-convex lenses of focal lengths $f_1 = 60$ cm and $f_2 = 50$ cm respectively.

speckle distributions obtained by the scattering of both ordinary Laguerre–Gauss beams and perfect optical vortex beams. The CCD camera is placed at a distance of 18 cm from the GGP for recording the speckles (without lens L2). It is clear from the figure that the size of the speckles decreases with the order for ordinary vortices whereas it remains same for POV beams. One should note that the intensity distribution of a POV beam is independent of the order while for the ordinary vortices it depends on the order. Therefore, one can say that the speckle distribution follows the intensity distribution falling on the random media rather than the field mode. The speckles corresponding to the POV beams also show structured

patterns which are same for all the orders at a given axicon parameter.

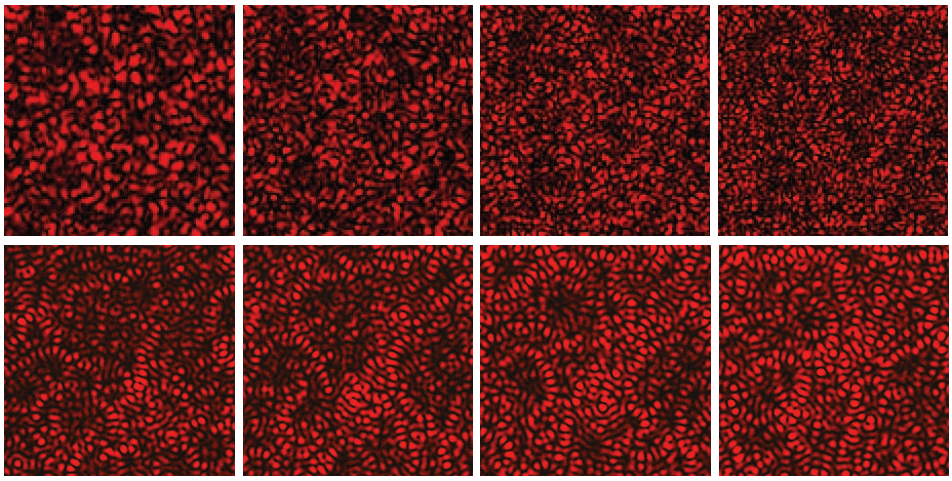

Figure 7.5: The speckle patterns correspond to scattering of the ordinary optical vortices (top) and the POV beams (bottom) of orders $m = 0$–3 (from left to right).

7.3 Non-diffracting speckles

Now, we show that the Fourier transform of speckles generated by the scattering of POV beams gives the non-diffracting speckle patterns. The Fourier transform has been taken using a lens (L2) of focal length 50 cm placed at a distance of 50 cm from the GGP. We have recorded these non-diffracting speckles at different distances from the lens starting from 12 cm to 57 cm at the intervals of 5 cm with a CCD camera of pixel size 4.65 μm. The recorded speckle patterns generated by the scattering of POV beams of orders m =2, 5, 8 and axicon parameter of 14.58 /mm are shown in Figure 7.6. It is clear from figure that the speckle size is invariant with propagation distance at a given axicon parameter for all orders. This confirms the non-diffracting or non-diverging nature of the generated speckles.

Figure 7.7 shows the intensity distributions of these speckles corresponding to the scattering of POV beams of orders m = 0, 3, 6, 9 with different axicon parameters at a given propagation distance of 37 cm from the collecting lens (L2). The size and distribution of speckle fields are independent of the order of POV beams. This confirms that the average speckle size and their distribution are mainly controlled by intensity distribution falling on the ground glass rather than its field distribution. With the increase in axicon parameter, the radius of POV beams increases that effectively increases the area of illumination on the GGP which controls the speckle size. The average size of speckles decreases with increase in

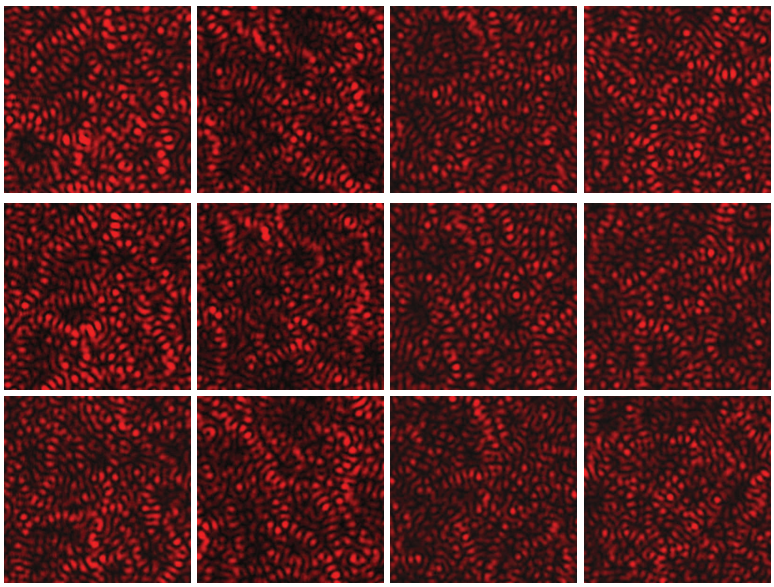

Figure 7.6: The intensity distributions of non-diffracting speckles obtained by taking the Fourier transform of speckles generated by the scattering of POV beams of orders m =2, 5, 8 (from top to bottom) at an axicon parameter of a = 14.58 /mm corresponding to different propagation distances of z = 0.12 m, 0.27 m, 0.42 m and 0.57 m (from left to right).

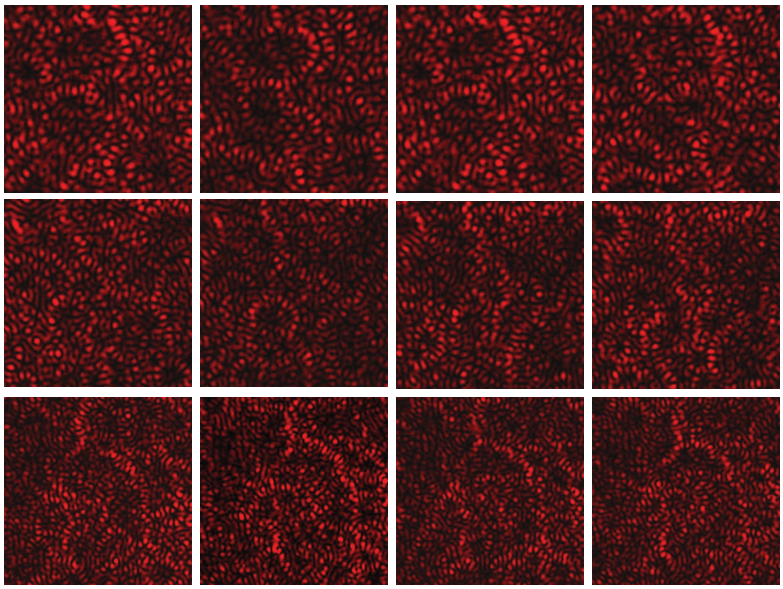

Figure 7.7: The intensity distribution of non-diffracting speckles obtained by taking the Fourier transform of speckles generated by the scattering of POV beams of orders m =0, 3, 6, 9 (from left to right) and at axicon parameters a =14.58, 17.01, 21.87 /mm (from top to bottom).

the axicon parameter due to the increase in area of the annular ring. As the phase singular density present in the speckle fields is inversely proportional to speckle size [72, 73], it can be controlled easily by changing the axicon parameter in our study.

We have verified the diffraction-free nature of speckles by quantifying the speckle size also using intensity auto-correlation method that calculates the correlation of speckles with themselves [99]. In this method, we fix one image of the speckles and observe its correlation

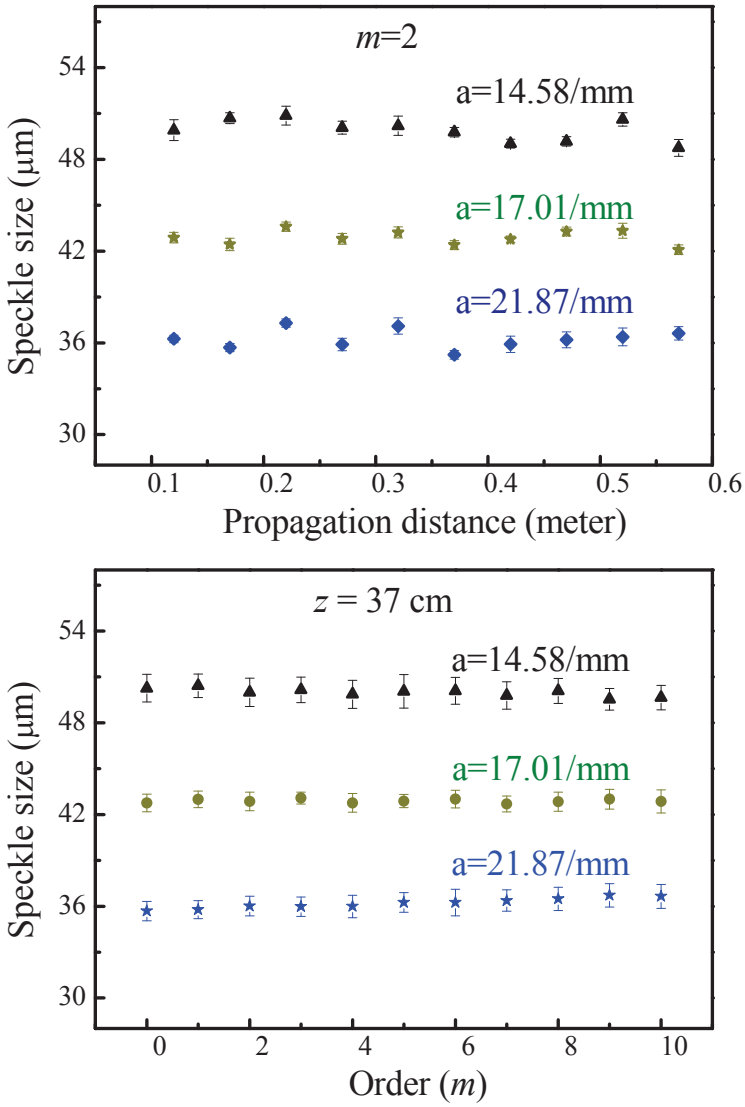

Figure 7.8: The variation of speckle size with the propagation distance (top) and the order (bottom) at different axicon parameters showing no difference with respect to either of them.

numerically with a number of images shifted in position. These shifts can be made pixel by pixel in both the transverse directions. We plot the results as a function of the shift. The

correlation factor is maximum if the two speckle distributions are completely overlapped and it decreases with the decrease in overlap. The correlation factor becomes zero if their overlap is less than the speckle size due to the random nature of speckles. The correlation curve has a Gaussian distribution whose full width at half maximum (FWHM) gives the speckle size in any of the transverse directions. Here, we have considered the normalized speckle patterns to determine the speckle size as they are overfilling the CCD camera. We have considered the average over ten images to measure the speckle size.

Figure 7.8 shows the variation of average speckle size with respect to both the propagation distance and the topological charge or order of the POV beams. The results show that for a given axicon parameter, the speckle size obtained by the scattering of a POV beam of order m =2 remains constant for all the propagation distances. We also verify that the speckle size is independent of the order for different axicon parameters at a given propagation distance, in this case z =37 cm. Thus confirming that the physical process of scattering is intensity dependent.

7.4 Conclusion

We experimentally generate the POV beams by taking the Fourier transform of the BG beams. We show that the distribution of speckles is controlled by the intensity distribution of the incident beam falling on the rough surface rather than the field distribution. The Fourier transform of the speckles generated by scattering of the POV beams gives the non-diffracting fields i.e. non-diverging speckles. These results may find applications in cryptography [169].

Chapter 8

Summary and Scope for Future Work

This thesis deals with the optical vortex beams and their scattering through random media. The optical vortices are generated using computer generated holograms as well as using a spiral phase plate. We also study the generation and scattering of a new type of vortices – perfect optical vortices (POV). The POV beams are generated using the Fourier transform of Bessel-Gauss beams. We use a ground glass plate for scattering the light beams. A novel description has been given for the intensity distribution of vortex beams along with their free space propagation. We use the effect of an astigmatic system on a pair of vortices embedded in a single host Gaussian beam to determine the net charge as well as the individual charges.

Next, we scatter the vortex beams through a GGP and record the generated speckle patterns. The intensity auto-correlation measurements show that the size of speckles as well as their divergence decrease with the increase in order of the vortex. We model the GGP using a δ-correlated Gaussian function which can be realized by the convolution of a 2-D spatial random function and the Gaussian correlation function. We also show how to recover the vorticity of a light beam after scattering using a single plano-convex lens. The recovered vorticity is confirmed using the properties of classical non-separable states of light.

At last, we generate the perfect optical vortices having order independent intensity distribution and scatter them through a GGP. The generated speckles are used to produce the non-diffracting random fields.

8.1 Summary of the work-done

Chapter 1 provides a brief introduction for the optical vortices and their generation using different techniques. We also describe briefly the speckles which are natural sources for

vortices along with scattering of the optical vortices. We introduce the concept of perfect optical vortices, whose core size is independent of the topological charge, and the methods for generating them in the laboratory.

In chapter 2, we discuss the intensity distribution of vortex beams using two new and novel parameters, inner and outer radii. We give the exact analytical expressions for these two parameters in terms of the order and verified using the numerical and the experimental results. Next, we have described the free space propagation of inner and outer radii that provides the divergence of vortex beams. We also show that the divergence varies as the corresponding radii at the source plane with the order. It helps in designing the fibres for vortex modes.

Chapter 3 discusses the propagation of a pair of vortices with arbitrary charges and separation through an astigmatic optical system, i.e a tilted lens. We provide an exact analytical equation for the propagation that uses incomplete two variable Hermite polynomials, for the first time in Optics. The intensity distribution of a beam past the tilted lens is used to find the net and individual charges embedded in the beam. The special kind of rectangular razor-blade structures are observed for the oppositely charged pair of vortices. The number of lobes present along the length and breadth of the structure give the individual magnitudes and their orientation gives the signs. In the case of vortices with same sign, the asymmetry present in the lobes gives the information about individual charges. We present the theoretical results along with the experimental verification.

The speckles generated by the scattering of higher order optical vortex beams through a ground glass plate are shown in chapter 4. The auto-correlation measurements show that the size of speckles decreases with the increase in order of the vortex. The propagation dynamics of speckles shows that the divergence of speckles decreases with the order. The scattering medium, i.e. a ground glass plate is modelled as δ-correlated Gaussian function and the results are verified. We have also discussed about the spatial intensity correlation properties of the scattered optical vortices which are similar to the temporal intensity correlations.

In chapter 5, we generate the ring-shaped beams by collecting the scattered LG and BG beams using a plano-convex lens. We show that the presence of dark core is independent of speed of the GGP. The size and darkness of the core gradually decreases with the decrease in incident beam width which is verified using the line profiles along the center of far field intensity distributions. We also observe that the size of the dark core increases with increase in the azimuthal index. We theoretically verify these experimental results using the propagation characteristics of partially coherent standard LG beams through a linear optical system.

In chapter 6, we recover the vorticity of a scattered vortex beam. After scattering through a random medium, the light beam gets completely randomized (in the form of speckles) and do not have any information regarding the vorticity. However, a plano-convex lens can recover the vorticity when we probe at the focal plane. We confirm the vorticity using the properties of a classical non-separable state of polarization and OAM. This state helps us to obtain the superposition of two equal and oppositely charged vortices which leads to the petal structure, number of petals being equal to twice the order. These petals are the characteristic of the azimuthal phase present in the vortex beams and thus confirm the vorticity.

Chapter 7 is devoted to the generation and scattering of perfect optical vortex beams. We generate these beams using an optical Fourier transform of the BG beams. These beams have topological charge independent intensity distribution and look like a thin annular ring. The radius of the ring is controlled by the axicon parameter and the width of the ring is controlled by the width of the Gaussian beam incident on the spatial light modulator. We confirm the presence of azimuthal phase using the superposition of two equal and oppositely charged vortices. Next, we scatter the POV beams through a ground glass plate and observe that the speckle size is independent of the order. We also show that the Fourier transform of the generated speckles gives the non-diffracting random fields i.e. speckles. We verify the non-diffracting nature by the invariant speckle size with propagation. These results may find applications for authentication in cryptography.

8.2 Scope for future work

The intensity distribution of vortex beams has been used for the geometrical characterization of coherence vortices, singularities present in the cross-correlation function of two fields obtained by the scatetring of two optical vortices having different topological charges [170]. It can also be used to generate the perfect coherence vortices. Since, we have studied the generation and scattering of POV beams, we would like to verify if the correlation singularities between two scattered POV beams have the order independent distribution. If so, we could extend our study to characterize their properties such as radius and width of the ring. Preliminary experiments have already been performed for this study.

We have studied the spatial intensity correlation properties of scattered optical vortices of different orders, however, to understand its properties, one needs a detailed study incorporating the effect of GGP. It would be worthwhile to see the dependence of intensity correlations on the degree of polarization. To take up this study, one can make the light

beams with varying degree of polarization using a classical non-maximal non-separable state of polarization and OAM.

The optical characterization of any material can be done with the use of Mueller matrix. We have proposed and verified a novel method for the determination of Mueller matrix using Simon-Mukunda polarization gadget or SU (2) universal polarization gadget [171]. This gadget can be used for quantum process tomography along with quantum state tomography for polarization entangled photons.

We plan to study the spontaneous parametric down conversion of POV beams through a second order non-linear BBO crystal [172]. It may be helpful in generating the higher order OAM spectra with a controlled spatial distribution. It can also be used to verify the dependence of down conversion on the spatial mode of pump light beam.

Bibliography

[1] H. J. Lugt, *Vortex flow in nature and technology,* New York, Wiley-Interscience, 1983, 305 p. Translation. **1** (1983).

[2] M. Matthews, B. Anderson, P. Haljan, D. Hall, C. Wieman, and E. Cornell, *Vortices in a Bose-Einstein condensate,* Physical Review Letters **83**, 2498 (1999).

[3] S. Prabhakar, R. P. Singh, S. Gautam, and D. Angom, *Annihilation of vortex dipoles in an oblate Bose–Einstein condensate,* Journal of Physics B: Atomic, Molecular and Optical Physics **46**, 125302 (2013).

[4] A. G. Peele, P. J. McMahon, D. Paterson, C. Q. Tran, A. P. Mancuso, K. A. Nugent, J. P. Hayes, E. Harvey, B. Lai, and I. McNulty, *Observation of an X-ray vortex,* Optics Letters **27**, 1752–1754 (2002).

[5] A. G. Peele, K. A. Nugent, A. P. Mancuso, D. Paterson, I. McNulty, and J. P. Hayes, *X-ray phase vortices: theory and experiment,* Journal of the Optical Society of America A **21**, 1575–1584 (2004).

[6] B. J. McMorran, A. Agrawal, I. M. Anderson, A. A. Herzing, H. J. Lezec, J. J. McClelland, and J. Unguris, *Electron vortex beams with high quanta of orbital angular momentum,* Science **331**, 192–195 (2011).

[7] J. Verbeeck, H. Tian, and P. Schattschneider, *Production and application of electron vortex beams,* Nature **467**, 301–304 (2010).

[8] M. Uchida and A. Tonomura, *Generation of electron beams carrying orbital angular momentum,* Nature **464**, 737–739 (2010).

[9] R. Dorn, S. Quabis, and G. Leuchs, *Sharper focus for a radially polarized light beam,* Physical Review Letters **91**, 233901 (2003).

[10] S. Slussarenko, V. D'Ambrosio, B. Piccirillo, L. Marrucci, and E. Santamato, *The polarizing Sagnac interferometer: a tool for light orbital angular momentum sorting and spin-orbit photon processing,* Optics Express **18**, 27205–27216 (2010).

[11] G. Gbur and T. D. Visser, *Coherence vortices in partially coherent beams,* Optics Communications **222**, 117–125 (2003).

[12] W. Wang, Z. Duan, S. G. Hanson, Y. Miyamoto, and M. Takeda, *Experimental study of coherence vortices: Local properties of phase singularities in a spatial coherence function,* Physical Review Letters **96**, 073902 (2006).

[13] G. Gbur and T. D. Visser, *Phase singularities and coherence vortices in linear optical systems,* Optics Communications **259**, 428–435 (2006).

[14] A. O'neil, I. MacVicar, L. Allen, and M. J. Padgett, *Intrinsic and extrinsic nature of the orbital angular momentum of a light beam,* Physical Review Letters **88**, 053601 (2002).

[15] G. Molina-Terriza, J. P. Torres, and L. Torner, *Twisted photons,* Nature Physics **3**, 305–310 (2007).

[16] J. P. Torres and L. Torner, *Twisted photons: applications of light with orbital angular momentum* (John Wiley & Sons, 2011).

[17] L. Allen, S. M. Barnett, and M. J. Padgett, *Optical angular momentum* (CRC Press, 2003).

[18] A. Mair, A. Vaziri, G. Weihs, and A. Zeilinger, *Entanglement of the orbital angular momentum states of photons,* Nature **412**, 313–316 (2001).

[19] S. Franke-Arnold, L. Allen, and M. Padgett, *Advances in optical angular momentum,* Laser & Photonics Reviews **2**, 299–313 (2008).

[20] B. Thidé, H. Then, J. Sjöholm, K. Palmer, J. Bergman, T. Carozzi, Y. N. Istomin, N. Ibragimov, and R. Khamitova, *Utilization of photon orbital angular momentum in the low-frequency radio domain,* Physical Review Letters **99**, 087701 (2007).

[21] F. Tamburini, E. Mari, A. Sponselli, B. Thidé, A. Bianchini, and F. Romanato, *Encoding many channels on the same frequency through radio vorticity: first experimental test,* New Journal of Physics **14**, 033001 (2012).

[22] F. Tamburini, B. Thidé, G. Molina-Terriza, and G. Anzolin, *Twisting of light around rotating black holes,* Nature Physics **7**, 195–197 (2011).

[23] N. Bozinovic, Y. Yue, Y. Ren, M. Tur, P. Kristensen, H. Huang, A. E. Willner, and S. Ramachandran, *Terabit-scale orbital angular momentum mode division multiplexing in fibers,* Science **340**, 1545–1548 (2013).

[24] S. Ramachandran and P. Kristensen, *Optical vortices in fiber,* Nanophotonics **2**, 455–474 (2013).

[25] A. Willner, H. Huang, Y. Yan, Y. Ren, N. Ahmed, G. Xie, C. Bao, L. Li, Y. Cao, Z. Zhao *et al.*, *Optical communications using orbital angular momentum beams,* Advances in Optics and Photonics **7**, 66–106 (2015).

[26] C. Brunet, P. Vaity, Y. Messaddeq, S. LaRochelle, and L. A. Rusch, *Design, fabrication and validation of an OAM fiber supporting 36 states,* Optics Express **22**, 26117–26127 (2014).

[27] D. G. Grier, *A revolution in optical manipulation,* Nature **424**, 810–816 (2003).

[28] C. P. Ellington, C. Van Den Berg, A. P. Willmott, and A. L. Thomas, *Leading-edge vortices in insect flight,* Nature **384**, 626–630 (1996).

[29] J. Nye and M. Berry, *Dislocations in wave trains,* Proceedings of the Royal Society of London A: Mathematical, Physical and Engineering Sciences **336**, 165–190 (1974).

[30] G. Gibson, J. Courtial, M. Padgett, M. Vasnetsov, V. Pas' ko, S. Barnett, and S. Franke-Arnold, *Free-space information transfer using light beams carrying orbital angular momentum,* Optics Express **12**, 5448–5456 (2004).

[31] J. Lin, X.-C. Yuan, S. Tao, and R. Burge, *Multiplexing free-space optical signals using superimposed collinear orbital angular momentum states,* Applied Optics **46**, 4680–4685 (2007).

[32] C. Paterson, *Atmospheric turbulence and orbital angular momentum of single photons for optical communication,* Physical Review Letters **94**, 153901 (2005).

[33] P. Martelli, A. Gatto, P. Boffi, and M. Martinelli, *Free-space optical transmission with orbital angular momentum division multiplexing,* Electronics Letters **47**, 972–973 (2011).

[34] F. Tamburini, G. Anzolin, G. Umbriaco, A. Bianchini, and C. Barbieri, *Overcoming the Rayleigh criterion limit with optical vortices,* Physical Review Letters **97**, 163903 (2006).

[35] J. E. Curtis and D. G. Grier, *Structure of optical vortices,* Physical Review Letters **90**, 133901 (2003).

[36] J. E. Curtis and D. G. Grier, *Modulated optical vortices,* Optics Letters **28**, 872–874 (2003).

[37] L. Allen, M. W. Beijersbergen, R. Spreeuw, and J. Woerdman, *Orbital angular momentum of light and the transformation of Laguerre-Gaussian laser modes,* Physical Review A **45**, 8185 (1992).

[38] B. E. Saleh and M. C. Teich, *Fundamentals of photonics* (Wiley New York, 1991).

[39] A. E. Siegman, *Lasers* (University Science Books, 1986).

[40] L. Zhu, Z. Guo, Q. Xu, J. Zhang, A. Zhang, W. Wang, Y. Liu, X. Wang, S. Qu *et al.*, *Calculating the torque of the optical vortex tweezer to the ellipsoidal micro-particles,* Optics Communications **354**, 34–39 (2015).

[41] M. Beijersbergen, L. Allen, H. Van der Veen, and J. Woerdman, *Astigmatic laser mode converters and transfer of orbital angular momentum,* Optics Communications **96**, 123–132 (1993).

[42] M. Padgett, J. Arlt, and N. Simpson, *An experiment to observe the intensity and phase structure of Laguerre-Gaussian laser modes,* American Journal of Physics **64**, 77–82 (2003).

[43] M. Beijersbergen, R. Coerwinkel, M. Kristensen, and J. Woerdman, *Helical-wavefront laser beams produced with a spiral phaseplate,* Optics Communications **112**, 321–327 (1994).

[44] S. Oemrawsingh, J. Van Houwelingen, E. Eliel, J. Woerdman, E. Verstegen, J. Kloosterboer, G. Hooft *et al.*, *Production and characterization of spiral phase plates for optical wavelengths,* Applied Optics **43**, 688–694 (2004).

[45] V. V. Kotlyar, H. Elfstrom, J. Turunen, A. A. Almazov, S. N. Khonina, and V. A. Soifer, *Generation of phase singularity through diffracting a plane or Gaussian beam by a spiral phase plate,* Journal of the Optical Society of America A **22**, 849–861 (2005).

[46] A. V. Carpentier, H. Michinel, J. R. Salgueiro, and D. Olivieri, *Making optical vortices with computer-generated holograms,* American Journal of Physics **76**, 916–921 (2008).

[47] C. Souza and A. Khoury, *A Michelson controlled-not gate with a single-lens astigmatic mode converter,* Optics Express **18**, 9207–9212 (2010).

[48] G. Nienhuis and L. Allen, *Paraxial wave optics and harmonic oscillators,* Physical Review A **48**, 656–665 (1993).

[49] C. Rotschild, S. Zommer, S. Moed, O. Hershcovitz, and S. G. Lipson, *Adjustable spiral phase plate,* Applied Optics **43**, 2397–2399 (2004).

[50] F. Tamburini, E. Mari, B. Thidé, C. Barbieri, and F. Romanato, *Experimental verification of photon angular momentum and vorticity with radio techniques,* Applied Physics Letters **99**, 204102 (2011).

[51] V. Y. Bazhenov, M. Vasnetsov, and M. Soskin, *Laser beams with screw dislocations in their wavefronts,* Journal of Experimental and Theoretical Physics Letters **52**, 429–431 (1990).

[52] N. Heckenberg, R. McDuff, C. Smith, and A. White, *Generation of optical phase singularities by computer-generated holograms,* Optics Letters **17**, 221–223 (1992).

[53] N. Heckenberg, R. McDuff, C. Smith, H. Rubinsztein-Dunlop, and M. Wegener, *Laser beams with phase singularities,* Optical and Quantum Electronics **24**, S951–S962 (1992).

[54] I. M. Firth, *Holography and Computer Generated Holograms* (Mills & Boon, 1972).

[55] B. Brown and A. Lohmann, *Computer-generated binary holograms,* IBM Journal of Research and Development **13**, 160–168 (1969).

[56] N. K. Sheridon, *Production of blazed holograms,* Applied Physics Letters **12**, 316–318 (1968).

[57] U. Efron, *Spatial light modulator technology: materials, devices, and applications* (CRC Press, 1994).

[58] J. W. Goodman, *Introduction to Fourier optics* (Roberts and Company Publishers, 2005).

[59] L. Lesem, P. Hirsch, and J. Jordan, *The kinoform: a new wavefront reconstruction device,* IBM Journal of Research and Development **13**, 150–155 (1969).

[60] P. Vaity, J. Banerji, and R. P. Singh, *Measuring the topological charge of an optical vortex by using a tilted convex lens,* Physics Letters A **377**, 1154–1156 (2013).

[61] S. G. Reddy, S. Prabhakar, A. Aadhi, J. Banerji, and R. P. Singh, *Propagation of an arbitrary vortex pair through an astigmatic optical system and determination of its topological charge,* Journal of the Optical Society of America A **31**, 1295–1302 (2014).

[62] A. Kumar, S. Prabhakar, P. Vaity, and R. P. Singh, *Information content of optical vortex fields,* Optics Letters **36**, 1161–1163 (2011).

[63] S. Prabhakar, A. Kumar, J. Banerji, and R. P. Singh, *Revealing the order of a vortex through its intensity record,* Optics Letters **36**, 4398–4400 (2011).

[64] C.-S. Guo, S.-J. Yue, and G.-X. Wei, *Measuring the orbital angular momentum of optical vortices using a multipinhole plate,* Applied Physics Letters **94**, 231104 (2009).

[65] C.-S. Guo, L.-L. Lu, and H.-T. Wang, *Characterizing topological charge of optical vortices by using an annular aperture,* Optics Letters **34**, 3686–3688 (2009).

[66] Y. Han and G. Zhao, *Measuring the topological charge of optical vortices with an axicon,* Optics Letters **36**, 2017–2019 (2011).

[67] J. Hickmann, E. Fonseca, W. Soares, and S. Chávez-Cerda, *Unveiling a truncated optical lattice associated with a triangular aperture using lights orbital angular momentum,* Physical Review Letters **105**, 053904 (2010).

[68] M. Berry, *Disruption of wavefronts: statistics of dislocations in incoherent Gaussian random waves,* Journal of Physics A: Mathematical and General **11**, 27 (1978).

[69] I. Freund, *Optical vortices in Gaussian random wave fields: statistical probability densities,* Journal of the Optical Society of America A **11**, 1644–1652 (1994).

[70] N. Shvartsman and I. Freund, *Vortices in random wave fields: nearest neighbor anticorrelations,* Physical Review Letters **72**, 1008 (1994).

[71] W. Wang, S. G. Hanson, Y. Miyamoto, and M. Takeda, *Experimental investigation of local properties and statistics of optical vortices in random wave fields,* Physical Review Letters **94**, 103902 (2005).

[72] J. W. Goodman, *Speckle phenomena in optics: theory and applications* (Roberts and Company Publishers, 2007).

[73] J. C. Dainty, *Laser speckle and related phenomena* (Springer, 1975).

[74] K. OHolleran, M. R. Dennis, F. Flossmann, and M. J. Padgett, *Fractality of lights darkness,* Physical Review Letters **100**, 053902 (2008).

[75] J. Leach, M. R. Dennis, J. Courtial, and M. J. Padgett, *Laser beams: knotted threads of darkness,* Nature **432**, 165–165 (2004).

[76] I. Vellekoop, A. Lagendijk, and A. Mosk, *Exploiting disorder for perfect focusing,* Nature Photonics **4**, 320–322 (2010).

[77] D. Leger and J. Perrin, *Real-time measurement of surface roughness by correlation of speckle patterns,* Journal of the Optical Society of America **66**, 1210–1217 (1976).

[78] U. Persson, *Real time measurement of surface roughness on ground surfaces using speckle-contrast technique,* Optics and Lasers in Engineering **17**, 61–67 (1992).

[79] O. V. Angelsky, *Optical Correlation Techniques and Applications* (SPIE Press, 2007).

[80] O. V. Angelsky, S. G. Hanson, and P. P. Maksimyak, *Use of optical correlation techniques for characterizing scattering objects and media* (SPIE Press, 1999).

[81] F. Roddier, J. Gilli, and G. Lund, *On the origin of speckle boiling and its effects in stellar speckle interferometry,* Journal of Optics **13**, 263 (1982).

[82] A. W. Lohmann, G. Weigelt, and B. Wirnitzer, *Speckle masking in astronomy: triple correlation theory and applications,* Applied Optics **22**, 4028–4037 (1983).

[83] M. P. Lavery, F. C. Speirits, S. M. Barnett, and M. J. Padgett, *Detection of a spinning object using lights orbital angular momentum,* Science **341**, 537–540 (2013).

[84] M. P. Lavery, S. M. Barnett, F. C. Speirits, and M. J. Padgett, *Observation of the rotational Doppler shift of a white-light, orbital-angular-momentum-carrying beam backscattered from a rotating body,* Optica **1**, 1–4 (2014).

[85] M. Harwit, *Photon orbital angular momentum in astrophysics,* The Astrophysical Journal **597**, 1266 (2003).

[86] O. S. Magana-Loaiza, M. Mirhosseini, R. M. Cross, S. M. H. Rafsanjani, and R. W. Boyd, *Hanbury Brown and Twiss interferometry with twisted light,* arXiv:1502.02086 (2015).

[87] D. Palacios, I. Maleev, A. Marathay, and G. Swartzlander Jr, *Spatial correlation singularity of a vortex field,* Physical Review Letters **92**, 143905 (2004).

[88] A. Kumar, J. Banerji, and R. P. Singh, *Intensity correlation properties of high-order optical vortices passing through a rotating ground-glass plate,* Optics Letters **35**, 3841–3843 (2010).

[89] A. Kumar, J. Banerji, and R. P. Singh, *Hanbury Brown–Twiss-type experiments with optical vortices and observation of modulated intensity correlation on scattering from rotating ground glass,* Physical Review A **86**, 013825 (2012).

[90] A. Kumar, P. Vaity, and R. P. Singh, *Diffraction characteristics of optical vortex passing through an aperture–iris diaphragm,* Optics Communications **283**, 4141–4145 (2010).

[91] A. S. Ostrovsky, C. Rickenstorff-Parrao, and V. Arrizón, *Generation of the perfect optical vortex using a liquid-crystal spatial light modulator,* Optics Letters **38**, 534–536 (2013).

[92] M. Chen, M. Mazilu, Y. Arita, E. M. Wright, and K. Dholakia, *Dynamics of microparticles trapped in a perfect vortex beam,* Optics Letters **38**, 4919–4922 (2013).

[93] J. García-García, C. Rickenstorff-Parrao, R. Ramos-García, V. Arrizón, and A. S. Ostrovsky, *Simple technique for generating the perfect optical vortex,* Optics Letters **39**, 5305–5308 (2014).

[94] P. Vaity and L. Rusch, *Perfect vortex beam: Fourier transformation of a Bessel beam,* Optics Letters **40**, 597–600 (2015).

[95] V. Arrizón, U. Ruiz, D. Sánchez-de-la Llave, G. Mellado-Villaseñor, and A. S. Ostrovsky, *Optimum generation of annular vortices using phase diffractive optical elements,* Optics Letters **40**, 1173–1176 (2015).

[96] R. L. Phillips and L. C. Andrews, *Spot size and divergence for Laguerre Gaussian beams of any order,* Applied Optics **22**, 643–644 (1983).

[97] M. J. Padgett, F. M. Miatto, M. Lavery, A. Zeilinger, and R. W. Boyd, *Divergence of an orbital-angular-momentum-carrying beam upon propagation,* New Journal of Physics **17**, 023011 (2015).

[98] A. Kumar, P. Vaity, Y. Krishna, and R. P. Singh, *Engineering the size of dark core of an optical vortex,* Optics and Lasers in Engineering **48**, 276–281 (2010).

[99] S. G. Reddy, S. Prabhakar, A. Kumar, J. Banerji, and R. P. Singh, *Higher order optical vortices and formation of speckles,* Optics Letters **39**, 4364–4367 (2014).

[100] V. Y. Bazhenov, M. Soskin, and M. Vasnetsov, *Screw dislocations in light wavefronts,* Journal of Modern Optics **39**, 985–990 (1992).

[101] G. Indebetouw, *Optical vortices and their propagation,* Journal of Modern Optics **40**, 73–87 (1993).

[102] F. S. Roux, *Spatial evolution of the morphology of an optical vortex dipole,* Optics Communications **236**, 433–440 (2004).

[103] F. S. Roux, *Canonical vortex dipole dynamics,* Journal of the Optical Society of America B **21**, 655–663 (2004).

[104] M. Chen and F. S. Roux, *Accelerating the annihilation of an optical vortex dipole in a Gaussian beam,* Journal of the Optical Society of America A **25**, 1279–1286 (2008).

[105] Z. Chen, J. Pu, and D. Zhao, *Tight focusing properties of linearly polarized Gaussian beam with a pair of vortices,* Physics Letters A **375**, 2958–2963 (2011).

[106] H. Chen, Z. Gao, H. Yang, F. Wang, and X. Huang, *Propagation of a pair of vortices through a tilted lens,* Optik-International Journal for Light and Electron Optics **124**, 4201–4205 (2013).

[107] S. Khan, M. Pathan, N. A. M. Hassan, and G. Yasmin, *Implicit summation formulae for Hermite and related polynomials,* Journal of Mathematical Analysis and Applications **344**, 408–416 (2008).

[108] G. Dattoli, *Hermite-Bessel and Laguerre-Bessel functions: a by-product of the monomiality principle* (Melfi, 1999).

[109] W. Magnus, F. Oberhettinger, and R. Soni, *Formulas and theorems for the special functions of mathematical physics*, vol. 52 (Springer Science & Business Media, 2013).

[110] G. Dattoli, *Incomplete 2d Hermite polynomials: properties and applications,* Journal of Mathematical Analysis and Applications **284**, 447–454 (2003).

[111] R. S. Sirohi, *A course of experiments with He-Ne laser* (New Age International, 1991).

[112] R. K. Singh, R. Vinu, and A. Sharma, *Recovery of complex valued objects from two-point intensity correlation measurement,* Applied Physics Letters **104**, 111108 (2014).

[113] G. Kirkbright, *R. Hanbury Brown: the intensity interferometer-its application to astronomy* (Taylor and Francis Ltd., London, 1975).

[114] R. J. Glauber, *Coherent and incoherent states of the radiation field,* Physical Review **131**, 2766 (1963).

[115] L. Mandel and E. Wolf, *Optical coherence and quantum optics* (Cambridge university press, 1995).

[116] C. Oliver, H. Cummins, and E. Pike, *Photon correlation and light beating spectroscopy,* Plenum Press, New York, London **197**, 151 (1974).

[117] G. Baym, *The physics of Hanbury Brown–Twiss intensity interferometry: from stars to nuclear collisions,* Acta Physica Polania B **29**, 1839 (1998).

[118] R. Dall, S. Hodgman, A. Manning, M. Johnsson, K. Baldwin, and A. Truscott, *Observation of atomic speckle and Hanbury Brown-Twiss correlations in guided matter waves,* Nature Communications **2**, 291 (2011).

[119] M. Yasuda and F. Shimizu, *Observation of two-atom correlation of an ultracold neon atomic beam,* Physical Review Letters **77**, 3090 (1996).

[120] W. D. Oliver, J. Kim, R. C. Liu, and Y. Yamamoto, *Hanbury Brown and Twiss-type experiment with electrons,* Science **284**, 299–301 (1999).

[121] H. Kiesel, A. Renz, and F. Hasselbach, *Observation of Hanbury Brown–Twiss anticorrelations for free electrons,* Nature **418**, 392–394 (2002).

[122] M. Henny, S. Oberholzer, C. Strunk, T. Heinzel, K. Ensslin, M. Holland, and C. Schönenberger, *The fermionic Hanbury Brown and Twiss experiment,* Science **284**, 296–298 (1999).

[123] M. Schellekens, R. Hoppeler, A. Perrin, J. V. Gomes, D. Boiron, A. Aspect, and C. I. Westbrook, *Hanbury Brown Twiss effect for ultracold quantum gases,* Science **310**, 648–651 (2005).

[124] T. Jeltes, J. M. McNamara, W. Hogervorst, W. Vassen, V. Krachmalnicoff, M. Schellekens, A. Perrin, H. Chang, D. Boiron, A. Aspect *et al.*, *Comparison of the Hanbury Brown–Twiss effect for bosons and fermions,* Nature **445**, 402–405 (2007).

[125] A. Perrin, R. Bücker, S. Manz, T. Betz, C. Koller, T. Plisson, T. Schumm, and J. Schmiedmayer, *Hanbury Brown and Twiss correlations across the Bose-Einstein condensation threshold,* Nature Physics **8**, 195–198 (2012).

[126] J. V. Gomes, A. Perrin, M. Schellekens, D. Boiron, C. I. Westbrook, and M. Belsley, *Theory for a Hanbury Brown Twiss experiment with a ballistically expanding cloud of cold atoms,* Physical Review A **74**, 053607 (2006).

[127] Y. Bromberg, Y. Lahini, E. Small, and Y. Silberberg, *Hanbury Brown and Twiss interferometry with interacting photons,* Nature Photonics **4**, 721–726 (2010).

[128] S. Crosby, S. Castelletto, C. Aruldoss, R. Scholten, and A. Roberts, *Modelling of classical ghost images obtained using scattered light,* New Journal of Physics **9**, 285 (2007).

[129] M. N. OSullivan, K. W. C. Chan, and R. W. Boyd, *Comparison of the signal-to-noise characteristics of quantum versus thermal ghost imaging,* Physical Review A **82**, 053803 (2010).

[130] K. W. C. Chan, M. N. O'Sullivan, and R. W. Boyd, *Optimization of thermal ghost imaging: high-order correlations vs. background subtraction,* Optics Express **18**, 5562–5573 (2010).

[131] F. Wang, Y. Cai, and O. Korotkova, *Experimental observation of focal shifts in focused partially coherent beams,* Optics Communications **282**, 3408–3413 (2009).

[132] K. C. Neuman, E. A. Abbondanzieri, and S. M. Block, *Measurement of the effective focal shift in an optical trap,* Optics Letters **30**, 1318–1320 (2005).

[133] F. Fatemi and M. Bashkansky, *Cold atom guidance using a binary spatial light modulator,* Optics Express **14**, 1368–1375 (2006).

[134] K. Gahagan and G. Swartzlander, *Trapping of low-index microparticles in an optical vortex,* Journal of the Optical Society of America B **15**, 524–534 (1998).

[135] G. Schweiger, R. Nett, B. Özel, and T. Weigel, *Generation of hollow beams by spiral rays in multimode light guides,* Optics Express **18**, 4510–4517 (2010).

[136] D. McGloin and K. Dholakia, *Bessel beams: diffraction in a new light,* Contemporary Physics **46**, 15–28 (2005).

[137] C. Zhao, Y. Cai, F. Wang, X. Lu, and Y. Wang, *Generation of a high-quality partially coherent dark hollow beam with a multimode fiber.* Optics Letters **33**, 1389–1391 (2008).

[138] Y. Cai, *Propagation of some coherent and partially coherent laser beams* (Royal Institute of Technology, 2006).

[139] F. Wang, Y. Cai, and O. Korotkova, *Partially coherent standard and elegant Laguerre-Gaussian beams of all orders,* Optics Express **17**, 22366–22379 (2009).

[140] Z. Mei and O. Korotkova, *Random sources generating ring-shaped beams,* Optics Letters **38**, 91–93 (2013).

[141] M. Gecevičius, R. Drevinskas, M. Beresna, and P. G. Kazansky, *Single beam optical vortex tweezers with tunable orbital angular momentum,* Applied Physics Letters **104**, 231110 (2014).

[142] R. Fickler, R. Lapkiewicz, M. Huber, M. P. Lavery, M. J. Padgett, and A. Zeilinger, *Interface between path and orbital angular momentum entanglement for high-dimensional photonic quantum information,* Nature Communications **5**, 4502 (2014).

[143] M. Krenn, R. Fickler, M. Fink, J. Handsteiner, M. Malik, T. Scheidl, R. Ursin, and A. Zeilinger, *Communication with spatially modulated light through turbulent air across Vienna,* New Journal of Physics **16**, 113028 (2014).

[144] G. Gbur and R. K. Tyson, *Vortex beam propagation through atmospheric turbulence and topological charge conservation,* Journal of the Optical Society of America A **25**, 225–230 (2008).

[145] B. Simon, S. Simon, F. Gori, M. Santarsiero, R. Borghi, N. Mukunda, and R. Simon, *Nonquantum entanglement resolves a basic issue in polarization optics,* Physical Review Letters **104**, 023901 (2010).

[146] L. Chen and W. She, *Single-photon spin-orbit entanglement violating a Bell-like inequality,* Journal of the Optical Society of America B **27**, A7–A10 (2010).

[147] R. Horodecki, P. Horodecki, M. Horodecki, and K. Horodecki, *Quantum entanglement,* Reviews of Modern Physics **81**, 865 (2009).

[148] L. Neves, G. Lima, A. Delgado, and C. Saavedra, *Hybrid photonic entanglement: Realization, characterization, and applications,* Physical Review A **80**, 042322 (2009).

[149] Q. Zhan, *Cylindrical vector beams: from mathematical concepts to applications,* Advances in Optics and Photonics **1**, 1–57 (2009).

[150] R. J. Spreeuw, *A classical analogy of entanglement,* Foundations of Physics **28**, 361–374 (1998).

[151] B. Simon, S. Simon, N. Mukunda, F. Gori, M. Santarsiero, R. Borghi, and R. Simon, *A complete characterization of pre-Mueller and Mueller matrices in polarization optics,* Journal of the Optical Society of America A **27**, 188–199 (2010).

[152] P. Ghose and A. Mukherjee, *Entanglement in classical optics,* Reviews in Theoretical Science **2**, 274–288 (2014).

[153] A. Luis, *Coherence, polarization, and entanglement for classical light fields,* Optics Communications **282**, 3665–3670 (2009).

[154] C. Borges, M. Hor-Meyll, J. Huguenin, and A. Khoury, *Bell-like inequality for the spin-orbit separability of a laser beam,* Physical Review A **82**, 033833 (2010).

[155] E. Karimi, J. Leach, S. Slussarenko, B. Piccirillo, L. Marrucci, L. Chen, W. She, S. Franke-Arnold, M. J. Padgett, and E. Santamato, *Spin-orbit hybrid entanglement of photons and quantum contextuality,* Physical Review A **82**, 022115 (2010).

[156] F. Töppel, A. Aiello, C. Marquardt, E. Giacobino, and G. Leuchs, *Classical entanglement in polarization metrology,* New Journal of Physics **16**, 073019 (2014).

[157] V. D'Ambrosio, N. Spagnolo, L. Del Re, S. Slussarenko, Y. Li, L. C. Kwek, L. Marrucci, S. P. Walborn, L. Aolita, and F. Sciarrino, *Photonic polarization gears for ultra-sensitive angular measurements,* Nature Communications **4**, 2432.

[158] M. Padgett and J. Courtial, *Poincaré-sphere equivalent for light beams containing orbital angular momentum,* Optics Letters **24**, 430–432 (1999).

[159] G. S. Agarwal, *SU (2) structure of the Poincaré sphere for light beams with orbital angular momentum,* Journal of the Optical Society of America A **16**, 2914–2916 (1999).

[160] S. G. Reddy, A. Kumar, S. Prabhakar, and R. P. Singh, *Experimental generation of ring-shaped beams with random sources,* Optics Letters **38**, 4441–4444 (2013).

[161] S. Prabhakar, S. G. Reddy, A. Aadhi, A. Kumar, P. Chithrabhanu, G. Samanta, and R. P. Singh, *Spatial distribution of spontaneous parametric down-converted photons for higher order optical vortices,* Optics Communications **326**, 64–69 (2014).

[162] J. Turunen, A. Vasara, and A. T. Friberg, *Propagation invariance and self-imaging in variable-coherence optics,* Journal of the Optical Society of America A **8**, 282–289 (1991).

[163] D. M. Cottrell, J. M. Craven, and J. A. Davis, *Nondiffracting random intensity patterns,* Optics Letters **32**, 298–300 (2007).

[164] A. Dudley, R. Vasilyeu, V. Belyi, N. Khilo, P. Ropot, and A. Forbes, *Controlling the evolution of nondiffracting speckle by complex amplitude modulation on a phase-only spatial light modulator,* Optics Communications **285**, 5–12 (2012).

[165] B.-Y. Wang, X.-L. Ge, Q.-Y. Yue, and C.-S. Guo, *Determining the vortex densities of random nondiffracting beams,* Optics Letters **40**, 1418–1421 (2015).

[166] F. Gori, G. Guattari, and C. Padovani, *Bessel-Gauss beams,* Optics Communications **64**, 491–495 (1987).

[167] P. L. Greene and D. G. Hall, *Properties and diffraction of vector Bessel–Gauss beams,* Journal of the Optical Society of America A **15**, 3020–3027 (1998).

[168] J. Vickers, M. Burch, R. Vyas, and S. Singh, *Phase and interference properties of optical vortex beams,* Journal of the Optical Society of America A **25**, 823–827 (2008).

[169] R. Pappu, B. Recht, J. Taylor, and N. Gershenfeld, *Physical one-way functions,* Science **297**, 2026–2030 (2002).

[170] C. R. Alves, A. J. Jesus-Silva, and E. J. Fonseca, *Characterizing coherence vortices through geometry,* Optics Letters **40**, 2747–2750 (2015).

[171] S. G. Reddy, S. Prabhakar, A. Aadhi, A. Kumar, M. Shah, R. P. Singh, and R. Simon, *Measuring the Mueller matrix of an arbitrary optical element with a universal SU (2) polarization gadget,* Journal of the Optical Society of America A **31**, 610–615 (2014).

[172] M. H. Rubin, *Transverse correlation in optical spontaneous parametric down-conversion,* Physical Review A **54**, 5349 (1996).

LIST OF PUBLICATIONS

Publications contributing to this thesis :

1. *Experimental generation of ring shaped beams with random sources*,
Salla Gangi Reddy, Ashok Kumar, Shashi Prabhakar, and R. P. Singh, Optics Letters **38**, 21, 4441-4444 (2013).

2. *Higher order optical vortices and formation of speckles*,
Salla Gangi Reddy, Shashi Prabhakar, Ashok Kumar, J. Banerji, and R. P. Singh, Optics Letters **39**, 15, 4364-4367 (2014).

3. *Propagation of an arbitrary vortex pair through an astigmatic optical system and determination of its topological charge*,
Salla Gangi Reddy, Shashi Prabhakar, A. Aadhi, J. Banerji, and R. P. Singh, Journal of the Optical Society of America A **31**, 6, 1295-1302 (2014).

4. *Recovering the vorticity of a light beam after scattering*,
Salla Gangi Reddy, Chithrabhanu P, Shashi Prabhakar, Ali Anwar, and R. P. Singh, Applied Physics Letters, **107**, 021104 (2015).

5. *Divergence of the optical vortex beams*,
Salla Gangi Reddy, Chithrabhanu P, Ali Anwar, Shashi Prabhakar, J. Banerji, and R. P. Singh, To be published in Applied Optics (2015).

6. *Perfect optical vortices and the non-diffracting speckles*,
Salla Gangi Reddy, Chithrabhanu P, Aadhi A, Pravin Vaity, Shashi Prabhakar, and R. P. Singh, Submitted to Optics Letters (Under Revision).

Other publications :

1. *Measuring the Mueller matrix of an arbitrary optical element with a universal SU (2) polarization gadget* ,
Salla Gangi Reddy, Shashi Prabhakar, A. Aadhi, A Kumar, M. Shah, R. P. Singh, R. Simon, Journal of the Optical Society of America A **31**, 3, 610-615 (2014).

2. *Spatial distribution of spontaneous parametric down-converted photons for higher order optical vortices*,
Shashi Prabhakar, **Salla Gangi Reddy**, A. Aadhi, Ashok Kumar, P. Chithrabhanu, G. K. Samanta, and R. P. Singh, Optics Communications **326**, 64-69 (2014).

3. *Scattering of non-separable states of light*,
Chithrabhanu P, **Salla Gangi Reddy**, Ali Anwar, Aadhi A, Shashi Prabhakar, and R. P. Singh, Optics Communications **355**, 301-305 (2015).

4. *Three particle hyper entanglement: Teleportation and quantum key distribution*,
P. Chithrabhanu, A. aadhi, **Salla Gangi Reddy**, Shashi Prabhakar, G. K. Samanta, G. Paul, and R. P. Singh, To be published in Quantum Information Processing (2015).

5. *Violation of Bell's inequality for phase singular beams*,
Shashi Prbhakar, **Salla Gangi Reddy**, A. Aadhi, P. Chithrabhanu, and R. P. Singh, Submitted to Physical Review A (Under Revision).

6. *Scattering of phase singular beams: A model for experimental results*,
Salla Gangi Reddy, Shashi Prabhakar, J. Banerji, and R. P. Singh, To be submitted to Physical Review A.

7. *Two component polarization gadget*,
Salla Gangi Reddy, Shashi Prabhakar, P. Chithrabhanu, R. P. Singh, and R. Simon, To be submitted to Journal of Biomedical optics.

Conference papers :

1. Shashi Prabhakar, Ashok Kumar, **Salla Gangi Reddy,** A. Aadhi, and R. P. Singh, *Determination of order of vortex from intensity distribution,* International Conference on Trends in Optics and Photonics, University of Calcutta, Koltata, India, pp. 115-119, December 7-9, 2011.

2. R. P. Singh, Pravin Vaity, Ashok Kumar, **Salla Gangi Reddy,** and A. Aadhi, *Dynamics of fractional charge optical vortices,* International Conference on Trends in Optics and Photonics, University of Calcutta, Koltata, India, pp. 217-220, December 7-9, 2011.

3. P. Vaity, Ashok Kumar, **Salla Gangi Reddy,** A. Aadhi, P. Chithrabhanu, and R. P. Singh, *Determining orbital angular momentum of light using simple convex lens,* in International Conference on Fibre Optics and Photonics, OSA Technical Digest (online) (Optical Society of America, 2012), paper MPo.4.

4. S. Prabhakar, **Salla Gangi Reddy,** A. Aadhi, Ashok Kumar, G. Samanta, and R. P. Singh, *Spatial distribution of Spontaneous Parametric Down-Converted Photons,*

in International Conference on Fibre Optics and Photonics, OSA Technical Digest (online) (Optical Society of America, 2012), paper T1C.2.

5. **Salla Gangi Reddy,** S. Prabhakar, A. Aadhi, Ashok Kumar, M. Shah, R. P. Singh, and R. Simon, *Determination of Mueller matrix of an optical element with Simon-Mukunda gadget,* in International Conference on Fibre Optics and Photonics, OSA Technical Digest (online) (Optical Society of America, 2012), paper M1B.2 (**Best Paper Award**).

6. **Salla Gangi Reddy,** Ashok Kumar, Shashi Prabhakar, and R. P. Singh, **Revival of the dark core in scattered optical vortices,** presented at SPIE optics and photonics during August 25-29, 2013 at San Diego, California, USA.

7. **Salla Gangi Reddy,** Shashi Prabhakar, Ashok Kumar, and R. P. Singh, *Spatial Intensity Distribution of optical vortex beams,* presented at Workshop in recent advances in Photonics during December 17-18, 2013 at IIT Delhi, New Delhi, India (**Best Paper Award**).

8. **Salla Gangi Reddy,** Shashi Prabhakar, Ashok Kumar, J. Banerji, and R. P. Singh, *Variation of speckle size with the order of an optical vortex,* presented at International conference on Optics and Optoelectronics during March 05-08, 2014 at IRDE Dehradun, India.

9. **Salla Gangi Reddy,** Ashok Kumar, J. Banerji, Shashi Prabhakar, and R. P. Singh, *Optical vortices through a ground glass,* presented at International conference on Optics and Optoelectronics during March 05-08, 2014 at IRDE Dehradun, India.

10. Chithrabhanu P, Aadhi A, **Salla Gangi Reddy,** Shashi Prabhakar, G. K. Samanta, and R. P. Singh, *A novel entangled source for higher dimensional quantum teleportation and QKD,* presented at International conference on Optics and Optoelectronics during March 05-08, 2014 at IRDE Dehradun, India (**Best Paper Award**).

11. **Salla Gangi Reddy,** Shashi Prabhakar, Ali Anwar, J. Banerji, and R. P. Singh, *Propagation of an arbitrary vortex pair through an astigmatic optical system,* presented at National Laser Symposium during December 03-06, 2014 at Sri Venkateswara University, Tirupathi, India.

12. Chithrabhanu, **Salla Gangi Reddy,** Aadhi A, Shashi Prabhakar, Ali Anwar, and R. P. Singh, *Scattering of non-separable light beams,* presented at National Laser Symposium during December 03-06, 2014 at Sri Venkateswara University, Tirupathi, India.

13. A. Aadhi, Chithrabhanu, **Salla Gangi Reddy,** Shashi Prabhakar, Jabir MV, G. K. Samanta, and R. P. Singh, *Measurement of Berry Phase by non-interferometric method,* presented at National Laser Symposium during December 03-06, 2014 at Sri Venkateswara University, Tirupathi, India.

14. **Salla Gangi Reddy,** Shashi Prabhakar, Ali Anwar, J. Banerji, and R. P. Singh, *Modelling of scattered optical vortices,* presented at Photonics 2014 during December 13-16, 2014 at IIT Kharagpur, India.

15. **Salla Gangi Reddy,** Chithrabhanu, Shashi Prabhakar, Ali Anwar, and R. P. Singh, *Revival of the vorticity in scattered optical vortices,* presented at Photonics 2014 during December 13-16, 2014 at IIT Kharagpur, India.

16. Chithrabhanu, A. Aadhi, **Salla Gangi Reddy,** Shashi Prabhakar, Ali Anwar, and R. P. Singh, *Construction of OAM Poincare sphere with both coherent and partially coherent light beams,* presented at Photonics 2014 during December 13-16, 2014 at IIT Kharagpur, India.

17. Shashi Prabhakar, **Salla Gangi Reddy,** Chithrabhanu, A. Aadhi, G. K. Samanta, and R. P. Singh, *Violation of Bells inequality with phase singular beams,* presented at Photonics 2014 during December 13-16, 2014 at IIT Kharagpur, India. to be presented at Photonics 2014 going to be held on December 13-16, 2014 at IIT Kharagpur, India (**Best Paper Award**).

18. **Salla Gangi Reddy,** Chithrabhanu, Shashi Prabhakar, Ali Anwar, and R. P. Singh, *Divergence of the optical vortex beams with measurable parameters,* presented at International conference on optics and photonics (ICOP 2015) during February 20-22, 2015 at Calcutta University, Kolkata, India.

19. Chithrabhanu, **Salla Gangi Reddy,** Ali Anwar, Aadhi A, Shashi Prabhakar, and R. P. Singh, *Generalized orbital angular momentum Poincaré sphere,* presented at International conference on optics and photonics (ICOP 2015) during February 20-22, 2015 at Calcutta University, Kolkata, India.

20. Aadhi A, Chithrabhanu, **Salla Gangi Reddy,** Apurv Chaitanya, G. K. Samanta, and R. P. Singh, *Superposition of polarization singularity,* presented at International conference on optics and photonics (ICOP 2015) during February 20-22, 2015 at Calcutta University, Kolkata, India.

21. **Salla Gangi Reddy,** Chithrabhanu, Shashi Prabhakar, Ali Anwar, and R. P. Singh, *Perfect optical vortices: Response to an astigmatic optical system,* to be presented at Third international conference on optical angular momentum (ICOAM 2015) going to be held on August 4-7, 2015 at City college of New York, New York, USA.

22. Chithrabhanu P, **Salla Gangi Reddy,** Ali Anwar, Aadhi A, Shashi Prabhakar, and R. P. Singh, *Scattering of light beams with non-separable polarization and orbital angular momentum states,* to be presented at Third international conference on optical angular momentum (ICOAM 2015) going to be held on August 4-7, 2015 at City college of New York, New York, USA.

23. Aadhi A, Chithrabhanu P, **Salla Gangi Reddy,** Apurv Chaitanya, G. K. Samanta, and R. P. Singh, *Non-interferometric method to measure the Pancharatnam phase using a non-separable light beam,* to be presented at Third international conference on optical angular momentum (ICOAM 2015) going to be held on August 4-7, 2015 at City college of New York, New York, USA.

24. Aadhi A, Chithrabhanu P, **Salla Gangi Reddy,** Apurv Chaitanya, G. K. Samanta, and R. P. Singh, *Spatial superposition of vector vortex beams,* to be presented at Third international conference on optical angular momentum (ICOAM 2015) going to be held on August 4-7, 2015 at City college of New York, New York, USA.

25. **Salla Gangi Reddy,** Chithrabhanu, Shashi Prabhakar, J. Banerji, and R. P. Singh, *Correlations in scattered optical vortices,* to be presented at Correlation optics 2015 going to be held on September 14-18, 2015 at University of Chernivtsi, Chernivtsi, Ukraine (**Invited talk**).

Publications attached with the thesis

1. *Higher order optical vortices and formation of speckles*,
   Salla Gangi reddy, Shashi Prabhakar, Ashok Kumar, J. Banerji, and R. P. Singh, Optics Letters **39**, 15, 4364-4367 (2014).

2. *Propagation of an arbitrary vortex pair through an astigmatic optical system and determination of its topological charge*,
   Salla Gangi Reddy, Shashi Prabhakar, A. Aadhi, J. Banerji, and R. P. Singh, Journal of the Optical Society of America A **31**, 6, 1295-1302 (2014).

3. *Recovering the vorticity of a light beam after scattering*,
   Salla Gangi Reddy, Chithrabhanu P, Shashi Prabhakar, Ali Anwar, and R. P. Singh, Applied Physics Letters, **107**, 021104 (2015).